

000 001 002 003 004 005 006 007 008 009 010 011 012 013 014 015 016 017 018 019 020 021 022 023 024 025 026 027 028 029 030 031 032 033 034 035 036 037 038 039 040 041 042 043 044 045 046 047 048 049 050 051 052 053 ALIGNMENT-SENSITIVE MINIMAX RATES FOR SPECTRAL ALGORITHMS WITH LEARNED KERNELS

Anonymous authors

Paper under double-blind review

ABSTRACT

We study spectral algorithms in the setting where kernels are learned from data. We introduce the effective span dimension (ESD), an alignment-sensitive complexity measure that depends jointly on the signal, spectrum, and noise level σ^2 . The ESD is well-defined for arbitrary kernels and signals without requiring eigen-decay conditions or source conditions. We prove that for sequence models whose ESD is at most K , the minimax excess risk scales as $\sigma^2 K$. Furthermore, we analyze over-parameterized gradient flow and prove that it can reduce the ESD of a sequence model, which in turn moves the problem into an easier ESD class and lowers the corresponding minimax risk. This analysis suggests a general route to study how adaptive feature learning can improve generalization through signal-kernel alignment: adaptive learning procedures reshape the kernel so that the ESD decreases and the problem enters an easier ESD class. We also extend the ESD framework to linear models and RKHS regression, and we support the theory with numerical experiments. This framework provides a novel perspective on generalization beyond traditional fixed-kernel theories.

1 INTRODUCTION

Neural networks excel across many applications, yet a complete theoretical understanding of their efficiency remains an open problem. In the infinite-width limit, the Neural Tangent Kernel (NTK) theory approximates training dynamics as kernel regression (Jacot et al., 2018; Allen-Zhu et al., 2019), and it enables the study of generalization by leveraging the classical theory of kernel regression and Reproducing Kernel Hilbert Spaces (RKHS) (Bauer et al., 2007; Yao et al., 2007). However, the NTK theory does not explain why finite-width networks, which adapt their features during training, often outperform traditional methods (Ghorbani et al., 2020; Gatmiry et al., 2021; Karp et al., 2021; Shi et al., 2023; Wenger et al., 2023; Seleznova & Kutyniok, 2022).

A growing line of work directly studies adaptivity, i.e., learning representations or kernel properties during training (Ba et al., 2022; Kunin et al., 2024; Liu et al., 2024; Bordelon et al., 2025; Xu & Ziyin, 2025; Zhang et al., 2024). Simplified models show that learning *eigenvalues* (with eigenfunctions fixed) can align the kernel with the signal and improve performance (Li & Lin, 2024; 2025). The common thread is signal-kernel alignment: ***performance improves when the target's energy concentrates on leading eigenfunctions***. The importance of signal-kernel alignment is well-recognized in the literature (Arora et al., 2019; Woodworth et al., 2020; Kornblith et al., 2019; Radhakrishnan et al., 2024). In classical RKHS theory, signal-kernel alignment is often captured through ***source conditions*** (Engl et al., 1996; Caponnetto & De Vito, 2007). While powerful for static kernels, source conditions assume a fixed eigenbasis and become ill-defined if the kernel evolves over time as in adaptive learning. To explain the observed advantages of adaptive learning, we need a refined theoretical framework that goes beyond fixed-kernel assumptions.

In this paper, we propose the **Effective Span Dimension (ESD)**, which is a population complexity measure for the analysis of signal-kernel alignment. ESD counts the smallest number of leading eigenfunctions required so that the remaining signal energy matches the estimation variance. Unlike classical measures that ignore the signal, ESD depends on the *signal, spectrum, and noise level*. Our framework provides new theoretical insights that are absent in classical analyses. In particular, we achieve the following:

054 (i) We establish a sharp minimax optimal convergence rate using ESD, which not only subsumes
 055 classical rates but also extends to dynamic kernels where classical theory is silent.
 056

057 (ii) We provide a mechanistic explanation for how adaptive algorithms improve generalization through
 058 ESD reduction: they modify the induced kernel to better align with the signal, shrink the ESD, and
 059 thereby move the problem into a class with lower minimax risk. This mechanism is proved for
 060 over-parameterized gradient flow and observed empirically in deep linear networks.

061 (iii) We extend our definitions and theory from sequence models to linear regression and kernel
 062 regression, which demonstrates the broad applicability of our framework.

063 Our ESD framework bridges fixed-kernel theory and adaptive learning by quantifying signal-kernel
 064 alignment. We hope it will open avenues for deeper understanding of neural networks and novel
 065 adaptive algorithms.

066 *Notations.* Write $a \lesssim b$ if there exists a constant $C > 0$ such that $a \leq Cb$, and write $a \asymp b$ if $a \lesssim b$
 067 and $b \lesssim a$, where the dependence of the constants on other parameters is determined by the context.
 068 For $d \in \mathbb{N}_+$, let $[d] = \{1, 2, \dots, d\}$; for $d = \infty$, let $[d] = \mathbb{N}_+$. $\mathbf{1}_{\{\cdot\}}$ denotes an indicator function.
 069

070 2 BACKGROUND ON KERNEL METHODS

071 We first review kernel regression to provide context. Let $(\mathbf{x}_i, y_i)_{i=1}^n$ be i.i.d. samples from $y = f^*(\mathbf{x}) + \epsilon$, where $\mathbf{x} \sim \mu$ on a compact space \mathcal{X} , ϵ is an independent noise with $\mathbb{E}[\epsilon] = 0$, $\text{Var}(\epsilon) = \sigma_0^2$.
 072 For an estimator \hat{f} of the target function f^* , the excess risk is $\mathcal{R}(\hat{f}; f^*) = \mathbb{E}_{\mathbf{x} \sim \mu}[(\hat{f}(\mathbf{x}) - f^*(\mathbf{x}))^2]$.
 073

074 A symmetric, positive-definite, and continuous kernel $\mathbf{k}(\cdot, \cdot) : \mathcal{X} \times \mathcal{X} \rightarrow \mathbb{R}$ induces an RKHS
 075 $\mathcal{H} \subset L^2(\mathcal{X}, \mu)$ with inner product $\langle \cdot, \cdot \rangle_{\mathcal{H}}$ and norm $\|\cdot\|_{\mathcal{H}}$ (Wahba, 1990; Schölkopf & Smola, 2002).
 076 Assuming \mathbf{k} is bounded, Mercer's theorem yields

$$077 \mathbf{k}(\mathbf{x}, \mathbf{x}') = \sum_{j=1}^{\infty} \lambda_j \psi_j(\mathbf{x}) \psi_j(\mathbf{x}'), \quad \mathbf{x}, \mathbf{x}' \in \mathcal{X}, \quad (1)$$

078 where $\{\lambda_j\}_{j \geq 1}$ are eigenvalues and $\{\psi_j\}_{j \geq 1} \subset \mathcal{H}$ are eigenfunctions forming an orthonormal basis
 079 of $L^2(\mathcal{X}, \mu)$. For background, see Steinwart & Christmann (2008); Steinwart & Scovel (2012).
 080

081 Kernel regression estimates f^* using $f = \sum_j \beta_j \psi_j$ and regularizes via a filter of the kernel spectrum
 082 $\{\lambda_j\}$ (Rosasco et al., 2005; Caponnetto & Vito, 2007; Gerfo et al., 2008). If f^* satisfies the *Hölder*
 083 *source condition* $\sum_j \langle f^*, \psi_j \rangle^2 / \lambda_j^s \leq R_s$ for some positive constants s and R_s (Engl et al., 1996;
 084 Mathé & Pereverzev, 2003) and the spectrum decays polynomially $\lambda_j \asymp j^{-\gamma}$, then the minimax
 085 rate is $n^{-s\gamma/(s\gamma+1)}$ (Yao et al., 2007; Li et al., 2024; Wang et al., 2024). The choice of kernels can
 086 significantly affect the performance (Li & Lin, 2024; Zhang et al., 2024), so it is beneficial when the
 087 kernel eigenvalues align well with the expansion of the target function.
 088

089 Since the kernel is usually chosen without knowing f^* , fixed-kernel methods may encounter mis-
 090 alignment. To address this limitation, adaptive methods have recently emerged. For instance, Li
 091 & Lin (2025) propose adapting kernel eigenvalues while fixing eigenfunctions. Specifically, they
 092 consider the kernel $\mathbf{k}_{\mathbf{a}}(\mathbf{x}, \mathbf{x}') = \sum_{j \geq 1} a_j^2 \psi_j(\mathbf{x}) \psi_j(\mathbf{x}')$ indexed by $\mathbf{a} = (a_j)_{j \geq 1}$ and the candidate
 093 $f = \sum_{j \geq 1} \beta_j a_j \psi_j$, where a_j 's and β_j 's are learned jointly via gradient flow. Such adaptation often
 094 improves performances, yet classical analyses built on fixed spectral assumptions do not explain these
 095 gains, because (a) adapted eigenvalues typically deviate from standard eigenvalue decay assumptions,
 096 and (b) it is unclear whether the classical source condition holds with respect to the adapted kernel,
 097 and if so, what the value of s is. We therefore seek a refined theoretical framework that explicitly
 098 captures signal-kernel alignment and explain the gains achieved by kernel adaptation.
 099

100 **Bridge to the sequence model.** We next connect the RKHS regression with the sequence model to
 101 motivate our analysis in the next section. For any $j \in \mathbb{N}_+$, define

$$102 \theta_j^* = \langle f^*, \psi_j \rangle, \quad z_j = n^{-1} \sum_i y_i \psi_j(\mathbf{x}_i), \text{ and } \xi_j = n^{-1} \sum_i \epsilon_i \psi_j(\mathbf{x}_i). \quad (2)$$

103 For large n , we have $n^{-1} \sum_i \psi_j(\mathbf{x}_i) \psi_k(\mathbf{x}_i) \approx \mathbb{E}[\psi_j(\mathbf{x}) \psi_k(\mathbf{x})] = \mathbf{1}_{\{j=k\}}$, which implies that

$$104 z_j \approx \theta_j^* + \xi_j, \text{ and } \mathbb{E}[\xi_j] = 0, \text{Cov}(\xi_j, \xi_k) \approx n^{-1} \sigma_0^2 \mathbf{1}_{\{j=k\}}, \quad \forall j, k \in \mathbb{N}_+. \quad (3)$$

108 This reduction connects RKHS regression to a sequence model where the observations are $z_j = \theta_j^* + \xi_j$
 109 and the noise terms $\{\xi_j\}$ are uncorrelated with effective noise variance $\sigma_{\text{eff}}^2 := n^{-1}\sigma_0^2$. The error
 110 in the approximation due to finite n will inflate the estimation variance compared to the sequence
 111 model. This approximation error can be controlled if f^* is bounded; see Appendix B for a rigorous
 112 treatment.
 113

114 3 EFFECTIVE SPAN DIMENSION AND SPAN PROFILE

116 To bridge existing theory and adaptive kernel methods as discussed in Section 2, we propose a novel
 117 framework to characterize the alignment between spectrum and signal. To focus on the main idea, we
 118 use the reduction in Equation (3) and first present our framework using sequence models.
 119

120 **Sequence models.** A sequence model assumes observations are sampled as follows:

$$121 \quad z_j = \theta_j^* + \xi_j, \quad 1 \leq j \leq d, \quad (4)$$

123 where $d \in \{\infty\} \cup \mathbb{N}_+$, $\boldsymbol{\theta}^* = (\theta_j^*)_{j=1}^d$ is a sequence of unknown parameters, ξ_j 's are uncorrelated
 124 random variables with mean zero and variance σ^2 (the noise level). For an estimator $\widehat{\boldsymbol{\theta}} = (\widehat{\theta}_j)_{j=1}^d$, we
 125 consider the loss $\mathcal{L}(\widehat{\boldsymbol{\theta}}; \boldsymbol{\theta}^*) = \sum_{j=1}^d (\widehat{\theta}_j - \theta_j^*)^2$ and risk $\mathcal{R}(\widehat{\boldsymbol{\theta}}; \boldsymbol{\theta}^*) = \mathbb{E}\mathcal{L}(\widehat{\boldsymbol{\theta}}; \boldsymbol{\theta}^*)$. The sequence model
 126 captures core estimation phenomena while permitting explicit analysis (Brown et al., 2002; Johnstone,
 127 2017). In Appendix A, we use whitening to deal with correlated noise and analyze fixed-design
 128 linear regression. In Appendix B, we leverage the approximation in Equation (3) to analyze RKHS
 129 regression and random-design linear regression.
 130

131 **Spectral estimators.** Given eigenvalues $\boldsymbol{\lambda} = (\lambda_j)_{j=1}^d$, spectral estimators take the form $\widehat{\theta}_j =$
 132 $(1 - g_\nu(\lambda_j)) z_j$, where $g_\nu(\lambda)$ is a filter such that larger ν induces more shrinkage. Some examples
 133 are:

$$134 \quad \text{Ridge (R): } g_\nu^R(\lambda) = \frac{1}{1 + \lambda/\nu}, \quad \widehat{\theta}_j^{R,\nu} = \frac{\lambda_j}{\lambda_j + \nu} z_j. \quad (5)$$

$$135 \quad \text{Gradient Flow (GF): } g_\nu^{\text{GF}}(\lambda) = e^{-\lambda/\nu}, \quad \widehat{\theta}_j^{\text{GF},\nu} = (1 - e^{-\lambda_j/\nu}) z_j. \quad (6)$$

$$136 \quad \text{Principal Component (PC): } g_\nu^{\text{PC}}(\lambda) = \mathbf{1}_{\{\lambda < \nu\}}, \quad \widehat{\theta}_j^{\text{PC},\nu} = \mathbf{1}_{\{\lambda_j \geq \nu\}} z_j. \quad (7)$$

137 For spectral estimators, the risk decomposes into squared bias $\sum_j (g_\nu(\lambda_j))^2 \theta_j^2$ and variance $\sum_j (1 - g_\nu(\lambda_j))^2 \sigma^2$, where ν controls the bias-variance trade-off. Classical analyses often assume $\boldsymbol{\theta}^*$ lies in
 138 an ellipsoid $\Theta_{\mathbf{a}} = \left\{ \boldsymbol{\theta} : \sum_j a_j^2 \theta_j^2 \leq C^2 \right\}$ and derives convergence rates for sequences with $a_i \asymp i^\alpha$
 139 (Johnstone, 2017). Our theoretical framework aims to bypass these assumptions.
 140

141 3.1 EFFECTIVE SPAN DIMENSION

142 Our goal is to develop a measure that captures the interplay between signal structure $\boldsymbol{\theta}^*$, spectrum $\boldsymbol{\lambda}$,
 143 and noise variance σ^2 . To start, we examine the Principal Component (PC) estimator analytically. PC
 144 operates by truncating coordinates with small eigenvalues. Its risk is composed of variance from the
 145 retained components and squared bias from those truncated. By trading variance against tail bias, PC
 146 admits the optimal truncation point. This motivates our core definition.

147 **Definition 3.1.** Suppose $\{\lambda_j\}_{j \in [d]}$ are distinct, with π_i indexing the i -th largest so that $\lambda_{\pi_1} > \lambda_{\pi_2} > \dots$. We define the Effective Span Dimension (ESD) d^\dagger of $\boldsymbol{\theta}^*$ w.r.t. the spectrum $\boldsymbol{\lambda}$ and variance σ^2 as

$$148 \quad d^\dagger = d^\dagger(\sigma^2; \boldsymbol{\theta}^*, \boldsymbol{\lambda}) = \min\{k \in [d] : \frac{1}{k} \sum_{i=k+1}^d (\theta_{\pi_i}^*)^2 \leq \sigma^2\}.$$

149 Intuitively, the ESD d^\dagger is the number of leading coordinates (with leading eigenvalues λ_i) that are
 150 most critical for estimation at a given noise level σ^2 . It is the truncation point where the squared tail
 151 bias of the PC estimator first becomes comparable to (or less than) the estimation variance. The next
 152 theorem shows that d^\dagger describes the best achievable risk for the PC estimator.
 153

162 **Theorem 3.2** (Optimal PC Estimator Risk). *Let $\widehat{\boldsymbol{\theta}}^{\text{PC}, \nu}$ be the PC estimator for the sequence model in*
 163 *Equation (4). Denote by $\mathcal{R}_*^{\text{PC}}$ the minimal possible risk over all choices of ν . Let $d^\dagger = d^\dagger(\sigma^2; \boldsymbol{\theta}^*, \boldsymbol{\lambda})$*
 164 *be the ESD of $\boldsymbol{\theta}^*$ w.r.t. the spectrum $\boldsymbol{\lambda}$ and the variance σ^2 . It holds that*

$$165 \quad (d^\dagger - 1) \sigma^2 \leq \mathcal{R}_*^{\text{PC}} \leq 2 d^\dagger \sigma^2.$$

167 The well-tuned PC estimator is known to be minimax rate optimal under classical assumptions in
 168 sequence models that are analogous to the polynomial eigen-decay condition and the source condition
 169 in kernel regression (see Propositions 3.11 and 4.23 of Johnstone (2017)). In contrast, Theorem 3.2
 170 suggests that we can instead use $O(d^\dagger \sigma^2)$ to upper bound the minimax estimation error with no
 171 reliance on particular spectral decay or source conditions.

172 Although we motivate ESD via PC estimators, the definition of ESD itself is not tied to any specific
 173 estimator, just as the sparsity level is not tied exclusively to Lasso or best subset selection. Moreover,
 174 the following theorem confirms that $d^\dagger \sigma^2$ indeed characterizes the intrinsic difficulty of estimation.

175 **Theorem 3.3.** *For any $K \in [d]$, spectrum $\boldsymbol{\lambda} = \{\lambda_j\}_{j \in [d]}$ and variance σ^2 , define*

$$177 \quad \mathcal{F}_{K, \boldsymbol{\lambda}}^{(n)} = \left\{ \boldsymbol{\theta} \in \mathbb{R}^d : d^\dagger(\sigma^2; \boldsymbol{\theta}, \boldsymbol{\lambda}) \leq K \right\}. \quad (8)$$

178 Suppose the sample \mathbf{Z} is drawn from the sequence model in Equation (4). We have

$$181 \quad \inf_{\widehat{\boldsymbol{\theta}}} \sup_{\boldsymbol{\theta}^* \in \mathcal{F}_{K, \boldsymbol{\lambda}}^{(n)}} \mathcal{R}(\widehat{\boldsymbol{\theta}}, \boldsymbol{\theta}^*) \asymp K \sigma^2,$$

184 where \inf is taken over any estimator $\widehat{\boldsymbol{\theta}}$ based on \mathbf{Z} .

185 Theorem 3.3 considers the minimax risk over $\mathcal{F}_{K, \boldsymbol{\lambda}}^{(n)}$, a class of distributions whose ESDs are at most
 186 K . We interpret K as the quota for ESD: the larger K , the larger $\mathcal{F}_{K, \boldsymbol{\lambda}}^{(n)}$ and thus the higher the
 187 minimax risk. Theorem 3.3 highlights the usefulness of ESD: although we motivate the definition of
 188 ESD using the PC estimator, the minimax lower bound $K \sigma^2$ applies to all estimators and the ESD
 189 actually quantifies the best possible worst-case performance of *any estimator*.

190 We emphasize that the ESD is a population-level complexity measure for signal-spectrum alignment.
 191 It is not a tuning parameter for a specific algorithm, and it does not need to be estimated. Instead,
 192 it serves as a statistical complexity measure, playing a role analogous to sparsity levels in high-
 193 dimensional regression or smoothness indices in nonparametric statistics. While these quantities
 194 are unknown to the practitioner, they characterize the information-theoretic limits of the respective
 195 learning tasks. Estimating the ESD from data is an interesting problem on its own, and we defer it to
 196 future work because it goes beyond the goals in the current paper.

197 **Comparisons to other alignment measures.** Alternative alignment measures exist. The cosine
 198 similarity-based kernel-target alignment yields generalization bounds (Cortes et al., 2012; Cristianini
 199 et al., 2001), but these bounds are typically too loose to explain fast rates in adaptive kernel methods.
 200 Recently, Barzilai & Shamir (2023) extended benign-overfitting analyses (Bartlett et al., 2020b;
 201 Tsigler & Bartlett, 2023) to kernel ridge regression, which may encounter saturation effects that
 202 prevent optimal rates for overly smooth target functions.

203 **Comparisons to other effective dimensions.** There are some well-known measures used in the
 204 classical analysis of spectral methods. We discuss the differences between ESD and these measures.

205 Zhang (2005) introduces the effective dimension to quantify the complexity of any regularized method.
 206 For ridge regularization in Equation (5), the effective dimension is defined as $d_{\text{eff}}(\nu) = \sum_j \frac{\lambda_j}{\lambda_j + \nu}$
 207 (see Proposition A.1 in Zhang (2005)). $d_{\text{eff}}(\nu)$ depends only on the spectrum $\boldsymbol{\lambda}$ and the regularization
 208 parameter ν , but not on the signal $\boldsymbol{\theta}^*$ or the noise level σ^2 . Consequently, the effective dimension is
 209 not suitable for measuring signal-spectrum alignment. Furthermore, the effective dimension, as a
 210 function of ν , does not directly connect to any minimax risk.

211 In linear regression, Bartlett et al. (2020a) analyze the minimum-norm interpolator via the effective
 212 rank $r_k = \frac{\sum_{i>k} \lambda_{\pi_i}}{\lambda_{\pi_{k+1}}}$ (using the relationship in Equation (3)). They define the splitting index

216 $k^* = \min\{k \geq 0 : \sigma^2 r_k \geq b\}$ for some constant b and establish risk bounds using $\sigma^2 k^*$. While k^*
 217 may resemble ESD since both depend on λ and σ^2 , they differ in two important aspects: (i) k^* does
 218 not involve the signal and thus cannot measure signal-spectrum alignment; and (ii) k^* is tailored to
 219 the minimum-norm estimator and does not characterize the minimax risk over a class.

220 Both $d_{\text{eff}}(\nu)$ and k^* are **signal-agnostic**: they depend on the spectrum λ (and either ν or σ^2) only,
 221 and therefore remain invariant under any change in the alignment between the signal and the kernel's
 222 eigenfunctions. For instance, if adaptive training improves alignment by reordering the eigenfunctions
 223 to better align with the signal while preserving the set of eigenvalues, then both $d_{\text{eff}}(\nu)$ and k^* are
 224 unchanged. In contrast, the ESD $d^\dagger(\sigma^2; \theta^*, \lambda)$ is signal-aware, because it is defined by the bias-
 225 variance crossing for the specific θ^* . As signal-kernel alignment improves, the ESD decreases.
 226 Consequently, the ESD can mechanistically explain the generalization benefits of adaptive kernel
 227 learning, a phenomenon that signal-agnostic complexity measures like $d_{\text{eff}}(\nu)$ and k^* cannot capture.
 228

229 **Examples.** For the following canonical settings, the optimal PC risk satisfies

$$230 \quad \mathcal{R}_*^{\text{PC}} \asymp \begin{cases} \min\left\{\sigma^{\frac{2s\beta}{1+s\beta}}, d\sigma^2\right\}, & (1) \lambda_i = i^{-\beta}, \sum_{i=1}^d \lambda_i^{-s} \theta_i^{*2} \leq R, \beta, s > 0, \\ 231 \min\left\{\sigma^{2-\frac{2}{\alpha}}, d\sigma^2\right\}, & (2) \theta_i^* = i^{-\alpha/2}, \alpha > 1, \{\lambda_i\} \downarrow, \\ 232 \min\{d\sigma^2, \log(d\sigma^2/\log(d\sigma^2))\}, & (3) d < \infty, \theta_i^* = i^{-1/2}, \{\lambda_i\} \downarrow, \\ 233 d \min\{d^{-\alpha}, \sigma^2\}, & (4) d < \infty, 0 < \alpha < 1, \theta_i^* = i^{-\alpha/2}, \{\lambda_i\} \downarrow, \end{cases} \quad (9)$$

234 where $\{\lambda_i\} \downarrow$ means λ_i is decreasing. Details and proofs are deferred to Appendix D.3.

235 In Setting (1), we may take $\sigma^2 = \sigma_0^2/n$ in view of Equation (3), and then the upper bound becomes
 236 $\sigma_0^2 \min\left(n^{-\frac{s\beta}{1+s\beta}}, d/n\right)$, which matches the well-known optimal rate under the source condition and
 237 the polynomial eigen-decay condition in the case when $d = \infty$. When $d < \infty$, there is a phase
 238 transition around $d_0 \asymp n^{\frac{1}{1+s\beta}}$: if $d \lesssim d_0$, the upper bound is $d\sigma_0^2/n$; if $d \gtrsim d_0$, the upper bound is
 239 the same as if $d = \infty$.

240 Appendix C.1 illustrates a sparse signal example where the ESD provides a quantitative comparison
 241 of two different spectra while the existing measures like $d_{\text{eff}}(\nu)$ and k^* do not. These examples
 242 suggest that the notion of ESD allows us not only to recover classical results but also to explore new
 243 settings where the classical framework is inapplicable.

244 3.2 SPAN PROFILE

245 The definition of ESD explicitly depends on the noise level σ^2 , which distinguishes it from other
 246 complexity measures in the literature. The dependence on σ^2 reflects the bias-variance trade-off
 247 nature of ESD: as σ^2 decreases, more coordinates can be unbiasedly estimated while controlling the
 248 overall variance, thereby more bias is removed. To focus on the alignment between a given signal θ^*
 249 and a spectrum λ , we examine the ESD by varying the noise level.

250 **Definition 3.4.** We define the span profile of θ^* w.r.t. the spectrum λ as $\mathbf{D}_{\theta^*, \lambda} : \tau \mapsto d^\dagger(\tau; \theta^*, \lambda)$.

251 The span profile $\mathbf{D}_{\theta^*, \lambda}$ is a well-defined object that depends only on θ^* and the ordering of λ , and it
 252 summarizes how σ^2 affects the ESD. Theorem 3.2 suggests that for two spectra $\lambda^{(1)}$ and $\lambda^{(2)}$, we
 253 can compare their alignments with the signal by the ratio of $r(\tau) = \mathbf{D}_{\theta^*, \lambda^{(1)}}(\tau)/\mathbf{D}_{\theta^*, \lambda^{(2)}}(\tau)$ for
 254 small τ , because, if this ratio is very small (and in particular if the limit is 0 for $\tau \rightarrow 0$), then a kernel
 255 method using $\lambda^{(1)}$ can achieve a smaller risk than one that uses $\lambda^{(2)}$. Such comparisons are not as
 256 convenient in classical theory. See Appendix C for more illustrations.

257 A closely related object is the *trade-off function* of θ^* relative to λ , which is defined as

$$258 \quad \mathbf{H}_{\theta^*, \lambda}(k) = \frac{1}{k} \sum_{i=k+1}^d (\theta_{\pi_i}^*)^2 = \frac{1}{k} \sum_{i: \lambda_i < \lambda_{\pi_k}} (\theta_i^*)^2, k \in [d]. \quad (10)$$

259 The quantity $\sigma^{-2} \mathbf{H}_{\theta^*, \lambda}(k)$ equals the bias-variance ratio of the PC estimator using the k leading
 260 coordinates. Properties of span profiles and trade-off functions are summarized as follows.

270 **Proposition 3.5.** (1) Both $\mathbf{D}_{\theta^*, \lambda} : \tau \mapsto [d]$ and $\mathbf{H}_{\theta^*, \lambda} : [d] \mapsto [0, \infty)$ are nonincreasing. (2) For
 271 any τ , it holds that $\mathbf{D}_{\theta^*, \lambda}(\tau) = \min\{k \in [d] : \mathbf{H}_{\theta^*, \lambda}(k) \leq \tau\}$. (3) For two spectra $\lambda^{(1)}$ and $\lambda^{(2)}$,
 272 if $\mathbf{H}_{\theta^*, \lambda^{(1)}}(k) \leq \mathbf{H}_{\theta^*, \lambda^{(2)}}(k)$ for all $k \in [d]$, then $\mathbf{D}_{\theta^*, \lambda^{(1)}}(\tau) \leq \mathbf{D}_{\theta^*, \lambda^{(2)}}(\tau)$, $\forall \tau > 0$.
 273

274 Property (3) in Proposition 3.5 suggests that the faster $\mathbf{H}_{\theta^*, \lambda}(\cdot)$ decreases, the better the spectrum λ
 275 aligns with the signal θ^* . In the extreme case where the ordering of λ_i matches the ordering of $|\theta_i^*|^2$,
 276 the decay of $\mathbf{H}_{\theta^*, \lambda}(\cdot)$ is the fastest, which leads to the most favorable span profile.
 277

278 **Extensions.** To save space, we defer the extensions to linear models and kernel regression to
 279 Appendices A and B, respectively. For the kernel regression model in Equations (1) and (2), we
 280 define the ESD of f^* w.r.t. the kernel \mathbf{k} and the effective noise variance $\sigma_{\text{eff}}^2 := (\sigma_0^2 + \|f^*\|_{\infty}^2)/n$ as
 281

$$282 d^{\dagger}(\sigma_{\text{eff}}^2; f^*, \mathbf{k}) = \min\{k \in \mathbb{N}_+ \cup \{\infty\} : \mathbf{H}_{\theta^*, \lambda}(k) \leq \sigma_{\text{eff}}^2\}.$$

284 4 MINIMAX OPTIMAL CONVERGENCE RATES

286 When using the span profile to characterize the signal-spectrum alignment, it is of interest to establish
 287 the optimal convergence rates. Since the setting where $d = d_n$ is finite and grows along with n can
 288 be studied using Theorem 3.3 for every finite n , we focus on the case where $d = \infty$ and the spectrum
 289 λ is given with ordering denoted by $\{\pi_j\}$ such that $\lambda_{\pi_1} > \lambda_{\pi_2} > \dots$. In this asymptotic analysis, n
 290 is growing and the noise variance σ^2 is set to be σ_0^2/n where σ_0^2 is fixed.
 291

292 We begin by defining a class of populations whose span profile is bounded by a sequence of quotas
 293 $\mathbf{K} = \{K_n\}_{n=1}^{\infty}$. This leads to the following class of parameters:
 294

$$\mathcal{F}_{\mathbf{K}, \lambda} := \left\{ \boldsymbol{\theta} \in \mathbb{R}^{\infty} : \mathbf{D}_{\theta, \lambda}\left(\frac{\sigma_0^2}{n}\right) \leq K_n, \quad \forall n \geq n_0 \text{ for some } n_0 \right\}. \quad (11)$$

296 For each $\boldsymbol{\theta} \in \mathcal{F}_{\mathbf{K}, \lambda}$, the sequence model in Equation (4) with $\theta^* = \boldsymbol{\theta}$ and $\sigma^2 = \sigma_0^2/n$ will have an
 297 ESD no greater than K_n . For a sample $\mathbf{Z}^{(n)}$ from this sequence model and any estimator $\hat{\boldsymbol{\theta}}$ based on
 298 $\mathbf{Z}^{(n)}$, we aim to determine the convergence rate of the following minimax risk:
 299

$$300 \inf_{\hat{\boldsymbol{\theta}}} \sup_{\boldsymbol{\theta} \in \mathcal{F}_{\mathbf{K}, \lambda}} \mathcal{R}(\hat{\boldsymbol{\theta}}, \boldsymbol{\theta}). \quad (12)$$

303 We emphasize that \mathbf{K} is a *model-class descriptor*. It is not a parameter of the distribution, but rather
 304 describes a condition on the distribution. For example, the sparsity assumption in high-dimensional
 305 regression states that $\|\beta\|_0 \leq s$, so s describes a class of distributions; yet s is not a parameter of
 306 the distribution. Our minimax result requires a regularity condition on the quota sequence \mathbf{K} . Let
 307 $\bar{K} := \sup\{K_n\} \in \mathbb{N} \cup \{\infty\}$. For any $k \in [\bar{K}]$, let $M_k := \max\{n : K_n = k\}$ (the largest n such
 308 that $K_n = k$).
 309

Condition 4.1. (1) $K_{n+1} - K_n \leq 1$ for all n sufficiently large. (2) For all $k \in [\bar{K}]$, it holds that
 310 $(k+1)/M_{k+1} \leq k/M_k$.
 311

Condition 4.1 ensures that K_n does not grow faster than n , and the ratio sequence $\{k/M_k\}$ is
 312 nonincreasing. Condition 4.1 is easily satisfied by common growth laws.
 313

Example 4.2. (1) Suppose $K_n \asymp n^a$ where $0 < a < 1$. For any k , we have $M_k \asymp k^{1/a}$. Since
 314 $k/k^{1/a}$ is decreasing, Condition 4.1 holds.
 315

(2) Suppose $K_n \asymp (\log n)^b$ where $b > 0$. For any k , we have $M_k \asymp e^{k^{1/b}}$. Since $k/e^{k^{1/b}}$ is
 316 decreasing, Condition 4.1 holds.
 317

318 The next theorem provides a lower bound on the minimax risk in Equation (12).
 319

Theorem 4.3. Suppose Condition 4.1 holds for a quota sequence $\mathbf{K} = \{K_n\}_{n=1}^{\infty}$. Let $c_0 = 1/4$. If
 320 $\mathbf{Z}^{(n)}$ is drawn from the sequence model with $\theta^* = \boldsymbol{\theta}$ and $\sigma^2 = \sigma_0^2/n$, it holds that
 321

$$322 \inf_{\hat{\boldsymbol{\theta}}} \sup_{\boldsymbol{\theta} \in \mathcal{F}_{\mathbf{K}, \lambda}} \mathcal{R}(\hat{\boldsymbol{\theta}}, \boldsymbol{\theta}) \geq c_0 \sigma_0^2 \frac{K_n}{n}.$$

Theorem 4.3 shows that given a quota sequence \mathbf{K} , no estimator can, uniformly over the class $\mathcal{F}_{\mathbf{K}, \lambda}$, achieve a faster convergence rate of risk than $\sigma_0^2 K_n/n$. On the other hand, Theorem 3.2 (using $\sigma^2 = \sigma_0^2/n$) provides a matched upper bound on the risk of the optimal PC estimator, which is $2\sigma_0^2 K_n/n$. We thus conclude that the minimax optimal rate over $\mathcal{F}_{\mathbf{K}, \lambda}$ is $\sigma_0^2 K_n/n$.

Our theory suggests that the ESD is an essential quantity, and the span profile provides a useful characterization of the attainable error rate for spectral methods. Our theory does not invoke any source condition or eigenvalue-decay condition and is more general than classical analysis:

1. The ESD framework recovers classical minimax rates. For spectra with polynomial decay $\lambda_j \asymp j^{-\gamma}$ and signals satisfying source conditions with smoothness index s , the ESD quota is $K_n \asymp n^{\frac{1}{1+s\gamma}}$. Consequently, our rate $\sigma_0^2 K_n/n$ recovers the standard optimal rate $n^{-\frac{s\gamma}{1+s\gamma}}$ (see Example D.3 for the full derivation).
2. The ESD framework can provide sharp rates for irregular classes where standard theory is silent. The next example presents a case where the minimax convergence rate is faster than the standard rate in classical analysis based on source conditions.

Example 4.4. Let $b \geq 1$ be a constant and $K_n = \lceil (\log n)^{1/b} \rceil$ for $n \in \mathbb{N}_+$. Suppose $\{\lambda_j\}_{j=1}^\infty$ is decreasing and $\theta_{j+1}^* = \sqrt{\sigma_0^2 [je^{-jb} - (j+1)e^{-(j+1)b}]}$ for $j \geq 1$ and $\theta_1^* = 0$. Then, $\theta^* \in \mathcal{F}_{\mathbf{K}, \lambda}$ and the optimal rate is $\sigma_0^2 (\log n)^{1/b} n^{-1}$. In contrast, the traditional convergence rate based on the source condition is $\sigma_0^2 n^{-\alpha/(1+\alpha)}$ for arbitrary $\alpha > 0$, which is not sharp.

4.1 TRACKING DYNAMIC ALIGNMENT

The key advantage of the ESD framework over classical theories is its utility in analyzing adaptive learning, where the main difficulty is that the signal-kernel alignment changes during training.

As discussed in Section 2, the polynomial eigenvalue decay condition ($\lambda_j \asymp j^{-\gamma}$) fails to hold and the Hölder source condition $\sum_j \langle f^*, \psi_j \rangle^2 / \lambda_j^s \leq R_s$ is ill-defined in adaptive learning. In adaptive learning, the learned kernel's eigenvalues and eigenfunctions evolve, making it analytically intractable to track the smoothness index s and radius R_s along the training trajectory.

In contrast, ESD is valid for evolving eigenfunctions. For any time-dependent kernel path $(\mathbf{k}_t)_{t \geq 0}$, the quantity $d^\dagger(\sigma_{\text{eff}}^2; f^*, \mathbf{k}_t)$ remains a well-defined population measure of complexity at each training time t , even when both eigenvalues and eigenfunctions evolve. This allows us to mathematically track the improvement in kernel-signal alignment during training, a dynamic that classical notions cannot easily describe. This *pathwise ESD* framework is further discussed in Appendix C.2.

Using the pathwise ESD, we can provide a mechanistic explanation for the generalization benefits of feature learning. An adaptive learning algorithm aligns the kernel's leading eigenfunctions with the signal, so that a signal that is poorly aligned with a large ESD at initialization may become well-aligned with a small ESD after training. By reducing the ESD, the algorithm actively moves the problem from a model class with high minimax risk to one with low minimax risk.

The above mechanistic explanation is supported by our minimax theorems (Theorem 3.3 and Theorem B.6). We rigorously establish the ESD reduction in Theorem 5.2 for the adaptive sequence model studied by Li & Lin (2024), where we prove the ESD is guaranteed to decrease over time. This result is obtained in a stylized model and should be viewed as a tractable case study of dynamic signal-kernel alignment. We expect similar ESD reduction to appear for other adaptive algorithms, including finite-width neural networks trained with stochastic gradient descent, but the dynamics of learned kernels in those settings are often analytically intractable and establishing such guarantees remains an open problem. Nonetheless, we provide empirical validation using a four-layer deep linear network in Appendix C.2, which demonstrates that ESD tracks the decay of prediction risk even when eigenfunctions evolve.

5 ADAPTIVE EIGENVALUES VIA OVER-PARAMETERIZED GRADIENT FLOW

This section will investigate the benefits of learning eigenvalues via over-parameterized gradient flow (OP-GF) in sequence models (Li & Lin, 2024) through the lens of ESDs.

378 Inspired by the over-parameterized nature of deep neural networks, Li & Lin (2024) parameterized
 379 $\theta_j = a_j b_{j,1} \cdots b_{j,D} \beta_j$, where D stands for the number of layers and $(a_j, b_{j,i}, \beta_j)$ are parameters to
 380 be learned. The gradient flow w.r.t. the empirical loss $L = \frac{1}{2} \sum_j (\theta_j - y_j)^2$ is given by
 381

$$\begin{aligned} 382 \dot{a}_j &= -\nabla_{a_j} L, \quad \dot{b}_{j,i} = -\nabla_{b_{j,i}} L \quad (i \in [D]), \quad \dot{\beta}_j = -\nabla_{\beta_j} L, \\ 383 a_j(0) &= \lambda_j^{1/2}, \quad b_{j,i}(0) = b_0 > 0, \quad (i \in [D]), \quad \beta_j(0) = 0, \quad j \in [d], \end{aligned} \quad (13)$$

385 where λ_j 's are the initial eigenvalues and b_0 is the common initialization of all $b_{j,i}$. At time t , the
 386 learned eigenvalues are given by $\tilde{\lambda}_j(t) = (a_j(t)b_{j,1}(t) \cdots b_{j,D}(t))^2$ and the OP-GF estimates are
 387 $\hat{\theta}_j^{OP}(t) = \tilde{\lambda}_j^{1/2}(t)\beta_j(t)$ for $j \in [d]$. Li & Lin (2024) consider infinite-dimensional sequence models
 388 with a polynomial decay condition on the initial eigenvalues and establish upper bounds on the risk
 389 of the OP-GF estimator with proper early stopping.
 390

391 Here we study the dynamics of eigenvalues in OP-GF and how it changes the ESD. At time t , the
 392 learned eigenvalues are $\tilde{\lambda}(t) := (\tilde{\lambda}_j(t))_{j \in [d]}$, and the ESD is $d^\dagger(t) = d^\dagger(\sigma^2; \theta^*, \tilde{\lambda}(t))$. We aim to
 393 show that under some regularity conditions, OP-GF can adjust the ordering of eigenvalues $\tilde{\lambda}(t)$ to
 394 reduce the ESD $d^\dagger(t)$, which leads to a better signal-spectrum alignment.

395 We begin with some notations for the sequence model in Equation (4). Following the asymptotic
 396 framework in Section 4, we set $\sigma^2 = \frac{\sigma_0^2}{n}$ and $\sigma_0 = 1$ without loss of generality. Denote $\tilde{d} = \sum_{i=1}^d \lambda_i$
 397 (i.e., sum of initial eigenvalues). Let $\pi_t^{-1}(i)$ denote the rank of $\tilde{\lambda}_i(t)$ at time t .

398 **Assumption 5.1.** We assume (1) Each noise ξ_j in Equation (4) is sub-Gaussian with variance proxy
 399 bounded by $C_{proxy}\sigma^2$. (2) Let $\varepsilon = 2C_{proxy}^{-1/2}n^{-1/2}\sqrt{\ln n \tilde{d} \cdot \ln n}$ and $\varepsilon' = 2C_{proxy}^{-1/2}n^{-1/2}\sqrt{\ln n}$.
 400 Define $S := \{j \in [d] : |\theta_j^*| > \varepsilon\}$. We have $|S| \leq n$. (3) $\inf_{j \in S} \lambda_j > n^{-\delta}$ for some $\delta \in (0, 1)$.

401 **Theorem 5.2.** Suppose that Assumption 5.1 holds and the initialization in Equation (13) is $b_0 =$
 402 $c_B D^{\frac{D+1}{D+2}} \varepsilon^{\frac{1}{D+2}}$. Define $t_2 = C \cdot D^{\frac{D}{D+2}}(\varepsilon)^{-\frac{2D+2}{D+2}}$. There exist some constants $c, C, C_M, C_{max}, C_\eta$,
 403 c_η, c_B , and c' , such that with probability larger than $1 - 4/n$, we have

$$404 d^\dagger(t_2) \leq d^\dagger(t_1)$$

405 for any $t_1 \in [0, t_2]$ if the followings hold:

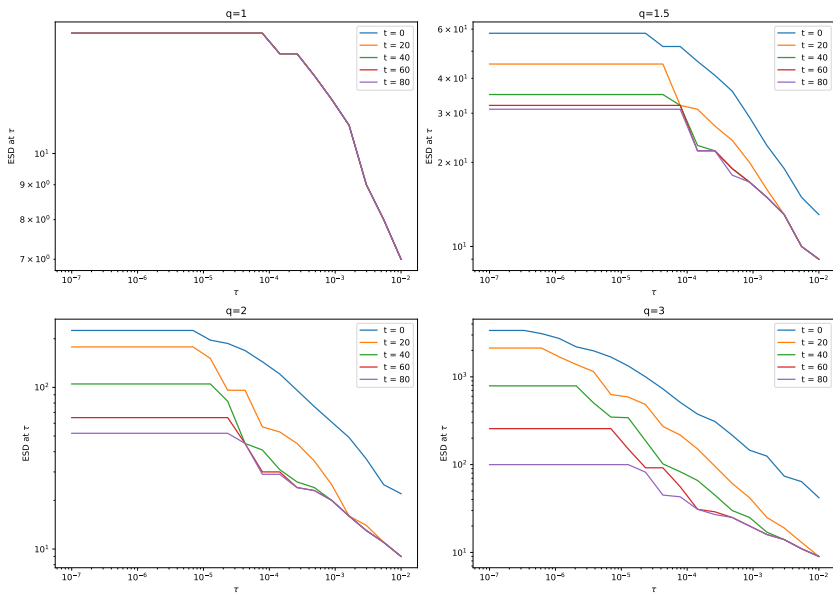
- 406 1. For any $j \in S$, we have $M \leq |\theta_j^*|$, where $M := C_M \varepsilon$;
- 407 2. For any $j \in S^c$, we have $|\theta_j^*| \leq \tilde{\sigma}$, where $\tilde{\sigma} = c' \varepsilon$.
- 408 3. For any $i, j \in S$, let $\eta_{i,j} := |\theta_i^*| - |\theta_j^*|$. At least one of the followings hold: (a) $\eta_{i,j} \leq 0$, (b)
 409 $\eta_{i,j} \geq C_\eta \varepsilon$ and $|\theta_i^*| \leq C_{max} M$, or (c) $\frac{|\theta_i^*|}{|\theta_j^*|} > (1 + \frac{c_\eta}{D})$.
- 410 4. At time t_1 , define two subsets of S^c : $A_1 := \{i \in S^c : \pi_{t_1}^{-1}(i) < d^\dagger(t_1), \lambda_i < c \cdot D^{-\frac{D}{D+2}} \cdot$
 411 $M^{\frac{2}{D+2}}\}$ and $B_1 := \{i \in S^c : \pi_{t_1}^{-1}(i) > d^\dagger(t_1)\}$, and define a subset of S : $B_2 := \{i \in S : \pi_{t_1}^{-1}(i) > d^\dagger(t_1)\}$. It holds that $|B_2| + \min[|A_1| - |B_2|]_+, |B_1| \leq |B_2|(C_M/c')^2$.

412 Theorem 5.2 shows that OP-GF reduces the ESD. The proof is highly technical, but the underlying
 413 idea is simple: the gradient flow dynamics increase the eigenvalues much more rapidly along
 414 directions where the signal energy $|\theta_j^*|^2$ is large and slower along directions where the signal is small.
 415 This dynamics explicitly reorders the spectrum to match the signal structure.

416 Li & Lin (2024) have analyzed the risk of the OP-GF algorithm, showing that the generalization is
 417 improved during training, but they did not provide a complexity measure to explain why the risk
 418 improves. Our work fills this gap by using ESD as the explanatory variable to show that the risk
 419 improvement results from the reduction of ESD. Initially, the learning problem lies in a model class
 420 with a large quota $K_{t_1} = d^\dagger(t_1)$ and as the ESD reduces, the problem lies in a model class with a
 421 smaller quota $K_{t_2} = d^\dagger(t_2)$. Since the minimax risk scales as $O(\sigma^2 K)$, the ESD reduction suggests
 422 that the learning problem has been moved from a harder class to an easier class. This explains the
 423 potential for generalization improves over time.

432 6 NUMERICAL EXPERIMENTS

434 **Data Generation.** We utilize the **misalignment** setting in Li & Lin (2024) to specify a d -dimensional
 435 sequence model. We fixed the eigen-decay rate $\gamma > 0$, the signal decay rate $p > 0$, and the number of
 436 nonzero signals J . Given any misalignment parameter $q \geq 1$, we set eigenvalues as $\lambda_j = j^{-\gamma}$, $j \in [d]$,
 437 and set the true nonzero parameters as $\theta_{\ell(j)}^* = C \cdot j^{-\frac{p+1}{2}}$, where $\ell(j) = [j^q]$ and $j \leq J$. Here all other
 438 elements of θ^* are zero and $d \geq J^q$ so $\|\theta^*\|_0 = J$. The observations are sampled as $y_i \sim N(\theta_i^*, \sigma^2)$.
 439 This setting provides a flexible way to control the alignment between the signal structure and the
 440 spectrum. When $q = 1$, the ordering of θ^* align perfectly with the ordering of λ . As q increases,
 441 more nonzero elements of θ^* are located on the tail where the eigenvalues are smaller, and more
 442 large eigenvalues are associated with zero signals, creating a worse signal-spectrum alignment.
 443



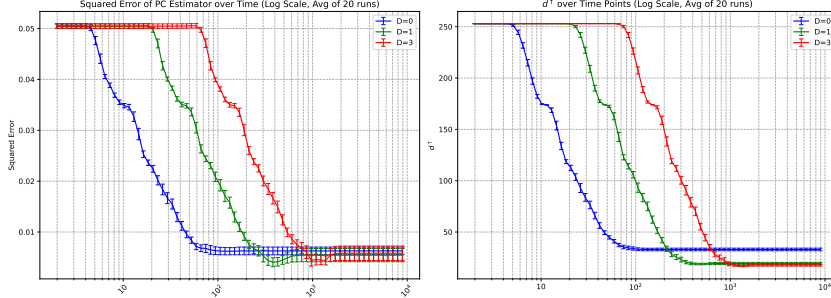
463 Figure 1: Evolution of span profiles during the training of an over-parameterized gradient flow. The misalignment
 464 level q varies from 1 to 3. Fixed parameters are $n = 10000$, $\sigma_0 = 1$, $d = 5000$, $J = 15$, $p = 2.5$, and $\gamma = 1$.
 465

466 **Evolution of Span Profile** The first experiment visualizes the span profile of the signal w.r.t.
 467 the learned spectrum at various stages in the OP-GF process with $D = 0$. Given a sample, we
 468 approximate the gradient flow in Equation (13) by discrete-time gradient descent and obtain the
 469 solution $\{(a_j(t), \beta_j(t))_{t \geq 0} : j \in [d]\}$. The trained eigenvalue sequence $\tilde{\lambda}(t)$ at time t is given by
 470 $\tilde{\lambda}_j(t) = a_j^2(t)$ for $j \in [d]$. Here we focus on time points before the optimal stopping time. Figure 1
 471 illustrates the evolution of the span profile w.r.t. the learned spectrum for different training times t
 472 and various values of q .
 473

474 When $q = 1$ (Top-Left panel), the span profiles at different training times t are nearly identical.
 475 This is because the initial spectrum already aligns perfectly with the signal and there is no room for
 476 improvement. For $q > 1$ (Top-Right, Bottom-Left, Bottom-Right panels), we observe that as the
 477 training time t increases 0 to 80, the span profile shifts downwards. This suggests that the training
 478 process refines the alignment between the spectrum and the signal. In addition, the reduction in the
 479 span profile is more significant for $q = 3$ compared to $q = 1.5$, because $q = 3$ corresponds to a
 480 greater initial misalignment between the signal and the spectrum, rendering the improvement from
 481 OP-GF more substantial.
 482

483 **Evolution of ESD and Estimation Error of PC Estimators** We next empirically investigate the
 484 evolution of the ESD d^\dagger and the estimation error as well as the impact of layers D . At any time
 485 t , we compute the ESD $d^\dagger(t)$ based on the learned eigenvalue sequence $\tilde{\lambda}(t)$ $\tilde{\lambda}(t)$ and also the PC
 486 estimate $\tilde{\theta}(t)$ based on $\tilde{\lambda}(t)$, with number of components determined by $d^\dagger(t)$. Theorems 3.2 and 3.3

486 suggest that the PC estimator tuned by the ESD can achieve the minimax risk rate, so we expect $\hat{\theta}(t)$
 487 to perform well.
 488



500 Figure 2: Averaged squared error of the tuned PC estimator and ESD as a function of the training time. Each
 501 average is computed based on 20 replications and each error bar represents a standard deviation.
 502

503 The empirical evaluation involved 20 Monte Carlo repetitions. Figure 2 displays the averaged $d^\dagger(t)$
 504 and the averaged estimation error of $\hat{\theta}(t)$ in Figure 2 as a function of training time t . We observe
 505 that both the ESD and the squared error of the tune PC estimator exhibit a general decay trend
 506 over training time t . Furthermore, for the shallow model with $D = 0$ (with no $b_{i,j}$ parameters),
 507 the initial decrease in ESD and MSE occurs earlier compared to the deeper models with $D = 1$ or
 508 $D = 3$. However, with sufficient training iterations, the deeper models with $D = 1$ or $D = 3$ can
 509 achieve lower ESD values than the shallow model with $D = 0$. These findings suggest that increased
 510 model depth ($D > 0$) may facilitate a better adaptation of the spectrum, and thus lead to lower
 511 estimation error. This observation offers a perspective on the benefits of depth in spectral learning,
 512 but a comprehensive study for general models is left for future research.
 513

514 7 DISCUSSION

515 This paper introduces the effective span dimension (ESD) and span profile to analyze the interplay
 516 between the signal structure and the kernel spectrum. Our framework moves beyond classical static
 517 assumptions relative to a fixed kernel (e.g., source conditions and polynomial eigenvalue decay)
 518 and offers a dynamic, noise-dependent perspective on signal complexity. Unlike traditional source
 519 conditions, the ESD is more flexible and remains applicable when the spectrum itself is learned from
 520 data.
 521

522 **Quantifying adaptivity.** Like the sparsity level in high-dimensional statistics, the ESD is a population
 523 quantity for theoretical analyses rather than an input to training. It serves as a quantitative target
 524 for adaptive algorithms on the population level: by comparing the ESD of a particular signal w.r.t.
 525 different kernels, we can determine which kernel permits better generalization for this signal.
 526

527 **Connecting adaptivity and generalization.** Our framework clarifies why adaptive learning methods
 528 often outperform classical fixed-kernel approaches. As detailed in Section 4.1, a fixed kernel $\lambda^{(0)}$
 529 forces the signal into a class $\mathcal{F}_{\mathbf{K}^{(0)}}$ characterized by high minimax risk. By contrast, successful
 530 adaptation modifies the kernel to reduce the span profile $D_{\theta^*, \lambda^{(a)}}$ of the same signal w.r.t. the adapted
 531 kernel spectrum $\lambda^{(a)}$. This adaptation places the signal into a class $\mathcal{F}_{\mathbf{K}^{(a)}}$ with a smaller quota $\mathbf{K}^{(a)}$,
 532 which implies lower minimax risk.
 533

534 **Analysis of ESD dynamics.** The theoretical analysis of ESD dynamics in Theorem 5.2 utilizes a
 535 tractable proxy model to rigorously study the OP-GF. This provides a mechanistic prototype where
 536 feature learning is formalized as ESD reduction. In numerical studies, the ESD dynamics can be
 537 empirically measured in various learning settings. However, establishing rigorous theoretical results
 538 for specific adaptive algorithms remains an important open problem.
 539

In summary, the ESD framework provides a novel view of generalization that connects classical kernel
 methods with modern adaptive learning. We expect to relate this framework to learned representations
 in neural networks to explain their superior generalization performance.

540 REPRODUCIBILITY STATEMENT
541542 There is no new datasets used. We will release anonymized source code in the supplementary material,
543 which enables reproduction of all experiments.
544545 LARGE LANGUAGE MODELS STATEMENT
546548 Large language models were used to improve the clarity of the manuscript and to facilitate experi-
549
550
551551 REFERENCES
552553 Anish Agarwal, Devavrat Shah, Dennis Shen, and Dogwoon Song. On robustness of principal
554 component regression. *Advances in Neural Information Processing Systems*, 32, 2019.555 Zeyuan Allen-Zhu, Yuanzhi Li, and Zhao Song. A convergence theory for deep learning via over-
556 parameterization. In *International conference on machine learning*, pp. 242–252. PMLR, 2019.558 Sanjeev Arora, Simon Du, Wei Hu, Zhiyuan Li, and Ruosong Wang. Fine-grained analysis of
559 optimization and generalization for overparameterized two-layer neural networks. In *International
560 Conference on Machine Learning*, pp. 322–332. PMLR, 2019.561 Jimmy Ba, Murat A. Erdogdu, Taiji Suzuki, Zhichao Wang, Denny Wu, and Greg Yang. High-
562 dimensional asymptotics of feature learning: How one gradient step improves the representation,
563 May 2022.564 Peter L. Bartlett, Philip M. Long, Gábor Lugosi, and Alexander Tsigler. Benign overfitting in linear
565 regression. *Proceedings of the National Academy of Sciences*, 117(48):30063–30070, December
566 2020a. ISSN 0027-8424, 1091-6490. doi: 10.1073/pnas.1907378117.568 Peter L Bartlett, Philip M Long, Gábor Lugosi, and Alexander Tsigler. Benign overfitting in linear
569 regression. *Proceedings of the National Academy of Sciences*, 117(48):30063–30070, 2020b.571 Daniel Barzilai and Ohad Shamir. Generalization in kernel regression under realistic assumptions.
572 *arXiv preprint arXiv:2312.15995*, 2023.573 Frank Bauer, Sergei Pereverzev, and Lorenzo Rosasco. On regularization algorithms in learning
574 theory. *Journal of complexity*, 23(1):52–72, 2007. doi: 10.1016/j.jco.2006.07.001.576 Xin Bing, Florentina Bunea, Seth Strimas-Mackey, and Marten Wegkamp. Prediction under latent
577 factor regression: Adaptive pcr, interpolating predictors and beyond. *Journal of Machine Learning
578 Research*, 22(177):1–50, 2021.580 Blake Bordelon, Alexander Atanasov, and Cengiz Pehlevan. How feature learning can improve neural
581 scaling laws. In *The Thirteenth International Conference on Learning Representations*, 2025. URL
582 <https://openreview.net/forum?id=dEypApI1MZ>.583 Lawrence D. Brown, T. Tony Cai, Mark G. Low, and Cun-Hui Zhang. Asymptotic equivalence theory
584 for nonparametric regression with random design. *The Annals of Statistics*, 30(3):688–707, 2002.
585 ISSN 0090-5364. doi: 10.1214/aos/1028674838.586 Andrea Caponnetto and Ernesto De Vito. Optimal rates for the regularized least-squares al-
587 gorithm. *Foundations of Computational Mathematics*, 7(3):331–368, 2007. doi: 10.1007/
588 s10208-006-0196-8.590 Andrea Caponnetto and Ernesto De Vito. Optimal rates for the regularized least-squares algorithm.
591 *Foundations of Computational Mathematics*, 7(3):331–368, 2007.593 Corinna Cortes, Mehryar Mohri, and Afshin Rostamizadeh. Algorithms for learning kernels based on
594 centered alignment. *The Journal of Machine Learning Research*, 13(1):795–828, 2012.

594 Nello Cristianini, John Shawe-Taylor, Andre Elisseeff, and Jaz Kandola. On kernel-target alignment.
 595 *Advances in neural information processing systems*, 14, 2001.
 596

597 Heinz Werner Engl, Martin Hanke, and A Neubauer. *Regularization of Inverse Problems*, volume
 598 375. Springer Science & Business Media, 1996.

599 Khashayar Gatmiry, Stefanie Jegelka, and Jonathan Kelner. Optimization and Adaptive Generalization
 600 of Three layer Neural Networks. In *International Conference on Learning Representations*, October
 601 2021. URL <https://openreview.net/forum?id=dPyRNUlttBv>.

602 Daniel Gedon, Antônio H Ribeiro, and Thomas B Schön. No double descent in principal component
 603 regression: A high-dimensional analysis. In *Forty-first International Conference on Machine
 604 Learning*, 2024.

605 L. Lo Gerfo, Lorenzo Rosasco, Francesca Odone, E. De Vito, and Alessandro Verri. Spectral
 606 algorithms for supervised learning. *Neural Computation*, 20(7):1873–1897, 2008.

607 Behrooz Ghorbani, Song Mei, Theodor Misiakiewicz, and Andrea Montanari. When do neural
 608 networks outperform kernel methods? *Advances in Neural Information Processing Systems*, 33:
 609 14820–14830, 2020.

610 Alden Green and Elad Romanov. The high-dimensional asymptotics of principal component regres-
 611 sion. *arXiv preprint arXiv:2405.11676*, 2024.

612 Ningyuan Teresa Huang, David W Hogg, and Soledad Villar. Dimensionality reduction, regularization,
 613 and generalization in overparameterized regressions. *SIAM Journal on Mathematics of Data
 614 Science*, 4(1):126–152, 2022.

615 Laura Hucke and Martin Wahl. A note on the prediction error of principal component regression in
 616 high dimensions. *Theory of Probability and Mathematical Statistics*, 109:37–53, 2023.

617 Arthur Jacot, Franck Gabriel, and Clement Hongler. Neural tangent kernel: Convergence and general-
 618 ization in neural networks. In S. Bengio, H. Wallach, H. Larochelle, K. Grauman, N. Cesa-Bianchi,
 619 and R. Garnett (eds.), *Advances in Neural Information Processing Systems*, volume 31. Curran As-
 620 sociates, Inc., 2018. URL <https://proceedings.neurips.cc/paper/2018/file/5a4be1fa34e62bb8a6ec6b91d2462f5a-Paper.pdf>.

621 Iain M. Johnstone. Gaussian estimation: Sequence and wavelet models. 2017.

622 Stefani Karp, Ezra Winston, Yuanzhi Li, and Aarti Singh. Local signal adaptivity: Provable feature
 623 learning in neural networks beyond kernels. *Advances in Neural Information Processing Systems*,
 624 34:24883–24897, 2021.

625 Simon Kornblith, Mohammad Norouzi, Honglak Lee, and Geoffrey Hinton. Similarity of neural
 626 network representations revisited. In *International conference on machine learning*, pp. 3519–3529.
 627 PMLR, 2019.

628 Daniel Kunin, Allan Raventós, Clémentine Dominé, Feng Chen, David Klindt, Andrew Saxe, and
 629 Surya Ganguli. Get rich quick: exact solutions reveal how unbalanced initializations promote rapid
 630 feature learning. *Advances in Neural Information Processing Systems*, 37:81157–81203, 2024.

631 Yicheng Li and Qian Lin. Improving adaptivity via over-parameterization in sequence models. In
 632 *The Thirty-eighth Annual Conference on Neural Information Processing Systems*, 2024. URL
 633 <https://openreview.net/forum?id=UfLH4T676K>.

634 Yicheng Li and Qian Lin. Diagonal over-parameterization in reproducing kernel hilbert spaces as an
 635 adaptive feature model: Generalization and adaptivity. *arXiv preprint arXiv:2501.08679*, 2025.

636 Yicheng Li, Weiye Gan, Zuoqiang Shi, and Qian Lin. Generalization error curves for analytic spectral
 637 algorithms under power-law decay. *arXiv preprint arXiv:2401.01599*, 2024.

638 Yuhan Helena Liu, Aristide Baratin, Jonathan Cornford, Stefan Mihalas, Eric Todd SheaBrown, and
 639 Guillaume Lajoie. How connectivity structure shapes rich and lazy learning in neural circuits. In
 640 *The Twelfth International Conference on Learning Representations*, 2024.

648 Peter Mathé and Sergei V Pereverzev. Geometry of linear ill-posed problems in variable hilbert scales.
 649 *Inverse problems*, 19(3):789, 2003.
 650

651 Adityanarayanan Radhakrishnan, Daniel Beaglehole, Parthe Pandit, and Mikhail Belkin. Mechanism
 652 for feature learning in neural networks and backpropagation-free machine learning models. *Science*,
 653 383(6690):1461–1467, 2024.

654 Lorenzo Rosasco, Ernesto De Vito, and Alessandro Verri. Spectral methods for regularization in
 655 learning theory. *DISI, Università degli Studi di Genova, Italy, Technical Report DISI-TR-05-18*,
 656 2005.

657 Bernhard Schölkopf and Alexander J. Smola. *Learning with Kernels: Support Vector Machines,
 658 Regularization, Optimization, and Beyond*. MIT Press, 2002.

659 Maria Seleznova and Gitta Kutyniok. Analyzing finite neural networks: Can we trust neural tangent
 660 kernel theory? In *Mathematical and Scientific Machine Learning*, pp. 868–895. PMLR, 2022.
 661 URL <https://proceedings.mlr.press/v145/seleznova22a.html>.

662 Zhenmei Shi, Junyi Wei, and Yingyu Liang. Provable guarantees for neural networks via gradient
 663 feature learning. *Advances in Neural Information Processing Systems*, 36:55848–55918, 2023.

664 Ingo Steinwart and Andreas Christmann. *Support vector machines*. Springer Science & Business
 665 Media, 2008.

666 Ingo Steinwart and C. Scovel. Mercer’s Theorem on General Domains: On the Interaction between
 667 Measures, Kernels, and RKHSs. 2012. doi: 10.1007/S00365-012-9153-3.

668 Alexander Tsigler and Peter L Bartlett. Benign overfitting in ridge regression. *Journal of Machine
 669 Learning Research*, 24(123):1–76, 2023.

670 Grace Wahba. *Spline Models for Observational Data*, volume 59 of *CBMS-NSF Regional Conference
 671 Series in Applied Mathematics*. SIAM, 1990.

672 Chao Wang, Xin He, Yuwen Wang, and Junhui Wang. On the target-kernel alignment: a unified
 673 analysis with kernel complexity. *Advances in Neural Information Processing Systems*, 37:40434–
 674 40485, 2024.

675 Jonathan Wenger, Felix Dangel, and Agustinus Kristiadi. On the disconnect between theory and
 676 practice of overparametrized neural networks, September 2023. URL <http://arxiv.org/abs/2310.00137>.

677 Blake Woodworth, Suriya Gunasekar, Jason D. Lee, Edward Moroshko, Pedro Savarese, Itay Golan,
 678 Daniel Soudry, and Nathan Srebro. Kernel and rich regimes in overparametrized models. In
 679 *Proceedings of Thirty Third Conference on Learning Theory*, pp. 3635–3673. PMLR, July 2020.
 680 URL <https://proceedings.mlr.press/v125/woodworth20a.html>.

681 Denny Wu and Ji Xu. On the optimal weighted ℓ_2 regularization in overparameterized linear
 682 regression. *Advances in Neural Information Processing Systems*, 33:10112–10123, 2020.

683 Ji Xu and Daniel J Hsu. On the number of variables to use in principal component regression.
 684 *Advances in neural information processing systems*, 32, 2019.

685 Yizhou Xu and Liu Ziyin. Three mechanisms of feature learning in a linear network. In *The Thirteenth
 686 International Conference on Learning Representations*, 2025.

687 Yuan Yao, Lorenzo Rosasco, and Andrea Caponnetto. On early stopping in gradient descent learning.
 688 *Constructive Approximation*, 26:289–315, August 2007. doi: 10.1007/s00365-006-0663-2.

689 Bin Yu. Assouad, fano, and le cam. In *Festschrift for Lucien Le Cam: research papers in probability
 690 and statistics*, pp. 423–435. Springer, 1997.

691 Haobo Zhang, Yicheng Li, and Qian Lin. On the optimality of misspecified spectral algorithms,
 692 March 2023.

702 Haobo Zhang, Jianfa Lai, Yicheng Li, Qian Lin, and Jun S Liu. Towards a statistical understanding
 703 of neural networks: Beyond the neural tangent kernel theories. *arXiv preprint arXiv:2412.18756*,
 704 2024.

705 Tong Zhang. Learning bounds for kernel regression using effective data dimensionality. *Neural*
 706 *Computation*, 17(9):2077–2098, 2005. doi: 10.1162/0899766054323008.

709 A EXTENSION TO CORRELATED NOISE AND FIXED-DESIGN LINEAR MODEL

712 This section extends the concepts of ESD and span profile, developed in Section 3 for the sequence
 713 model, to the setting of fixed-design linear regression. In addition, we demonstrate how the minimax
 714 optimal prediction risk in this setting can be characterized using the span profile, paralleling the
 715 analysis in Section 4.

716 A.1 STRATEGY OF REDUCTION

718 Before introducing the linear model, it is helpful to outline our general transformation strategy in the
 719 context of a sequence model with correlated noise. Suppose $d \in \mathbb{N}_+$ and the observations are

$$721 \mathbf{Z} = \boldsymbol{\theta}^* + \boldsymbol{\xi}, \quad \boldsymbol{\xi} \sim \mathcal{N}_d(0, \sigma^2 \boldsymbol{\Sigma}_\xi) \quad (14)$$

722 where $\boldsymbol{\Sigma}_\xi \in \mathbb{R}^{d \times d}$ is known, symmetric, and positive definite. For a correlated sequence model, it is
 723 usually of interest to measure the estimation error using the squared Mahalanobis distance defined as
 724 $L(\boldsymbol{\theta}^*, \widehat{\boldsymbol{\theta}}^*) = (\widehat{\boldsymbol{\theta}}^* - \boldsymbol{\theta}^*)^\top \boldsymbol{\Sigma}_\xi^{-1} (\widehat{\boldsymbol{\theta}}^* - \boldsymbol{\theta}^*)$.
 725

726 Let $\mathbf{L} = \boldsymbol{\Sigma}_\xi^{-1/2}$ be a symmetric square root of $\boldsymbol{\Sigma}_\xi^{-1}$. Define the whitened observation and transformed
 727 parameters as

$$728 \tilde{\mathbf{Z}} = \mathbf{L}\mathbf{Z}, \quad \tilde{\boldsymbol{\theta}}^* = \mathbf{L}\boldsymbol{\theta}^*.$$

730 It follows that $\tilde{\mathbf{Z}} = \tilde{\boldsymbol{\theta}}^* + \tilde{\boldsymbol{\xi}}$, where $\tilde{\boldsymbol{\xi}} = \mathbf{L}\boldsymbol{\xi} \sim \mathcal{N}_d(0, \sigma^2 \mathbf{I}_d)$. Accordingly, any estimator $\widehat{\boldsymbol{\theta}}$ for $\boldsymbol{\theta}^*$ is
 731 equivalent to the estimator $\widehat{\boldsymbol{\theta}} := \mathbf{L}\widehat{\boldsymbol{\theta}}^*$ for $\boldsymbol{\theta}^*$, whose squared loss is $\|\widehat{\boldsymbol{\theta}} - \boldsymbol{\theta}^*\|^2 = (\widehat{\boldsymbol{\theta}}^* - \boldsymbol{\theta}^*)^\top \boldsymbol{\Sigma}_\xi^{-1} (\widehat{\boldsymbol{\theta}}^* - \boldsymbol{\theta}^*) = L(\boldsymbol{\theta}^*, \widehat{\boldsymbol{\theta}}^*)$.
 732

734 Therefore, the transformed model is equivalent to the standard sequence model with uncorrelated
 735 noise in Equation (4) and the estimation is equivalent to the estimation therein. Consequently, the
 736 ESD and span profile for the model in Equation (14) can be naturally defined using the original
 737 definitions for the transformed model. Specifically, for the correlated-noise model, we define the
 738 ESD w.r.t. $\boldsymbol{\Sigma}_\xi$ as

$$739 d_{\boldsymbol{\Sigma}_\xi}^\dagger(\tau; \boldsymbol{\theta}^*) := d^\dagger\left(\tau; \tilde{\boldsymbol{\theta}}^* = \mathbf{L}\boldsymbol{\theta}^*\right).$$

741 Note that for the risk $\mathbb{E}L(\boldsymbol{\theta}^*, \widehat{\boldsymbol{\theta}}^*)$, our minimax risk characterization still applies, i.e., the minimax
 742 risk scales as $K\sigma^2$ across all distributions whose ESD $d_{\boldsymbol{\Sigma}_\xi}^\dagger(\sigma^2; \boldsymbol{\theta}^*)$ is bounded by K .
 743

744 The relationship between Euclidean distance and Mahalanobis distance satisfies that

$$745 \lambda_{\min}(\boldsymbol{\Sigma}_\xi) L(\boldsymbol{\theta}^*, \widehat{\boldsymbol{\theta}}^*) \leq \|\boldsymbol{\theta}^* - \widehat{\boldsymbol{\theta}}^*\|^2 \leq \lambda_{\max}(\boldsymbol{\Sigma}_\xi) L(\boldsymbol{\theta}^*, \widehat{\boldsymbol{\theta}}^*),$$

747 so the minimax risk in terms of $\mathbb{E}\|\boldsymbol{\theta}^* - \widehat{\boldsymbol{\theta}}^*\|^2$ can still be characterized sharply when the condition
 748 number of $\boldsymbol{\Sigma}_\xi$ is bounded.

749 This strategy of reducing a complex model to a simple model will be used in our analysis of the linear
 750 model and in RKHS regression in Appendix B.
 751

752 A.2 LINEAR MODEL

754 Consider the following fixed-design linear regression model:

$$755 \mathbf{Y} = \mathbf{X}\boldsymbol{\beta}^* + \boldsymbol{\epsilon}, \quad (15)$$

756 where $\mathbf{Y} \in \mathbb{R}^n$ is the vector of observations, $\mathbf{X} \in \mathbb{R}^{n \times p}$ is the fixed-design matrix of rank $r \leq$
757 $\min(n, p)$, $\beta^* \in \mathbb{R}^p$ is the unknown vector of true coefficients, and $\epsilon \in \mathbb{R}^n$ is the noise vector. We
758 assume the components of ϵ are uncorrelated with mean zero and variance σ_0^2 . For this model, we
759 consider the loss (in-sample prediction error) $\mathcal{L}(\hat{\beta}; \beta^*) = \frac{1}{n} \|\mathbf{X}(\hat{\beta} - \beta^*)\|^2$ and risk $\mathcal{R}(\hat{\beta}; \beta^*) =$
760 $\mathbb{E}\mathcal{L}(\hat{\beta}; \beta^*)$. For random design linear regression, we treat it as a special case of RKHS regression
761 and discuss it in Appendix B.

763 To connect this model to the sequence model analysis presented earlier, we utilize the Singular Value
764 Decomposition (SVD) of the design matrix \mathbf{X} as follows:

$$765 \quad 766 \quad 767 \quad \frac{1}{\sqrt{n}} \mathbf{X} = \mathbf{U} \mathbf{S} \mathbf{V}^\top, \quad (16)$$

768 where $\mathbf{U} \in \mathbb{R}^{n \times n}$ and $\mathbf{V} \in \mathbb{R}^{p \times p}$ are orthogonal matrices, and $\mathbf{S} \in \mathbb{R}^{n \times p}$ is a rectangular diagonal
769 matrix with non-negative singular values $s_1 \geq s_2 \geq \dots \geq s_r > 0$ on its diagonal, and $s_j = 0$ for
770 $j > r$.

771 For any matrix \mathbf{A} and subsets R and T , we write $\mathbf{A}_{\cdot, R}$ for the submatrix formed by the columns of
772 \mathbf{A} with indices in R , and write $\mathbf{A}_{T, \cdot}$ for the submatrix formed by the rows of \mathbf{A} with indices in T .

773 Multiplying the model in Equation (15) by $\frac{1}{\sqrt{n}} \mathbf{U}_{\cdot, [r]}^\top$, we obtain a r -dimensional transformed model:

$$774 \quad 775 \quad \mathbf{Z} = \theta^* + \xi, \quad (17)$$

776 where we have defined $\mathbf{Z} = \frac{1}{\sqrt{n}} \mathbf{U}_{\cdot, [r]}^\top \mathbf{Y}$, $\theta^* = \frac{1}{\sqrt{n}} \mathbf{U}_{\cdot, [r]}^\top \mathbf{X} \beta^* = \mathbf{S}_{[r], \cdot} \mathbf{V}^\top \beta^*$, and $\xi = \frac{1}{\sqrt{n}} \mathbf{U}_{\cdot, [r]}^\top \epsilon$.
777 Since \mathbf{U} is orthogonal, the transformed noise vector ξ still has uncorrelated components with mean
778 zero and variance $\sigma_{\text{eff}}^2 := \sigma_0^2/n$.

779 The transformed model in Equation (17) is analogous to the sequence model in Equation (4), where
780 the signal is θ^* and the noise variance for each component is σ_{eff}^2 . The ‘‘spectrum’’ relevant to this
781 problem is derived from the singular values of \mathbf{X} . Specifically, we define the eigenvalues as $\lambda_j = s_j^2$
782 for $j = 1, \dots, r$, and $\lambda_j = 0$ for $j > r$. Let $\{\pi_k\}_{k=1}^r$ denote the indices corresponding to the
783 eigenvalues sorted in descending order, $\lambda_{\pi_1} \geq \lambda_{\pi_2} \geq \dots \geq \lambda_{\pi_r} > 0$.

784 For any estimator $\hat{\beta}$ for the linear model Equation (15), define $\hat{\theta} = \mathbf{S}_{[r], \cdot} \mathbf{V}^\top \hat{\beta}$. We can then write the
785 prediction risk as $n^{-1} \mathbb{E} \|\mathbf{X} \hat{\beta} - \mathbf{X} \beta^*\|^2 = \mathbb{E} \|\mathbf{USV}^\top \hat{\beta} - \mathbf{USV}^\top \beta^*\|^2 = \mathbb{E} \|\hat{\theta} - \theta^*\|^2$. Conversely,
786 given an estimator $\hat{\theta}$ for the sequence model Equation (17), we can define $\tilde{\beta} = \mathbf{VS}^\dagger \hat{\theta}$ where
787 $\mathbf{S}^\dagger \in \mathbb{R}^{p \times r}$ is a diagonal matrix whose diagonal elements are $\{1/s_j\}_{j \in [r]}$. It is easy to check that
788 $\mathbf{S}_{[r], \cdot} \mathbf{V}^\top \tilde{\beta} = \hat{\theta}$. Therefore, we establish an equivalence between the model Equation (17) and the
789 model Equation (15).

790 The usual ridge regression estimator for the linear model Equation (15) is given by

$$791 \quad 792 \quad \hat{\beta}_\nu = (\mathbf{X}^\top \mathbf{X} + \nu \mathbf{I}_p)^{-1} \mathbf{X}^\top \mathbf{Y},$$

793 which transforms into

$$794 \quad 795 \quad \hat{\theta}_\nu = \mathbf{S}_{[r], \cdot} \mathbf{V}^\top \hat{\beta}_\nu = (\mathbf{I}_r - g_\nu(\text{Diag}(\lambda_1, \dots, \lambda_r))) \mathbf{Z}, \quad \text{where } g_\nu(\lambda) = \frac{1}{\lambda/\nu + 1}.$$

796 In the above expression, we have used the identity that $\mathbf{S}_{[r], \cdot} \mathbf{S}_{[r], \cdot}^\top = \text{Diag}(s_1^2, \dots, s_r^2)$ and $g_\nu(\cdot)$ is
797 applied element-wise. If we replace $g_\nu(\lambda)$ by other functions as discussed in Section 3, we recover
798 other spectral methods.

802 A.3 ESD FOR LINEAR MODELS

804 We can now adapt the definitions from Section 3 to linear models.

805 **Definition A.1** (ESD for Linear Regression). *Suppose the SVD of the design matrix \mathbf{X} is given in
806 Equation (16). The Effective Span Dimension (ESD) of β^* with respect to the design \mathbf{X} and the per
807 component variance σ_0^2/n is defined as*

$$808 \quad 809 \quad d^\dagger = d^\dagger(\sigma_0^2/n; \beta^*, \mathbf{X}) = \min\{k \in [r] : \mathbf{H}_{\theta^*, \lambda}(k) \leq \sigma_0^2/n\},$$

where $\theta^* = \mathbf{S}_{\cdot, [r]} \mathbf{V}^\top \beta^*$ and $\lambda_j = s_j^2$.

The Principal Component Regression (PCR) estimator for β^* corresponds to the Principal Component (PC) estimator in the transformed space Equation (17). Specifically, for any $k \in [r]$, define $\hat{\beta}^{\text{PC},k} = \frac{1}{\sqrt{n}} \mathbf{V} \mathbf{S}_k^\dagger \mathbf{U}_{\cdot,[r]}^\top \mathbf{Y}$, where $\mathbf{S}_k^\dagger \in \mathbb{R}^{p \times r}$ is a diagonal matrix whose diagonal elements are $\{\frac{1}{s_j} \mathbf{1}_{\{s_j \geq s_{\pi_k}\}}\}$. In the \mathbf{Z} space, this means

$$\hat{\theta}_j^{\text{PC},k} = \mathbf{1}_{\{s_j \geq s_{\pi_k}\}} Z_j, \quad j \in [r]. \quad (18)$$

Analogous to Theorem 3.2, the minimal prediction risk achievable by PCR over k is characterized by the ESD.

Proposition A.2 (Optimal PCR Prediction Risk). *Let $\hat{\beta}^{\text{PC},k}$ be the PCR estimator using the first k principal components. Let $\mathcal{R}_*^{\text{PC}}$ be the minimal possible prediction risk over $k \in [r]$, i.e., $\mathcal{R}_*^{\text{PC}} = \min_{k \in [r]} \mathcal{R}(\hat{\beta}^{\text{PC},k}; \beta^*)$. It holds that*

$$(d^\dagger - 1)\sigma_0^2/n \leq \mathcal{R}_*^{\text{PC}} \leq 2d^\dagger\sigma_0^2/n,$$

where $d^\dagger = d^\dagger(\sigma_0^2/n; \beta^*, \mathbf{X})$ is the ESD defined in Definition A.1.

Proposition A.2 directly follows from Theorem 3.2 and its proof is omitted. This result shows that the optimal prediction risk for PCR is determined by the ESD d^\dagger , which measures the effective number of principal components needed to balance the bias-variance trade-off.

We can further extend the minimax analysis from Theorem 3.3. Let K be a quota on ESD. Define a class of coefficient vectors based on this quota:

$$\mathcal{B}_K^{(n)} = \{\beta^* \in \mathbb{R}^p : d^\dagger(\sigma_0^2/n; \beta^*, \mathbf{X}) \leq K\}, \quad (19)$$

This class contains signals whose ESD relative to the design \mathbf{X} is controlled by K . We can establish the minimax optimal rate for prediction over this class.

Theorem A.3 (Minimax Prediction Risk for Linear Regression). *Suppose $K \leq r$. For the linear model Equation (15) with noise variance σ_0^2 , the minimax prediction risk over the class $\mathcal{B}_K^{(n)}$ defined in Equation (19) satisfies:*

$$\inf_{\hat{\beta}} \sup_{\beta^* \in \mathcal{B}_K^{(n)}} \mathcal{R}(\hat{\beta}; \beta^*) \asymp \sigma_0^2 \frac{K}{n}.$$

The proof of Theorem A.3 is essentially the same as that of Theorem 3.3 and is omitted.

Through this extension, the span profile framework connects the optimal prediction performance in fixed-design linear regression to the alignment between the signal structure (transformed via the design matrix) and the spectrum derived from the design matrix's singular values.

A.4 NUMERICAL ILLUSTRATION

This section illustrates the ESD in fixed-design linear models in two examples. Throughout, we fix the noise variance at $\sigma_0^2 = 1$, the sample size at $n = 300$, and the dimension at $p = 400$.

Experimental setup The baseline design matrix \mathbf{X}_0 is randomly generated with covariance matrix $\Sigma = \text{Diag}\{\lambda_j\}_{j \in [p]}$ and then held fixed. We consider two cases:

1. *Geometric decay spectrum and polynomial decay signal:* $\lambda_j \propto 0.95^j$ and $\beta_j^* = j^{-0.2}$;
2. *Logarithmic decay spectrum and signal:* $\lambda_j = 1/\log(j+1)$ with $\beta_j^* = 1/\log(j+1)$.

The response will be generated from $\mathbf{Y} = \mathbf{X}_0 \beta^* + \epsilon$ with random noise ϵ .

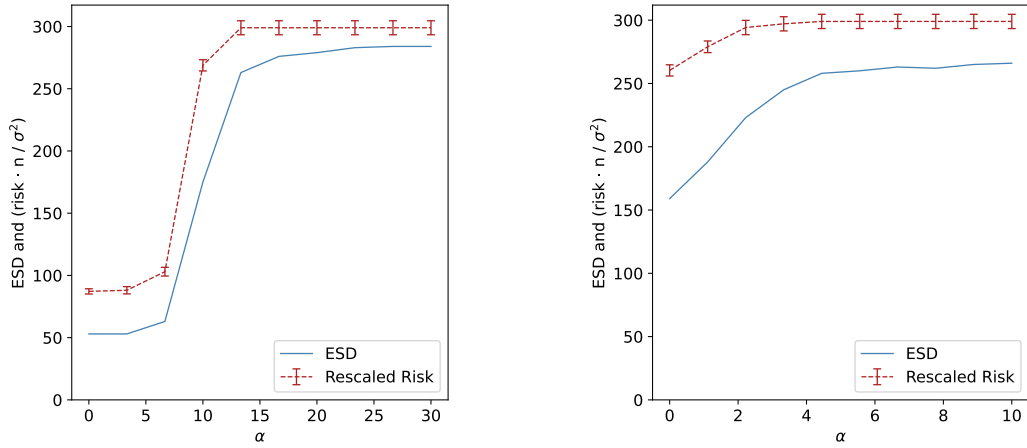
We are interested in the ESD and the minimum risk for different transformations of the design matrix. For this purpose, we introduce a class of non-orthogonal column transformations indexed by $\alpha > 0$ as follows:

$$\mathbf{A}(\alpha) = \text{diag}(\exp\{\alpha t_j\}), \quad t_j = (j-1)/(p-1) - 1/2, \quad j \in [p].$$

The transformed design $\mathbf{X}(\alpha) = \mathbf{X}_0 \mathbf{A}(\alpha)$ and the correspondingly transformed coefficient vector is $\beta(\alpha) = \mathbf{A}(\alpha)^{-1} \beta^*$. These transformations will change the ordering of the spectrum, from well-aligned to misaligned. We are interested in the following at each α :

864
 865
 866
 867
 868
 869
 870
 871
 872
 873
 874
 875
 876
 877
 878
 879
 880
 881
 882
 883
 884

- Effective Span Dimension: $d^\dagger(\alpha) = d^\dagger(\sigma_0^2/n; \beta(\alpha), \mathbf{X}(\alpha))$;
- Minimal PCR risk: $\mathcal{R}_*(\alpha) = \min_k \mathbb{E}[n^{-1} \|\mathbf{X}(\alpha) \hat{\beta}_k - \mathbf{X}(\alpha) \beta(\alpha)\|^2]$, where $\hat{\beta}_k$ is the k -component principal-component estimator based on $(\mathbf{Y}, \mathbf{X}(\alpha))$.



885 **Figure 3: Oracle PCR risk versus Effective Span Dimension** for (a) geometric eigen-decay and (b) logarithmic
 886 eigen-decay. The dashed line plots Risk $\times n/\sigma_0^2$; the solid line is $d^\dagger(\alpha)$. The risk is computed based on 20
 887 replications and the error bar represents the standard deviation.

888 Figure 3 plots $d^\dagger(\alpha)$ (solid) and the rescaled oracle risk defined as $n\mathcal{R}_*(\alpha)/\sigma_0^2$ (dashed) against α .
 889 The two curves coincide over the entire path, which empirically verifies the bound in Proposition A.2
 890 that $\mathcal{R}_*(\alpha) \asymp \frac{\sigma_0^2}{n} d^\dagger(\alpha)$. As α grows, the diagonal stretch $\mathbf{A}(\alpha)$ shifts signal energy towards
 891 directions that carry smaller singular values. This raises d^\dagger , and consequently, the achievable risk.

892 This experiment illustrates that ESD, rather than raw spectral decay, is the pivotal measure governing
 893 learnability.

896 B EXTENSION TO RKHS REGRESSION

897 This section extends the concepts of Effective Span Dimension (ESD) and span profile, developed
 898 in Section 3, to the setting of RKHS regression. Since our goal is to develop a population level
 899 complexity measure, we focus on the simple case where the eigenfunctions of the kernel are fully
 900 known and computable, and leave a thorough analysis in future studies.

903 B.1 RKHS REGRESSION

905 We recall the standard random-design kernel regression model from Section 2:

906
$$y_i = f^*(x_i) + \epsilon_i, \quad \epsilon_i \text{ are i.i.d. with } \mathbb{E}[\epsilon_i] = 0, \text{Var}(\epsilon_i) = \sigma_0^2, \quad i = 1, \dots, n, \quad (20)$$

907 where $x_i \stackrel{\text{i.i.d.}}{\sim} \mu$, and $f^* \in L^2(\mathcal{X}, \mu)$ is the target function. We use a kernel $\mathbf{k}(\cdot, \cdot)$ with Mercer
 908 decomposition $\mathbf{k}(x, x') = \sum_{j=1}^{\infty} \lambda_j \psi_j(x) \psi_j(x')$, where $\{\psi_j\}_{j=1}^{\infty}$ form an orthonormal basis for
 909 $L^2(\mathcal{X}, \mu)$ and $\lambda = \{\lambda_j\}_{j \geq 1}$ is the sequence of eigenvalues not necessarily sorted. For simplicity,
 910 we assume there are no ties among the eigenvalues and let π be the permutation that sorts them
 911 in descending order, so that $\lambda_{\pi_1} > \lambda_{\pi_2} > \dots > \lambda_{\pi_k} > \dots$. The coefficients of f^* in this basis
 912 are $\theta_j^* = \langle f^*, \psi_j \rangle_{L^2(\mu)}$. An estimator \hat{f} has risk $\mathcal{R}(\hat{f}; f^*) = \mathbb{E}\|\hat{f} - f^*\|_{L^2(\mu)}^2$. If we define
 913 $\hat{\theta}_j = \langle \hat{f}, \psi_j \rangle_{L^2(\mu)}$, we can also write the risk as
 914

915
$$\mathcal{R}(\hat{f}; f^*) = \mathbb{E}\|\hat{f} - f^*\|_{L^2(\mu)}^2 = \mathbb{E}\left[\sum_{j=1}^{\infty} (\hat{\theta}_j - \theta_j^*)^2\right] = \sum_{j=1}^{\infty} \mathbb{E}(\hat{\theta}_j - \theta_j^*)^2. \quad (21)$$

918 The expression in Equation (21) suggests that we can equivalently estimate each θ_j^* separately using
 919 the transformed observation $z_j = n^{-1} \sum_i y_i \psi_j(x_i)$ for any $j \geq 1$ as introduced in Equation (2).
 920

921 Here we kindly remind the reader that in RKHS, we use subscript i for samples and subscript j for
 922 eigen-coordinates. The subscript j aligns with the use of notation in the sequence model, where we
 923 use indices j to denote coordinates.

924 **Inflated variance in Equation (3).** Before we introduce the definition of ESD, we demonstrate
 925 that the approximation in Equation (3) can be made exact by increasing the variance to absorb the
 926 approximation error.
 927

928 For each $j \geq 1$, we can write the transformed observation as

$$\begin{aligned}
 z_j &= \frac{1}{n} \sum_{i=1}^n y_i \psi_j(x_i) \\
 &= \frac{1}{n} \sum_{i=1}^n (f^*(x_i) + \epsilon_i) \psi_j(x_i) \\
 &= \frac{1}{n} \sum_{i=1}^n \left(\sum_{k \geq 1} \theta_k^* \psi_k(x_i) \right) \psi_j(x_i) + \frac{1}{n} \sum_{i=1}^n \epsilon_i \psi_j(x_i) \\
 &= \sum_{k \geq 1} \underbrace{\theta_k^* \left(\frac{1}{n} \sum_{i=1}^n \psi_k(x_i) \psi_j(x_i) \right)}_{:= G_{kj}} + \underbrace{\frac{1}{n} \sum_{i=1}^n \epsilon_i \psi_j(x_i)}_{:= \xi_j} \\
 &= \sum_{k \geq 1} G_{kj} \theta_k^* + \xi_j,
 \end{aligned}$$

945 where $G_{kj} := \frac{1}{n} \sum_{i=1}^n \psi_k(x_i) \psi_j(x_i)$ are entries of the empirical feature correlation matrix. For ξ_j ,
 946 we have $\mathbb{E}(\xi_j | \{x_i\}_{i \in [n]}) = 0$ and $\mathbb{E}(\xi_j \xi_k | \{x_i\}_{i \in [n]}) = n^{-1} \sigma_0^2 G_{jk}$.
 947

948 Since $x_i \stackrel{\text{i.i.d.}}{\sim} \mu$ and $\{\psi_j\}$ are orthonormal in $L^2(\mathcal{X}, \mu)$, we have $\mathbb{E}[G_{kj}] = \mathbf{1}_{\{k=j\}}$. Hence $\mathbb{E}[z_j] = \theta_j^*$.
 949

950 We may further decompose z_j as follows

$$z_j - \theta_j^* = (G_{jj} - 1)\theta_j^* + \left(\sum_{k \geq 1, k \neq j} G_{kj} \theta_k^* \right) + \xi_j = \Delta_j + \xi_j,$$

955 where we have defined $\Delta_j = (G_{jj} - 1)\theta_j^* + \left(\sum_{k \geq 1, k \neq j} G_{kj} \theta_k^* \right)$. This term does not appear in
 956 the sequence model; its randomness arises solely from the random covariates x_i . As $n \rightarrow \infty$, this
 957 term vanishes because $G_{jj} = n^{-1} \sum_i \psi_j(x_i)^2 \rightarrow 1$ and $G_{kj} = n^{-1} \sum_{i=1}^n \psi_j(x_i) \psi_{j'}(x_i) \rightarrow 0$ for
 958 $k \neq j$. Furthermore, since $\mathbb{E}(\xi_j | \{x_i\}_{i \in [n]}) = 0$, we have
 959

$$\mathbb{E}(\Delta_j \xi_j) = \mathbb{E}(\Delta_j \mathbb{E}(\xi_j | \{x_i\}_{i \in [n]})) = 0.$$

960 The presence of Δ_j effectively inflates the variance in z_j to $\sigma_0^2/n + \text{Var}(\Delta_j)$. One can show that
 961 $\text{Var}(\Delta_j) = \text{Var}(f^*(x) \psi_j(x))$, which is bounded by $\|f^*\|_\infty^2$. This is how we will control the impact
 962 of Δ_j in the following development.
 963

964 B.2 ESD FOR RKHS REGRESSION

965 We start by analyzing the counterpart of the PC estimator, the Kernel Principal Component Projection
 966 Estimator (KPCPE), defined as
 967

$$\hat{f}_k^{\text{PC}}(x) := \sum_{j: \lambda_j \geq \lambda_{\pi_k}} z_j \psi_j(x), \quad (22)$$

972 where k is the number of leading eigenfunctions to be included.
 973

974 The risk $\mathcal{R}_k := \mathbb{E}\|\hat{f}_k^{\text{PC}} - f^*\|_{L^2(\mu)}^2$ decomposes into squared bias $B(k)$ and variance $V(k)$. Since
 975 $\mathbb{E}[\psi_{j'}(x_i)\psi_j(x_i)] = \mathbf{1}_{\{j=j'\}}$, we have $\mathbb{E}[z_j] = \theta_j^*$. Therefore, the bias is due to truncation as
 976

$$977 \quad B(k) = \sum_{j=k+1}^{\infty} (\theta_j^*)^2. \quad (23)$$

978

980 The integrated variance is $V(k) = \sum_{j:\lambda_j \geq \lambda_{\pi_k}} \text{Var}(z_j)$. Using the law of total variance, we have
 981

$$982 \quad \text{Var}(z_j) = \frac{1}{n} \text{Var}(y_i \psi_j(x_i)) = \frac{1}{n} (\sigma_0^2 + \tau_j^2), \quad \text{where } \tau_j^2 := \text{Var}(f^*(x) \psi_j(x)). \quad (24)$$

983

984 The term τ_j^2 arises from the randomness of the design x . To ensure $V(k)$ grows at the rate of k/n ,
 985 we need to uniformly bound the design-induced variance τ_j^2 . To illustrate the idea, we assume f^* is
 986 bounded in the sense that $|f^*(X)| \leq \|f^*\|_{\infty}$, μ -almost surely. Here, $\|f^*\|_{\infty}$ denotes the essential
 987 supremum of $|f^*|$ w.r.t. the measure μ .

988 **Assumption B.1** (Bounded target). $f^* \in L^{\infty}(\mathcal{X}, \mu)$ and $\|f^*\|_{\infty} = \text{ess sup } |f^*|$.
 989

990 Assumption B.1 is very mild: for compact \mathcal{X} , if f is continuous, then f is bounded.
 991

992 Under Assumption B.1, $\tau_j^2 \leq \mathbb{E}[f^*(x)^2 \psi_j(x)^2] \leq \|f^*\|_{\infty}^2$. Subsequently, the variance is bounded by
 993 $V(k) \leq \frac{k}{n} (\sigma_0^2 + \|f^*\|_{\infty}^2)$. This motivates us to define the effective noise variance per component as
 994

$$995 \quad \sigma_{\text{eff}}^2 := \frac{\sigma_0^2 + \|f^*\|_{\infty}^2}{n}. \quad (25)$$

996

997 The effective noise variance σ_{eff}^2 includes the term $\|f^*\|_{\infty}^2/n$, which inflates the noise compared to
 998 an idealized sequence model.
 999

1000 We can now adapt the definitions from Section 3.1 using the effective noise variance σ_{eff}^2 .
 1001

1002 **Definition B.2** (ESD for RKHS Regression). *The Effective Span Dimension (ESD) of f^* with respect
 1003 to the kernel \mathbf{k} and the effective noise variance $\sigma_{\text{eff}}^2 = (\sigma_0^2 + \|f^*\|_{\infty}^2)/n$ is defined as*
 1004

$$1005 \quad d^{\dagger} = d^{\dagger}(\sigma_{\text{eff}}^2; f^*, \mathbf{k}) = \min\{k \in \mathbb{N}_+ \cup \{\infty\} : \mathbf{H}_{\theta^*, \lambda}(k) \leq \sigma_{\text{eff}}^2\}, \quad (26)$$

1006 where $\theta^* = \{\theta_j^*\}_{j \geq 1}$ and $\mathbf{H}_{\theta^*, \lambda}(k)$ is defined as in Equation (10).
 1007

1008 The risk of the KPCPE estimator can be bounded using this ESD.
 1009

1010 **Proposition B.3** (Optimal KPCPE Risk Bound). *Let \hat{f}_k^{PC} be the KPCPE estimator defined in
 1011 Equation (22). Let $\mathcal{R}_*^{\text{PC}} = \min_{k \geq 1} \mathcal{R}(\hat{f}_k^{\text{PC}}; f^*)$. Under Assumption B.1, it holds that:*
 1012

$$1013 \quad (d^{\dagger} - 1) \frac{\sigma_0^2}{n} \leq \mathcal{R}_*^{\text{PC}} \leq 2d^{\dagger} \sigma^2 = 2d^{\dagger} \frac{\sigma_0^2 + \|f^*\|_{\infty}^2}{n}, \quad (27)$$

1014 where $d^{\dagger} = d^{\dagger}(\sigma_{\text{eff}}^2; f^*, \mathbf{k})$ is the ESD from Definition B.2. In particular, if $\|f^*\|_{\infty}^2 \lesssim \sigma_0^2$, we can
 1015 conclude that $\mathcal{R}_*^{\text{PC}} \asymp d^{\dagger} \sigma_0^2/n$.
 1016

1017 We comment that Zhang et al. (2023) have established the minimax optimality of the well-tuned
 1018 PC estimator. Proposition B.3 suggests that the risk of the well-tuned PC estimator scales as d^{\dagger}/n .
 1019 Therefore, we essentially express the minimax rate therein using the ESD without reliance on the
 1020 classical eigen-decay conditions or source conditions.
 1021

1022 We can also extend the minimax framework in Section 4 to RKHS regression. Let K be a quota on
 1023 the ESD, and let C_0 be a constant. Define the class based on the span profile as follows:
 1024

$$1025 \quad \mathcal{F}_{K, \mathbf{k}}^{(n)} = \{f^* \in L^2(\mathcal{X}, \mu) \cap L^{\infty}(\mathcal{X}, \mu) : \|f^*\|_{\infty} \leq \sigma_0 C_0, \quad d^{\dagger}(\bar{\sigma}^2/n; f^*, \mathbf{k}) \leq K\}, \quad (28)$$

1026 where $\bar{\sigma}^2 = \sigma_0^2(1 + C_0^2)$. We further impose the following assumption on the spectrum.
 1027

1028 **Assumption B.4.** *The kernel \mathbf{k} is said to be (K, n) -regular if there are some constants $c_1 \in (0, 1)$
 1029 and C_1 such that $\sum_{i \leq c_1 K} \lambda_{\pi_i}^{-1} \leq C_1 n$.*

1026
1027 **Theorem B.5** (Minimax Risk over Span Profile Classes). *If \mathbf{k} is (K, n) -regular, then the minimax
1028 risk over $\mathcal{F}_{K, \mathbf{k}}^{(n)}$ satisfies:*

1029
$$\inf_{\hat{f}} \sup_{f^* \in \mathcal{F}_{K, \mathbf{k}}^{(n)}} \mathcal{R}(\hat{f}; f^*) \asymp \frac{\sigma_0^2 K}{n}, \quad (29)$$

1030
1031

1032 where the infimum is over all estimators \hat{f} .

1033 Combining Theorem B.5 and Proposition B.3, the optimally tuned KPCPE estimator is minimax rate
1034 optimal over $\mathcal{F}_{K, \mathbf{k}}^{(n)}$, with rate $\sigma_0^2 K/n$.

1035 The KPCPE serves as a simple benchmark for spectral methods. This analysis, via the ESD,
1036 characterizes the performance of the optimally tuned KPCPE based directly on the properties of
1037 the specific signal f^* (via θ^*) and kernel spectrum λ , without requiring standard assumptions like
1038 source conditions or polynomial eigenvalue decay. Therefore, we consider the ESD evaluated at the
1039 design-adjusted noise level σ_{eff}^2 as a key measure of statistical complexity in RKHS regression. In
1040 summary, the span profile framework provides a unified perspective on the generalization performance
1041 of spectral methods across a variety of models.

1042 **Minimax convergence rates.** Following the framework in Section 4, we can quantify a class of
1043 populations using a quota sequence $\mathbf{K} = \{K_n\}_{n=1}^\infty$. For some $n_0 \in \mathbb{N}_+$, define

1044
$$\mathcal{F}_{\mathbf{K}, \mathbf{k}} = \{f^* \in L^2(\mathcal{X}, \mu) \cap L^\infty(\mathcal{X}, \mu) : \|f^*\|_\infty \leq \sigma_0 C_0, \quad d^\dagger(\bar{\sigma}^2/n; f^*, \mathbf{k}) \leq K_n, \forall n \geq n_0\}, \quad (30)$$

1045

1046 where $\bar{\sigma}^2 = \sigma_0^2(1 + C_0^2)$. For a sample $\{(x_i, y_i)\}_{i=1}^n$ drawn from the model in Equation (20) and any
1047 estimator \hat{f} , we aim to determine the optimal convergence rate of the following minimax risk:

1048
$$\inf_{\hat{f}} \sup_{f^* \in \mathcal{F}_{\mathbf{K}, \mathbf{k}}} \mathcal{R}(\hat{f}, f^*). \quad (31)$$

1049

1050 We have the following result.

1051 **Theorem B.6.** *Suppose Condition 4.1 holds for a quota sequence $\mathbf{K} = \{K_n\}_{n=1}^\infty$. Furthermore, suppose \mathbf{k} is (K_n, n) -regular for all $n \geq n_0$. If $\{(x_i, y_i)\}_{i=1}^n$ is drawn from the model in Equation (20), it holds that*

1052
$$\inf_{\hat{f}} \sup_{f^* \in \mathcal{F}_{\mathbf{K}, \mathbf{k}}} \mathcal{R}(\hat{f}, f^*) \asymp \bar{\sigma}^2 \frac{K_n}{n}.$$

1053

1054 Assumption B.4 is a mild condition. The following is an example where we use Theorem B.6 to
1055 recover the minimax convergence rate derived under the classical polynomial eigen-decay conditions
1056 and source conditions.

1057 **Example B.7.** *Suppose \mathbf{k} admits spectrum such that $\lambda_{\pi_i} \asymp i^{-\beta}$ with $\beta > 0$. Let $K_n = \lfloor n^{\frac{1}{1+s\beta}} \rfloor$ for
1058 any $s \geq 1$. It is easy to see that*

1059
$$\sum_{i \leq c_1 K_n} \lambda_{\pi_i}^{-1} \asymp (c_1 K_n)^{\beta+1} \asymp n^{\frac{\beta+1}{s\beta+1}} \lesssim n.$$

1060

1061 Therefore, the minimax optimal rate for the class $\mathcal{F}_{\mathbf{K}, \mathbf{k}}$ is $\frac{\bar{\sigma}^2 K_n}{n} \asymp \sigma_0^2 n^{-\frac{s\beta}{1+s\beta}}$, which is the same as
1062 the optimal rate given by the source condition with smoothness parameter s .

1063 **Remark B.8.** *In Section 2, we simplify our discussion by assuming that \mathbf{k} is positive definite. In
1064 practice, positive semi-definite (PSD) kernels may also be used. In the case where \mathbf{k} has rank $d < \infty$,
1065 spectral algorithms inevitably induce a systematic (squared) bias*

1066
$$\Delta_{f^*, \mathbf{k}} = \|f^*\|_{L^2(\mu)}^2 - \sum_{j \in [d]} (\theta_{\pi_j}^*)^2,$$

1067

1068 regardless the regularization parameter. In that case, we may modify the definition of ESD by adding
1069 the systematic bias into the summation to the sum of squared tails.

1070 Specifically, for a PSD kernel \mathbf{k} of rank $d < \infty$, we modify the definition of ESD in Definition B.2 as

1071
$$\bar{d}^\dagger = \bar{d}^\dagger(\sigma_{\text{eff}}^2; f^*, \mathbf{k}) = \min \left\{ j \in [d] : \frac{1}{j} \left[\Delta_{f^*, \mathbf{k}} + \sum_{i=j+1}^d (\theta_{\pi_i}^*)^2 \right] \leq \sigma_{\text{eff}}^2 \right\}.$$

1072

1073 Again, $\sigma_{\text{eff}}^2 \bar{d}^\dagger$ characterizes the risk of the well-tuned PC estimator as in Proposition B.3.

1080
1081

B.3 CONNECTION TO RANDOM DESIGN LINEAR REGRESSION

1082
1083
1084
1085

The analysis in this section also covers an important case: random-design linear regression (as opposed to fixed-design linear regression). This is because linear regression can be viewed as an RKHS regression w.r.t. any positive-definite linear kernels $\mathbf{k}(x, x') = x^\top \mathbf{K} x'$ for $x, x' \in \mathbb{R}^p$, where $\mathbf{K} \in \mathbb{R}^{p \times p}$ is positive definite.

1086
1087

Let the support \mathcal{X} be a compact subset of \mathbb{R}^p . Suppose $\Sigma_x = \mathbb{E}_{x \sim \mu}(xx^\top)$ is positive definite and \mathbf{L} is a symmetric square root of Σ_x . Let the eigen-decomposition of \mathbf{LKL} be

1088
1089
1090
1091

$$\mathbf{LKL} = \sum_{j=1}^p \lambda_j v_j v_j^\top = \mathbf{V} \mathbf{\Lambda} \mathbf{V}^\top,$$

1092

where \mathbf{V} is the matrix with columns formed by v_j and $\mathbf{\Lambda} = \text{Diag}(\lambda_1, \dots, \lambda_p)$.

1093

Define $\Psi = \mathbf{L}^{-1} \mathbf{V}$. Then $\Psi^\top \Sigma_x \Psi = \mathbf{V}^\top \mathbf{V} = \mathbf{I}_p$. Furthermore, we have

1094
1095

$$\mathbf{K} = \mathbf{L}^{-1} \mathbf{V} \mathbf{\Lambda} \mathbf{V}^\top \mathbf{L}^{-1} = \Psi \mathbf{\Lambda} \Psi^\top,$$

1096
1097

Suppose the columns of Ψ are ψ_j . We can then write

1098
1099

$$\mathbb{E}_{x \sim \mu} [\langle \psi_j, x \rangle \langle \psi_j, x \rangle] = (\Psi^\top \Sigma_x \Psi)_{jk} = \mathbf{1}_{\{j=k\}}, \quad \forall j, k \in [p],$$

1100

so $\{\psi_j\}$ is an orthonormal system in $L^2(\mathcal{X}, \mu)$. Furthermore, the kernel can be expressed as

1101
1102
1103

$$\mathbf{k}(x, x') = x^\top \mathbf{K} x' = \sum_{j=1}^p \lambda_j \langle \psi_j, x \rangle \langle \psi_j, x' \rangle.$$

1104
1105

Hence, $(\{\lambda_j\}, \{\psi_j\})$ is the eigenpair for \mathbf{k} .

1106
1107

For linear regression where $y = f^*(x) + \epsilon$ and $f^*(x) = \langle \beta^*, x \rangle$. Define $\theta^* = \Psi^{-1} \beta^* = \mathbf{V}^\top \mathbf{L} \beta^*$. We can write

1108
1109
1110

$$f^*(x) = \langle \beta^*, x \rangle = \langle \Psi^{-1} \beta^*, \Psi^\top x \rangle = \sum_{j=1}^p \theta_j^* \langle \psi_j, x \rangle.$$

It is also clear that $\|f^*\|_\infty \leq \sup_{x \in \mathcal{X}} \langle \beta^*, x \rangle \leq \|\beta^*\|_2 C_{\mathcal{X}} < \infty$, where $C_{\mathcal{X}}$ is finite and depends on \mathcal{X} . We can define the effective noise level $\sigma_{\text{eff}}^2 = n^{-1} (\sigma_0^2 + \|f^*\|_\infty^2)$.

1113
1114

Therefore, with respect to the kernel \mathbf{k} and the basis $\{\psi_j\}$, we define the ESD exactly as in Definition B.2 using the coefficients $\{\theta_j^*\}$ and eigenvalues $\{\lambda_j\}$.

1115

B.4 NUMERICAL ILLUSTRATION

1116
1117
1118
1119
1120
1121
1122

This section provides numerical validation of the relationship between the ESD and the optimally tuned KPCPE risk, mirroring the setup for linear models in Appendix A.4. We use the cosine basis eigenfunctions $\psi_j(x) = \sqrt{2} \cos(2\pi j x)$ on the domain $[0, 1]$ with inputs sampled as $x_i \stackrel{\text{i.i.d.}}{\sim} \text{Unif}[0, 1]$. The sample size is fixed at $n = 400$, and for numerical purpose, we consider the first $J = 800$ eigenfunctions. The noise variance is set as $\sigma_0^2 = 1$.

1123
1124
1125
1126

Experimental Setup: We set the baseline kernel eigenvalue spectrum as $\lambda_{j,0} = j^{-1.1}$ and the fixed signal coefficients as $\theta_j^* = j^{-4}$. To study the impact of misalignment between the kernel spectrum and the signal, we introduce a severity parameter $\alpha \geq 0$ and define the modified eigenvalue spectrum as

1127
1128

$$\lambda_j(\alpha) = \lambda_{j,0} \exp(\alpha t_j), \quad t_j = \frac{j-1}{D-1} \text{ for } j \leq D, \text{ and } t_j = 0 \text{ otherwise,}$$

1129
1130
1131
1132

with $D = 80$. As α increases, the leading D eigenvalues become progressively magnified, with the largest index having the most significant increase. Consequently, the modified kernel places more emphasis on directions that receive less signal energy, so the optimal KPCPE selects more principal components.

1133

As the severity parameter α grows, only the first D eigenvalues are changed while the rest of the spectrum is untouched. Among the changed ones, the leading eigenvalues are magnified by a smaller

1134 constant, so that the resulting kernel has its leading subspaces being on the directions in which the
 1135 signal has less of its energy and thus increases the misalignment.
 1136

1137 For each α in a specified grid, we compute two quantities:

1138 • The Effective Span Dimension
 1139

1140
$$d_{\text{eff}}^{\dagger}(\alpha) = d^{\dagger}(\sigma_{\text{eff}}^2; f^*, \lambda(\alpha)), \quad \sigma_{\text{eff}}^2 := \frac{\sigma_0^2 + \|f^*\|_{\infty}^2}{n},$$

 1141

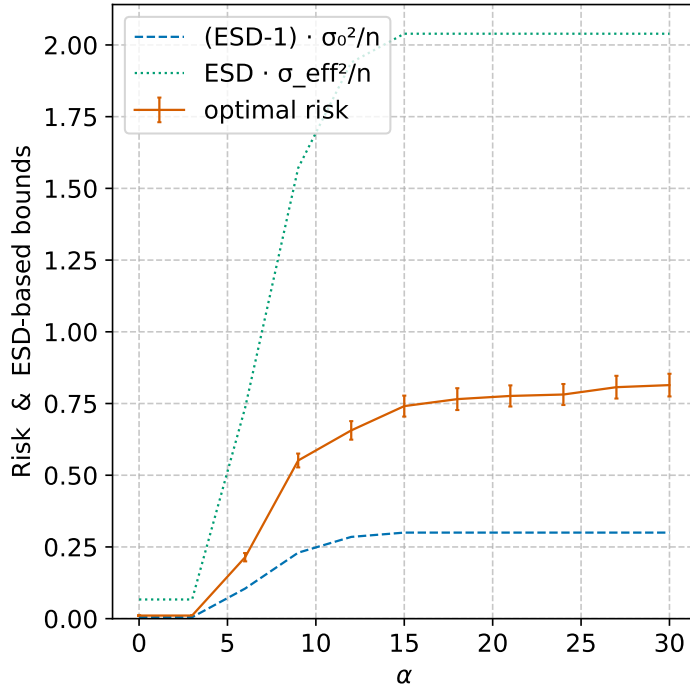
1142 where $\|f^*\|_{\infty} = \text{ess sup}_x |f^*(x)|$ is approximated by evaluating f^* on a dense grid of input
 1143 points and taking the maximum absolute value.
 1144

1145 • The optimally tuned KPCPE risk
 1146

1147
$$\mathcal{R}_*(\alpha) = \min_k \mathbb{E} \|\hat{f}_k^{\text{PC}}(\alpha) - f^*\|_{L^2(\mu)}^2,$$

 1148

1149 where the estimator $\hat{f}_k^{\text{PC}}(\alpha)$ is computed using the spectrum $\lambda(\alpha)$ and the expectation is
 1150 estimated by averaging prediction error over $B = 10$ Monte Carlo replications.
 1151



1176 Figure 4: Effective Span Dimension and Optimal KPCPE risk. The dashed line plots Risk $\times n/\sigma_0^2$; the solid line
 1177 is $d^{\dagger}(\alpha)$. The risk is computed based on 20 replications and the error bar represents the standard deviation.
 1178

1179 Figure 4 plots the empirically computed optimal KPCPE risk (orange solid line) alongside the
 1180 theoretical lower bound $(d^{\dagger} - 1)\sigma_0^2/n$ (blue dashed line) and upper bound $2d^{\dagger}\sigma_{\text{eff}}^2$ (green dotted line).
 1181 The empirical risk consistently lies between the two theoretical curves, confirming the validity of the
 1182 bounds derived in Proposition B.3.

1183 As the severity parameter α increases, the resulting spectral perturbation shifts energy into higher-
 1184 index eigenfunctions. This inflates the ESD and consequently the minimal achievable risk.
 1185

1186 Overall, this experiment demonstrates that our span profile framework provides an accurate and
 1187 robust characterization of generalization performance in RKHS regression, consistent with earlier
 1188 observations made for the sequence and linear regression models.

1188 **C MEASURING ALIGNMENT VIA ESD**
 1189

1190 We illustrate how the notion of ESD can be used to measure the alignment between the signal and the
 1191 kernel.
 1192

1193 **C.1 AN EXAMPLE COMPARING SIGNAL-SPECTRUM ALIGNMENT**
 1194

1195 The following simple example illustrates how to compare signal-spectrum alignment across the
 1196 spectra discussed in Section 3.2.
 1197

1198 Suppose θ^* is s -sparse with support $S \subset [d]$ and $s = |S| \ll d$. Consider the following two spectra
 1199 with the same set of eigenvalues but different allocations:
 1200

1200 (1) The k largest eigenvalues of $\lambda^{(1)}$ are located on S ;
 1201 (2) The k largest eigenvalues of $\lambda^{(2)}$ are located on $S^c = [d] \setminus S$.
 1202

1203 Intuitively, $\lambda^{(1)}$ aligns better with θ^* than $\lambda^{(2)}$. However, a quantitative analysis is not straightforward
 1204 without using the notion of ESD.
 1205

1206 First, we note that the effective dimensions (Zhang, 2005) is the same for both spectra because they
 1207 share the same sets of eigenvalues. Similarly, the covariance-splitting index k^* (Bartlett et al., 2020a)
 1208 is the same for both spectra. Thus, these signal-agnostic complexity measures do not distinguish
 1209 signal-spectrum alignment between the two spectra.
 1210

Next, we consider the ESD and the span profile. Rigorously, we can show for any τ ,

$$D_{\theta^*, \lambda^{(1)}}(\tau) \leq s, \text{ and } D_{\theta^*, \lambda^{(2)}}(\tau) \geq \min(d - s, \|\theta^*\|^2 / \tau).$$

Hence, for sufficiently small τ , their ratio

$$r(\tau) = D_{\theta^*, \lambda^{(1)}}(\tau) / D_{\theta^*, \lambda^{(2)}}(\tau) \leq s / (d - s) \ll 1.$$

In view of Theorem 3.3, this suggests that the minimax risk under $\lambda^{(1)}$ is substantially lower than
 under $\lambda^{(2)}$ when the noise level is small. Therefore, spectral estimators using $\lambda^{(1)}$ are preferred.
 1216
 1217
 1218

1219 **C.2 PATHWISE ESD FOR LEARNED KERNELS**
 1220

1221 Section 5 analyzes eigenvalue learning because OP-GF admits tractable dynamics under a fixed
 1222 eigenbasis. This is a limitation of that specific analysis, not of the ESD concept. In fact, ESD
 1223 applies to general representation learning. We illustrate how decreases in ESD explain minimax risk
 1224 reduction for learned kernels, whether adaptation acts through eigenvalues, eigenfunctions, or both.
 1225

1226 Let \mathbf{k}_t be the kernel learned at training time t , with eigenvalues $\{\lambda_j(t)\}$ (sorted in decreasing order)
 1227 and eigenfunctions $\{\psi_j^{(t)}\}$ that are orthonormal in $L^2(\mathcal{X}, \mu)$. To understand how the signal-kernel
 1228 alignment evolves, we define the pathwise ESD as
 1229

$$d^\dagger(t) := d^\dagger(\sigma^2; f^*, \mathbf{k}_t), t \geq 0,$$

1230 where we have followed Definition B.2 to define $d^\dagger(\sigma^2; f^*, \mathbf{k}_t)$ as the ESD of f^* w.r.t. the kernel \mathbf{k}_t
 1231 using $\theta_j^{*,(t)} = \langle f^*, \psi_j^{(t)} \rangle$ and $\sigma^2 = n^{-1}(\sigma_0^2 + \|f^*\|_\infty^2)$.
 1232

1233 Let $\mathbf{H}_t(k) := \frac{1}{k} \sum_{i>k} [\theta_i^{*,(t)}]^2$. If training aligns the leading eigenfunctions $\psi_j^{(t)}$ better with f^* ,
 1234 then $\{\theta_j^{*,(t)}\}$ concentrate more on the leading indices, and thus $\mathbf{H}_t(k)$ decreases for all k , which
 1235 implies a decrease in $d^\dagger(t)$.
 1236

1237 **Experiment on Deep Linear Networks.** To demonstrate this pathwise perspective, we simulate a
 1238 random-design linear regression.
 1239

1240 Each covariate coordinate is drawn independently from $\{\pm 1\}$, so $\Sigma_x = \mathbb{E}(XX^\top) = \mathbf{I}_p$ and
 1241 $\|X\|_\infty = 1$. We set $p = 900$, and specify the true parameters as follows: β^* follows a power-law

1242 decay with $\beta_j^* = j^{-1.1}$ for $1 \leq j \leq 200$ and $\beta_j^* = 0$ for $j > 200$. The response is $Y = \langle \beta^*, X \rangle + \varepsilon$
 1243 with $\varepsilon \sim N(0, \sigma_0^2)$ and $\sigma_0 = 0.1$.
 1244

1245 We draw $n = 1000$ samples and train a deep *linear network* with $D = 4$ hidden affine layers without
 1246 bias using full-batch Adam with learning rate 10^{-4} . The hidden weight matrices of the network are
 1247 $\mathbf{W}_\ell(t) \in \mathbb{R}^{p \times p}$ for $\ell = 1, \dots, D$ (using a near-identity initialization), and the weight of the final
 1248 linear layer is $w(t) \in \mathbb{R}^p$.

1249 The estimated function at time t is given by $f_t(x) = w(t)^\top \mathbf{A}(t)x$, where $\mathbf{A}(t) := \mathbf{W}_D(t) \cdots \mathbf{W}_1(t)$.
 1250 We form the learned kernel $\mathbf{k}_t(x, x') = \langle \mathbf{A}(t)x, \mathbf{A}(t)x' \rangle = x^\top \mathbf{G}_t x'$, where $\mathbf{G}_t := \mathbf{A}(t)^\top \mathbf{A}(t)$. We
 1251 then follow the derivation in Appendix B.3 and define the ESD $d^\dagger(t)$ of f^* w.r.t. the kernel \mathbf{k}_t . Since
 1252 $\|X\|_\infty = 1$ μ -a.s., we have $\|f^*\|_\infty^2 = \|\beta^*\|_1^2$; this is used in computing the effective noise level.
 1253

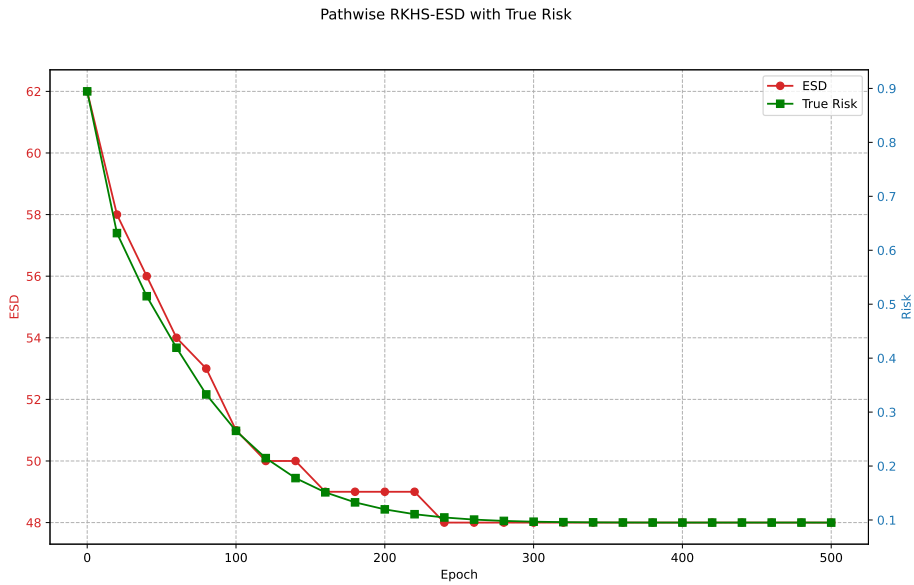


Figure 5: Pathwise ESD and risk under a learned kernel using a 4-layer linear network.

Figure 5 shows that adaptive representation learning progressively reduces the ESD $d^\dagger(t)$ over training time, along with the true risk. This confirms that ESD captures the evolving alignment between signal and kernel.

D PROOF

D.1 PROOFS OF RESULTS ON ESD OF SEQUENCE MODELS

Proof of Theorem 3.2. For any $\nu > 0$, define

$$k_\Lambda(\nu) = \#\{j : \lambda_j \geq \nu\},$$

which counts how many eigenvalues exceed the threshold ν . The KPCR estimator sets

$$\hat{\theta}_i^\nu = \mathbf{1}_{\{\lambda_i \geq \nu\}} z_i, \quad i \in [d].$$

Its squared bias and variance are given by

$$B^{\text{PC}}(v) = \sum_{i:\lambda_i < v} (\theta_i^*)^2, \quad V^{\text{PC}}(v) = \sum_{i:\lambda_i \geq v} \sigma^2 = k_\Lambda(v) \sigma^2.$$

For any threshold v , we can reparameterize the bias and variance using $k = k_\Lambda(v)$ as

$$B^{\text{PC}}(k) = \sum_{i=k+1}^d (\theta_{\pi_i}^*)^2, \quad \text{and} \quad V^{\text{PC}}(k) = k \sigma^2, \quad k = 0, 1, \dots, d.$$

1296 The function $B^{\text{PC}}(k)$ decreases in k , while $V^{\text{PC}}(k)$ increases in k . The risk function is given by
 1297 $\mathcal{R}^{\text{PC}}(k) = B^{\text{PC}}(k) + V^{\text{PC}}(k)$.
 1298

1299 For any integer $k \geq 1$, we have

$$1300 \quad \mathcal{R}^{\text{PC}}(k) = k \left(\sigma^2 + \frac{1}{k} \sum_{i: \lambda_i < \lambda_{\pi_k}} (\theta_i^*)^2 \right).$$

1303
 1304 **Upper bound** For $k = d^\dagger$, we have $\frac{1}{k} \sum_{i: \lambda_i < \lambda_{\pi_k}} (\theta_i^*)^2 \leq \sigma^2$. By definition of the optimal risk, we
 1305 have

$$1306 \quad \mathcal{R}_*^{\text{PC}} \leq \mathcal{R}^{\text{PC}}(d^\dagger) \leq 2d^\dagger \sigma^2.$$

1307 Therefore, the upper bound is proved.

1309 **Lower bound** Without loss of generality, assume $d^\dagger \geq 2$. For any $k \leq d^\dagger - 1$, we have

$$1311 \quad \mathcal{R}^{\text{PC}}(k) \geq B^{\text{PC}}(k) = \sum_{i=k+1}^d (\theta_{\pi_i}^*)^2 \geq \sum_{i=d^\dagger}^d (\theta_{\pi_i}^*)^2 > (d^\dagger - 1)\sigma^2,$$

1314 where the last inequality comes from the definition of d^\dagger . For any $k \in [d^\dagger, d]$, we have

$$1315 \quad \mathcal{R}^{\text{PC}}(k) \geq k\sigma^2 \geq d^\dagger \sigma^2.$$

1317 Therefore, the lower bound is proved. \square

1319 D.2 PROOF ON MINIMAX RESULTS

1320 *Proof of Theorem 4.3.* Throughout the proof, the quota sequence is fixed. Recall the definition of
 1321 M_k in Condition 4.1. Define $\psi(k) = \sigma_0^2 \frac{k}{M_k}$ for any $k \in \bar{K}$. Also define $\mathbf{S}_{\theta, \lambda}(k) = k\mathbf{H}_{\theta, \lambda}(k)$.

1323 We can express $\mathcal{F}_{K, \lambda}$ as follows.

1324 **Lemma D.1.** *Under Condition 4.1, we have*

$$1326 \quad \mathcal{F}_{K, \lambda} = \left\{ \theta \in \mathbb{R}^\infty : \mathbf{S}_{\theta, \lambda}(k) \leq \psi(k) \text{ for all } k \in [\bar{K}] \right\}.$$

1328 *Proof of Lemma D.1.* Observe the relation that

$$1330 \quad \theta \in \mathcal{F}_{K, \lambda} \iff \mathbf{D}_{\theta, \lambda}\left(\frac{\sigma_0^2}{n}\right) \leq K_n, \quad \forall n \geq 1 \iff \mathbf{S}_{\theta, \lambda}(K_n) \leq \sigma_0^2 \frac{K_n}{n}, \quad \forall n \geq 1.$$

1332 By (1) of Condition 4.1, we have

$$1334 \quad \mathbf{S}_{\theta, \lambda}(K_n) \leq \sigma_0^2 \frac{K_n}{n}, \quad \forall n \geq 1 \iff \mathbf{S}_{\theta, \lambda}(k) \leq \psi(k) \text{ for all } k \in [\bar{K}].$$

1336 Therefore, we can rewrite

$$1337 \quad \mathcal{F}_{K, \lambda} = \left\{ \theta \in \mathbb{R}^\infty : \mathbf{S}_{\theta, \lambda}(k) \leq \psi(k) \text{ for all } k \in [\bar{K}] \right\}.$$

1340 \square

1341 Fix any n . Define $\delta = \sqrt{c\sigma_0^2/n}$ with the constant $c = \frac{1}{4} \wedge \tau$, where τ comes from Condition 4.1.
 1342 Consider assigning nonzero signals on the block $B_n = \{\pi_1, \dots, \pi_{K_n}\}$ to construct a subset of
 1343 populations.

1345 Specifically, we define the collection of hypercubes vertices $\mathcal{V} = \{-1, 1\}^{K_n}$. For every vertex $v \in \mathcal{V}$,
 1346 define a parameter vector $\theta^{(v)} = (\theta_j^{(v)})_{j=1}^d$ as follows:

$$1348 \quad \theta_{\pi_i}^{(v)} = \delta v_i, \quad \text{for } i = 1, \dots, K_n, \quad \text{and } \theta_j^{(v)} = 0 \text{ for } j \notin B_n. \quad (32)$$

1349 There are 2^{K_n} such vectors $\{\theta^{(v)}\}$, and they satisfy the following property.

1350 **Lemma D.2.** For any $v \in \mathcal{V}$, the parameter vector $\theta^{(v)}$ constructed in Equation (32) lies in $\mathcal{F}_{K,\lambda}$.
 1351

1352 *Proof of Lemma D.2.* For any $k \in [\bar{K}]$, if $k \geq K_n$, then $\mathbf{S}_{\theta^{(v)},\lambda}(k)$ is 0.
 1353

1354 If $1 \leq k \leq K_n - 1$, then $\mathbf{S}_{\theta^{(v)},\lambda}(k) \leq K_n \delta^2 = c\sigma_0^2 K_n/n$. Denote $k_0 = K_n - 1$ and $L = 1 + M_{k_0}$.
 1355 By definition of M_{k_0} , we have $n \geq L$. Since $k \leq k_0$, we have $L \geq 1 + M_k$. We have
 1356

$$\begin{aligned} \frac{K_n}{n} &\leq \frac{K_n}{L} \\ &= \frac{k_0 + 1}{1 + M_{k_0}} \\ &\leq 2 \frac{k_0}{M_{k_0}} \\ &\leq 2 \frac{k}{M_k}, \end{aligned} \tag{33}$$

1366 where the second last inequality is because $(1 + k_0)/(1 + m) \leq 2k_0/m \Leftrightarrow m + k_0 m \leq 2k_0 + 2k_0 m$
 1367 and the last inequality is due to (2) of Condition 4.1. Since $2c < 1$, we see that $\sigma_0^2 c K_n/n \leq \psi(k)$ for
 1368 all $k < K_n$.

1369 In either case, we have $\mathbf{S}_{\theta^{(v)},\lambda}(k) \leq \psi(k)$ for all $k \in [\bar{K}]$, and thus $\theta^{(v)} \in \mathcal{F}_{K,\lambda}$. \square
 1370

1371 For each $v \in \mathcal{V}$, let P_v be the sampling distribution of the sequence model in Equation (4) with
 1372 $\theta^* = \theta^{(v)}$, $\sigma^2 = \sigma_0^2/n$, and $\{\xi_j\}_{j \in [d]}$ being i.i.d. from $N(0, \sigma^2)$. Let ρ be Hamming distance on \mathcal{V} .
 1373 If v and $w \in \mathcal{V}$ differ in exactly one coordinate (i.e., $\rho(v, w) = 1$), then
 1374

- $\|\theta^{(v)} - \theta^{(w)}\|^2 \geq (2\delta)^2$, and
- the Kullback-Leibler divergence between P_v and P_w satisfies $\text{KL}(P_v \parallel P_w) = \frac{1}{2\sigma^2}(2\delta)^2 = 2c \leq \frac{1}{2}$, and by the Pinsker's inequality, $\|P_v \wedge P_w\| = 1 - \text{TV}(P_v, P_w) \geq 1 - \sqrt{\text{KL}(P_v \parallel P_w)/2} \geq 1/2$.

1383 By Assouad's Lemma (Lemma 2 in Yu (1997)), for any estimator $\hat{\theta}$ based on a sample $Y^{(n)}$ drawn
 1384 from P_v , we have
 1385

$$\sup_{v \in \mathcal{V}} \mathbb{E}_v \|\hat{\theta} - \theta^{(v)}\|^2 \geq K_n \frac{(2\delta)^2}{4} = c\sigma_0^2 \frac{K_n}{n}.$$

1388 \square
 1389

1390 *Proof of Theorem 3.3.* The upper bound is given by Theorem 3.2, so we only need to prove the lower
 1391 bound. The main idea is the same as the proof for Theorem 4.3.

1392 Let $\delta = \sqrt{c\sigma_0^2/n}$ with the constant $c = \frac{1}{4}$. Let $B_n = \{\pi_1, \dots, \pi_{K_n}\}$. We define the collection
 1393 of hypercubes vertices $\mathcal{V} = \{-1, 1\}^K$. For every vertex $v \in \mathcal{V}$, define a parameter vector $\theta^{(v)} =$
 1394 $(\theta_j^{(v)})_{j=1}^d$ as in Equation (32). There are 2^K such vectors $\{\theta^{(v)}\}$. For each $v \in \mathcal{V}$, let P_v be the
 1395 sampling distribution of the sequence model in Equation (4) with $\theta^* = \theta^{(v)}$, $\sigma^2 = \sigma_0^2/n$, and
 1396 $\{\xi_j\}_{j \in [d]}$ being i.i.d. normal. Let ρ be Hamming distance on \mathcal{V} . The rest of the proof is identical to
 1397 that of Theorem 4.3 and is omitted. \square
 1398

1400 **D.3 DETAILS OF EXAMPLES IN EQUATION (9)**
 1401

1402 We provide the details of Equation (9) for illustration of the concepts of ESD and span profile through
 1403 several examples.

Example D.3 (Polynomial spectrum with source condition). Assume $\lambda_i = i^{-\beta}$ for some $\beta > 0$ and the source condition $\sum_{i=1}^d \lambda_i^{-s} \theta_i^{*2} \leq R$ with $s > 0$. The trade-off function satisfies

$$\mathbf{H}_{\theta^*, \lambda}(k) = \frac{1}{k} \sum_{i>k} \theta_i^{*2} \leq \frac{\lambda_k^s}{k} \sum_{i>k} \lambda_i^{-s} \theta_i^{*2} \leq R k^{-(1+s\beta)},$$

which follows that $\mathbf{D}_{\theta^*, \lambda}(\sigma^2) \lesssim [\sigma^2]^{-\frac{1}{1+s\beta}}$. Since $\mathbf{D}_{\theta^*, \lambda}(\sigma^2) \leq d$, the optimal risk of PC estimator satisfies

$$\mathcal{R}_*^{\text{PC}} \lesssim \min \left([\sigma^2]^{\frac{s\beta}{1+s\beta}}, d\sigma^2 \right).$$

In Example D.3, we note that for $\sigma^2 = \sigma_0^2/n$, the upper bound becomes $\sigma_0^2 \min \left(n^{-\frac{s\beta}{1+s\beta}}, d/n \right)$. When $d = \infty$, this upper bound matches the well-known optimal rate under the source condition and the polynomial eigen-decay condition. When $d < \infty$, there is a phase transition around $d_0 \asymp n^{\frac{1}{1+s\beta}}$: if $d \lesssim d_0$, the upper bound is $d\sigma_0^2/n$; if $d \gtrsim d_0$, the upper bound is the same as if $d = \infty$. Using the span profile, we can extend classical results to finite-dimensional models and reveal new phenomena.

Example D.4 (Polynomial signals ($\alpha > 1$)). Suppose $\theta_i^* = i^{-\alpha/2}$ for some constant $\alpha > 1$, and $\{\lambda_i\}_1^d$ are decreasing. By an integral approximation, we can get $\mathbf{H}_{\theta^*, \lambda}(k) \leq \frac{1}{\alpha-1} k^{-\alpha}$. Therefore, we have $\mathbf{D}_{\theta^*, \lambda}(\sigma^2) \lesssim [\sigma^2]^{-\frac{1}{\alpha}}$. The optimal risk of PC estimator satisfies

$$\mathcal{R}_*^{\text{PC}} \leq 2\sigma^2 \mathbf{D}_{\theta^*, \lambda}(\sigma^2) \lesssim \min \left([\sigma^2]^{1-\frac{1}{\alpha}}, d\sigma^2 \right).$$

Example D.5 (Polynomial signals ($\alpha = 1$)). Suppose $d < \infty$, $\theta_i^* = i^{-1/2}$, and $\{\lambda_i\}_1^d$ are decreasing. We show in the supplementary material that for some constant C , if $d\sigma^2 \leq e$, then $\mathcal{R}_*^{\text{PC}} \leq C d\sigma^2$, and if $d\sigma^2 > e$, then $\mathcal{R}_*^{\text{PC}} \leq C \log(d\sigma^2 / \log(d\sigma^2))$.

Example D.6 (Polynomial signals ($\alpha < 1$)). Suppose $d < \infty$, $\theta_i^* = i^{-1/2}$, and $\{\lambda_i\}$ is decreasing. We show in the supplementary material that $\mathcal{R}_*^{\text{PC}} \lesssim d \min(d^{-\alpha}, \sigma^2)$.

These examples suggest that using our framework of span profile, we are able not only to recover classical results but also to extend it to various settings where the classical framework is inapplicable.

Details of Example D.5. We have $\mathbf{H}_{\theta^*, \lambda}(k) \leq k^{-1} \int_k^d \frac{1}{x} dx = k^{-1} (\log d - \log k)$.

By dropping the term $\log k$ in the numerator, it is easy to see that a sufficient condition for $\mathbf{H}_{\theta^*, \lambda}(k) \leq \sigma^2$ is given by $k \geq \sigma^{-2} \log(d)$. Therefore, we have $\mathbf{D}_{\theta^*, \lambda}(\sigma^2) \leq \lceil \sigma^{-2} \log(d) \rceil$.

The upper bound can be improved. Suppose $A > 1$ satisfies $d\sigma^2 \leq A \log A$. If $k \geq \sigma^{-2} \log A$, then

$$\frac{k}{d} \geq \frac{\log A}{d\sigma^2} \geq \frac{d\sigma^2/A}{d\sigma^2} = \frac{1}{A},$$

which follows that $\mathbf{H}_{\theta^*, \lambda}(k) \leq k^{-1} \log A \leq \sigma^2$. Therefore,

$$\mathbf{D}_{\theta^*, \lambda}(\sigma^2) \leq \min(d, \lceil \sigma^{-2} \log A \rceil).$$

By elementary calculus, if $y > e$, the solution to $x \log x = y$ satisfies that $x \in (e, y)$, and thus $\log x \in (1, \log(y))$, which implies $x > y/\log(y)$ and thus $x < y/\log(y/\log(y)) = y/(\log y - \log \log y) < 2y/\log(y)$.

If $d\sigma^2 \leq e$, we can take $A = e$ and conclude

$$\mathcal{R}_*^{\text{PC}} \leq 2\sigma^2 \mathbf{D}_{\theta^*, \lambda}(\sigma^2) \lesssim d\sigma^2.$$

If $d\sigma^2 > e$, then $\log(d\sigma^2) > 1$ and we can take $A = 2d\sigma^2 / \log(d\sigma^2)$, which implies that

$$\mathcal{R}_*^{\text{PC}} \leq 2\sigma^2 \mathbf{D}_{\theta^*, \lambda}(\sigma^2) \lesssim \log(d\sigma^2) - \log(\log(d\sigma^2)).$$

□

Detail of Example D.6. By an integral approximation, we see that

$$\mathbf{H}_{\theta^*, \lambda}(k) \asymp k^{-1} (d^{1-\alpha} - k^{1-\alpha}).$$

1458 **Case 1:** $\sigma^2 d^\alpha < 2$. We have the default bound $\mathbf{D}_{\theta^*, \lambda}(\sigma^2) \leq d$.
 1459
 1460 **Case 2:** $\sigma^2 d^\alpha \geq 2$. If $k \geq d^{1-\alpha}/\sigma^2$, then $\mathbf{H}_{\theta^*, \lambda}(k) \leq \sigma^2$. Therefore, we have $\mathbf{D}_{\theta^*, \lambda}(\sigma^2) \leq \lceil d^{1-\alpha}/\sigma^2 \rceil$, which is not larger than $\lceil d/2 \rceil$.
 1461
 1462 Combining both cases, we have $\mathbf{D}_{\theta^*, \lambda}(\sigma^2) \lesssim d \min(1/(d^\alpha \sigma^2), 1)$. Multiplying by $2\sigma^2$ on both
 1463 sides, we have
 1464

$$\mathcal{R}_*^{\text{PC}} \leq 2\sigma^2 \mathbf{D}_{\theta^*, \lambda}(\sigma^2) \lesssim d \min(d^{-\alpha}, \sigma^2).$$

□

1465
 1466
 1467 **D.4 DETAIL OF EXAMPLE 4.4**

1468 Let $f(x) = \sigma_0^2 x e^{-x^b}$. Then $(\theta_{j+1}^*)^2 = f(j) - f(j+1)$ for $j \geq 1$. Since $\theta_1^* = 0$, for any $k \geq 1$, the
 1469 tail sum is
 1470

$$\sum_{j=k+1}^{\infty} (\theta_j^*)^2 = \sum_{j=k}^{\infty} (f(j) - f(j+1)) = f(k) = \sigma_0^2 k e^{-k^b},$$

1471 since $f(N) \rightarrow 0$. As $\{\lambda_j\}$ is assumed to be decreasing, the trade-off function is $\mathbf{H}_{\theta^*, \lambda}(k) =$
 1472 $\frac{1}{k} \sum_{j=k+1}^{\infty} (\theta_j^*)^2 = \sigma_0^2 e^{-k^b}$.
 1473

1474 For any $n \geq 3$, let $k = K_n$. By definition of the ceiling function, $k \geq (\log n)^{1/b}$, which implies
 1475 $k^b \geq \log n$, and thus $e^{k^b} \geq n$. Then, $\mathbf{H}_{\theta^*, \lambda}(k) = \sigma_0^2 e^{-k^b} \leq \sigma_0^2/n$. By Proposition 3.5, we have
 1476 $\mathbf{D}_{\theta^*, \lambda}(\sigma_0^2/n) \leq k = K_n$.
 1477

1478 Since this holds for all sufficiently large n , we conclude that $\theta^* \in \mathcal{F}_K$. Theorem 4.3 guarantee the
 1479 optimal convergence rate is $\Theta(\sigma_0^2 K_n/n) = \Theta(\sigma_0^2 (\log n)^{1/b}/n)$.
 1480

1481 Lastly, we consider the standard source condition that for some $s > 0$, there is some constant R_s
 1482 such that
 1483

$$\sum_{j=1}^{\infty} \lambda_j^{-s} (\theta_j^*)^2 \leq R_s. \quad (34)$$

1484 Let's assume a polynomial eigenvalue decay $\lambda_j \asymp j^{-\gamma}$ for some $\gamma > 0$. Let S be the left hand side
 1485 of Equation (34). Since $\theta_1^* = 0$, we have
 1486

$$\begin{aligned} S &= \sum_{j=2}^{\infty} (j^{-\gamma})^{-s} (\theta_j^*)^2 = \sum_{j=2}^{\infty} j^{s\gamma} (\theta_j^*)^2 \\ &= \sum_{k=1}^{\infty} (k+1)^{s\gamma} (\theta_{k+1}^*)^2. \end{aligned}$$

1487 Using $(\theta_{k+1}^*)^2 = f(k) - f(k+1)$ with $f(x) = \sigma_0^2 x e^{-x^b}$:
 1488

$$S = \sum_{k=1}^{\infty} (k+1)^{s\gamma} (f(k) - f(k+1)).$$

1489 Using summation by part, we have
 1490

$$S = (1+1)^{s\gamma} f(1) - \lim_{N \rightarrow \infty} (N+1)^{s\gamma} f(N+1) + \sum_{k=1}^{\infty} ((k+2)^{s\gamma} - (k+1)^{s\gamma}) f(k+1).$$

1491 Since $\lim_{N \rightarrow \infty} (N+1)^{s\gamma} N e^{-N^b} = 0$ for $b \geq 1$, the limit term vanishes. $f(1) = \sigma_0^2 e^{-1}$. The
 1492 difference term $(k+2)^{s\gamma} - (k+1)^{s\gamma} > 0$. $f(k+1) = \sigma_0^2 (k+1) e^{-(k+1)^b} > 0$. The sum
 1493 $\sum_{k=1}^{\infty} ((k+2)^{s\gamma} - (k+1)^{s\gamma}) f(k+1)$ converges because $f(k+1)$ decays faster than any polynomial
 1494 grows. Specifically, $(k+2)^{s\gamma} - (k+1)^{s\gamma} \approx s\gamma k^{s\gamma-1}$, and the sum $\sum k^{s\gamma-1} (k+1) e^{-(k+1)^b}$
 1495 converges. Therefore, S converges for any $s > 0$ and any $\gamma > 0$.
 1496

1512 The classical theory predicts a rate of $n^{-\frac{s\gamma}{s\gamma+1}}$. Since the source condition holds for arbitrarily
 1513 large s , the classical rate can be made arbitrarily close to n^{-1} . However, this n^{-1} rate ignores the
 1514 logarithmic factor $(\log n)^{1/b}$ present in the true optimal rate $\Theta(\sigma_0^2(\log n)^{1/b}/n)$. Thus, the traditional
 1515 convergence analysis based on the source condition is not sharp for this signal.
 1516

1517 E PROOFS FOR RESULTS IN APPENDIX B

1519 *Proof of Proposition B.3. Upper bound:* Take $k = d^\dagger$, and we have $B(k) = k\mathbf{H}_{f^*,\lambda}(k) \leq k\sigma^2$.
 1520 The variance $V(k) = \sum_{j=1}^k (\sigma_0^2 + \tau_j^2)/n \leq k(\sigma_0^2 + \sigma_{f,4}^2)/n = k\sigma^2$. Thus $\mathcal{R}_*^{\text{PC}} \leq \mathcal{R}_k = B(k) +$
 1521 $V(k) \leq 2k\sigma^2 = 2d^\dagger\sigma^2$.

1523 **Lower bound:** Let k^* be the optimal tuning parameter. If $k^* \geq d^\dagger$, then $\mathcal{R}_* \geq d^\dagger\sigma_0^2/n$. If
 1524 $k^* \leq d^\dagger - 1$, by definition of ESD, we have $\mathcal{R}_* \geq B(k^*) \geq B(d^\dagger - 1) \geq (d^\dagger - 1)\sigma^2 \geq (d^\dagger - 1)\sigma_0^2/n$.
 1525

□

1527 *Proof of Theorem B.5. Upper bound:* The upper bound follows the proof of the upper bound in
 1528 Proposition B.3. To see this, we note that since $f^* \in \mathcal{F}_{K,\lambda,n}$, we have $\|f\|_\infty^2 \leq \sigma_0^2 C_0^2$. Therefore,
 1529 $\sigma^2 \leq \bar{\sigma}^2/n$. We can then apply the argument in Proposition B.3 with σ^2 replaced by $\bar{\sigma}^2/n$.
 1530

1531 **Lower bound:** We establish the lower bound using Assouad's method.

1532 Let $m = \lfloor c_1 K \rfloor$. Consider the first m eigenfunctions $\{\psi_{\pi_j}\}_{j \leq m}$ corresponding to the largest
 1533 eigenvalues $\{\lambda_{\pi_j}\}_{j \leq m}$. Define the collection of hypercubes vertices $\mathcal{V} = \{-1, 1\}^m$. For every vertex
 1534 $v \in \mathcal{V}$, define a function

$$1535 \quad 1536 \quad 1537 \quad f^{(v)}(x) = \gamma \sum_{j=1}^m v_j \psi_{\pi_j}(x), \quad (35)$$

1538 where the amplitude γ is to be chosen. Since \mathbf{k} is (K, n) -regular, we have

$$1539 \quad 1540 \quad 1541 \quad f^{(v)}(x)^2 \leq \gamma^2 \sum_{j \leq m} \lambda_{\pi_j}^{-1} \sum_{j \leq m} \lambda_j \psi_{\pi_j}^2(x) \leq \gamma^2 C_1 n \kappa^2, \quad (36)$$

1542 where $\kappa^2 = \sup_x \mathbf{k}(x, x) < \infty$ by assumption.

1543 We choose

$$1544 \quad 1545 \quad \gamma^2 = n^{-1} \min \left(\frac{\bar{\sigma}^2}{4(1 + C_0^2)}, \frac{\sigma_0^2 C_0^2}{C_1 \kappa^2} \right).$$

1546 It then follows that $\|f^{(v)}\|_\infty^2 \leq \sigma_0^2 C_0^2$.

1547 For each $v \in \mathcal{V}$, let P_v be the sampling distribution of $\{z_i = (x_i, y_i)\}_{i \leq n}$ from the regression model
 1548 Equation (20) with $f^* = f^{(v)}$. Let ρ be the Hamming distance on \mathcal{V} . If v and $w \in \mathcal{V}$ differ in exactly
 1549 one coordinate (i.e., $\rho(v, w) = 1$), then

- 1552 • $\|f^{(v)} - f^{(w)}\|_{L^2(\mu)}^2 \geq (2\gamma)^2$, and
- 1553 • the Kullback-Leibler divergence between P_v and P_w satisfies $\text{KL}(P_v \parallel P_w) = \frac{n}{2\sigma_0^2}(2\gamma)^2 \leq$
 1554 $\frac{1}{2}$, where the last equation is due to the definition of the constant c . By the Pinsker's
 1555 inequality, $\|P_v \wedge P_w\| = 1 - \text{TV}(P_v, P_w) \geq 1 - \sqrt{\text{KL}(P_v \parallel P_w)/2} = 1/2$.

1556 By Assouad's Lemma (Lemma 2 in Yu (1997)), for any estimator \hat{f} based on a sample $\{z_i =$
 1557 $(x_i, y_i)\}_{i \leq n}$ drawn from P_v , we have

$$1558 \quad 1559 \quad 1560 \quad \sup_{v \in \mathcal{V}} \mathbb{E}_v \|\hat{\theta} - \theta^{(v)}\|^2 \geq m \frac{(2\gamma)^2}{4} = c \frac{\sigma_0^2 K}{n},$$

1561 where c is a constant that depends on C_0, κ, c_1, C_1 .
 1562

□

1566 *Proof of Theorem B.6.* Since

$$1567 \quad \mathcal{F}_{\mathbf{K}, \mathbf{k}} = \bigcap_{n \geq n_0} \mathcal{F}_{K_n, \mathbf{k}}^{(n)},$$

1569 the upper bound $\bar{\sigma}^2 K_n / n$ is immediately implied by Theorem B.5.

1571 The lower bound follows the same argument as in the proof of Theorem 4.3, but replace the con-
 1572 struction of parameter vectors in Equation (32) by the construction of functions in Equation (35).
 1573 Following the proof for Theorem 4.3, we use Condition 4.1 to ensure the constructed functions
 1574 all belong to $\mathcal{F}_{\mathbf{K}, \mathbf{k}}$. Then the lower bound is given using Assouad’s Lemma as in the proof of
 1575 Theorem B.5. Below, we provide the details for completeness.

1576 Mercer’s theorem yields

$$1577 \quad \mathbf{k}(\mathbf{x}, \mathbf{x}') = \sum_{j=1}^{\infty} \lambda_j \psi_j(\mathbf{x}) \psi_j(\mathbf{x}'), \quad \mathbf{x}, \mathbf{x}' \in \mathcal{X}, \quad (37)$$

1581 where $\{\psi_j\}_{j \geq 1}$ is a $L^2(\mathcal{X}, \mu)$ -orthonormal eigenbasis. Without loss of generality, assume λ_j is sorted
 1582 decreasingly.

1583 Fix n and set $m := \lfloor c_1 K_n \rfloor$ where c_1 comes from Assumption B.4.

1585 For a sign vector $v = (v_j)_{j \leq m} \in \{-1, +1\}^m$, define the sequence of coefficients as

$$1586 \quad \theta_j^{(v)} := \begin{cases} \gamma v_j, & j \leq m, \\ 0, & j > m, \end{cases} \quad f_v(x) := \sum_{j \geq 1} \theta_j^{(v)} \psi_j(x) = \gamma \sum_{j \leq m} v_j \psi_j(x).$$

1589 Since \mathbf{k} is (K_n, n) -regular, Equation (36) holds and reads as

$$1590 \quad f^{(v)}(x)^2 \leq \gamma^2 C_1 n \kappa^2.$$

1592 If $\gamma^2 C_1 n \kappa^2 \leq \sigma_0^2 C_0^2$, then $\|f^{(v)}\|_{\infty}^2 \leq \sigma_0^2 C_0^2$. Furthermore, if $m \gamma^2 \leq (2n)^{-1} \sigma_0^2 K_n$, we can the
 1593 same argument in Lemma D.2 (in particular, using Condition 4.1 to derive Equation (33)) to show
 1594 that $f^{(v)} \in \mathcal{F}_{\mathbf{K}, \mathbf{k}}$.

1595 We choose

$$1597 \quad \gamma^2 = n^{-1} \min \left(\sigma_0^2, \frac{\bar{\sigma}^2}{4(1 + C_0^2)}, \frac{\sigma_0^2 C_0^2}{C_1 \kappa^2} \right),$$

1599 which implies $f^{(v)} \in \mathcal{F}_{\mathbf{K}, \mathbf{k}}$.

1600 We then follows the same argument in the proof of lower bound in Theorem B.5 to obtain

$$1602 \quad \sup_{v \in \mathcal{V}} \mathbb{E}_v \|\hat{\boldsymbol{\theta}} - \boldsymbol{\theta}^{(v)}\|^2 \geq m \frac{(2\gamma)^2}{4} = c \frac{\sigma_0^2 K}{n},$$

1604 where c is a constant that depends on C_0, κ, c_1, C_1 .

1605 \square

1608 F PROOFS FOR RESULT ON OVERPARAMETERIZED GRADIENT FLOW

1610 In this section, we prove Theorem 5.2. The high-level idea is as follows: To show the ESD decreases,
 1611 it is enough to show that the squared signal tail sorted by the learned eigenvalues at the new time
 1612 is smaller than that at the old time. The key idea is to study how the gradient flow changes the
 1613 eigenvalues depending on the signal’s strength. Our analysis reveals that eigenvalues associated
 1614 with the strong signal coordinates will often grow much faster than those associated with weak ones.
 1615 Consequently, more of the largest learned eigenvalues correspond to the strong signals. This implies
 1616 that the signal energy is concentrated in the top principal components of the learned kernel, which
 1617 reduces the signal tail and thus reduces the ESD.

1618 We first remark that for any $j \in [d]$, due to the same initialization $b_{j,k} = b_0$ for all k , one can
 1619 prove that throughout the time $b_{j,k}$ (for all k) have the same value b_j . Therefore, we can rewrite the
 over-parameterization as $\theta_j = a_j b_j^D \beta_j$, and consider the following gradient flow

$$\begin{aligned}\dot{a}_j &= -\nabla_{a_j} L_j = b_j^D \beta_j(z_j - \theta_j), \\ \dot{b}_j &= -\nabla_{b_j} L_j = D a_j b_j^{D-1} \beta_j(z_j - \theta_j), \\ \dot{\beta}_j &= -\nabla_{\beta_j} L_j = a_j b_j^D (z_j - \theta_j), \\ a_j(0) &= \lambda_j^{\frac{1}{2}} > 0, \quad \mathbf{b}(0) = b_0 > 0, \quad \boldsymbol{\beta}(0) = 0,\end{aligned}\tag{38}$$

where $L_j = \frac{1}{2}(z_j - \theta_j)^2$.

F.1 PROOF OF THEOREM 5.2

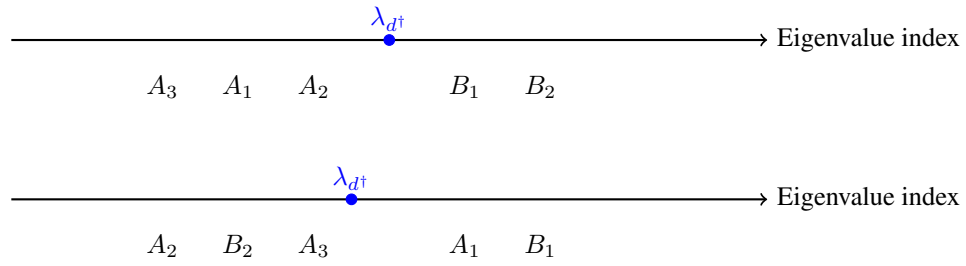
Recall that we define these sets as follows:

$$\begin{aligned} A_1 &:= \{i : \pi_{t_1}^{-1}(i) < d^\dagger(t_1), \lambda_i < c \cdot D^{-\frac{D}{D+2}} \cdot M^{\frac{2}{D+2}}, |\theta_i^*| < \tilde{\sigma}\}; \\ A_2 &:= \{i : \pi_{t_1}^{-1}(i) < d^\dagger(t_1), |\theta_i^*| > M\}; \\ A_3 &:= \{i : \pi_{t_1}^{-1}(i) < d^\dagger(t_1), |\theta_i^*| < \tilde{\sigma}\} \setminus A_1. \end{aligned}$$

and

$$B_1 := \{i : \pi_{t_1}^{-1}(i) > d^\dagger(t_1), |\theta_i^*| < \tilde{\sigma}\}; \quad B_2 := \{i : \pi_{t_1}^{-1}(i) > d^\dagger(t_1), |\theta_i^*| > M\}.$$

where $\tilde{\sigma}^2 \leq \min\{\frac{|B_1|}{C_{B_1}}\varepsilon^2, c'\varepsilon^2\}$, $C_{B_1} = \min\{1 \vee (|A_1| - |B_1|), |B_2|\}$ and c' is a constant ≤ 1 . Also recall from the assumption of Theorem 5.2 that suppose $|\theta_i^*| > |\theta_j^*| > M$, then if $C_{max}M > |\theta_i^*|$, $\eta_{i,j} = |\theta_i^*| - |\theta_j^*| > C_\eta \varepsilon'$; otherwise, $\frac{|\theta_i^*|}{|\theta_j^*|} > (1 + \frac{c_\eta}{D})$.



Throughout the proof, we assume all the events $\{E_k\}$ in Lemma F.9 hold. We divide the proof into several parts.

Part 1: Very small eigenvalues can be ignored. From Assumption 5.1, we have $\inf_{j \in S} \lambda_j > n^{-\delta}$, where δ is a constant. For $i \in R$, if $\lambda_i \leq n^{-(2.1\delta\vee 5)}$, Proposition F.2 implies that at t_2 , we have

$$\tilde{\lambda}_i(t_2) < n^{1.1} \cdot \lambda_i^{0.99} < n^{-\delta}.$$

If B_2 is empty, then all the signals in R is 0 by the definition of $\tilde{\sigma}$. Otherwise, for $\tilde{\lambda}_i < n^{-\delta}$, and $\lambda_{\pi_{t_1}(d^\dagger(t_1))} > n^{-\delta}$. According to the monotonicity of eigenvalues in Lemma F.4, any the index i such that $\lambda_i < n^{-(2.1\delta\vee 5)}$ can not rank among the first $d^\dagger(t_1)$ at time t_2 , i.e., it makes no difference to the variation of d^\dagger from t_1 to t_2 .

Part 2: Analysis for B_2

If $j \in B_2$, by Proposition F.1, we have $|\theta_j(t_2) - \theta_j^*| < \varepsilon' \leq \frac{1}{CM}M$. We apply Equation (50) to get $\beta^2 = a^2 - \lambda < a^2$ and $\beta^2 = D^{-1}(b^2 - b_0^2) < D^{-1}b^2$, and thus

$$|\theta_j(t)| = a_j(t) b_j^D(t) |\beta_j(t)| \leq a_j(t) b_j^D(t) \cdot a_j^{\frac{1}{D+1}}(t) \cdot D^{-\frac{D}{2(D+1)}} b_j^{\frac{D}{D+1}}(t) = D^{-\frac{D}{2(D+1)}} [a_j(t) b_j^D(t)]^{\frac{D+2}{D+1}}.$$

1674

Therefore, at time $t = t_2$, we have for some constants c and C that

1675

1676

1677

1678

1679

1680

1681

1682

1683

$$D^{-\frac{D}{2(D+1)}} [a_j(t)b_j^D(t)]^{\frac{D+2}{D+1}} \geq |\theta_j(t)| \geq (1-c)M, \implies a_j(t)b_j^D(t) \geq C \cdot D^{\frac{D}{2(D+2)}} M^{\frac{D+1}{D+2}}.$$

It follows that $\tilde{\lambda}_j(t_2) \geq cD^{\frac{D}{2(D+2)}} M^{\frac{2(D+1)}{D+2}}$. Moreover, for λ_j and $D^{-1}b_0^2$ that are much smaller than $c \cdot D^{-\frac{D}{D+2}} \cdot M^{\frac{2}{D+2}}$, we use Equation (50) to obtain

$$\beta_j^2 \asymp a_j^2 \asymp D^{-1}b_j^2 \asymp D^{-\frac{D}{D+2}} M^{\frac{2}{D+2}}. \quad (39)$$

Part 3: A_1 and B_2 will exchange

In the following, suppose $i \in A_1$ and $j \in B_2$. We will prove $\tilde{\lambda}_i(t_2) < \tilde{\lambda}_j(t_2)$ by contradiction.

If $\tilde{\lambda}_i(t_2) \geq \tilde{\lambda}_j(t_2)$, then by Proposition F.1, we have

$$|\theta_i(t_2) - \theta_i^*| < 2\varepsilon'.$$

By Lemma F.4, we have

$$|\theta_i(t_2)| < |\theta_i^*| + \kappa_i.$$

We have $|\theta_j| > C_D |\theta_i|$ where $C_D > 1 + \frac{c}{D}$ for $M = C_M \varepsilon > C_M |\kappa_i|$. At t_2 , the following holds:

$$|\beta_j(t_2)| > C_D |\beta_i(t_2)|.$$

It follows that $a_i^2(t_2)b_i^{2D}(t_2) > a_j^2(t_2)b_j^{2D}(t_2)$. Combined with Equation (50), we have

$$\frac{\beta_i^2(t_2) + \lambda_i}{\beta_j^2(t_2) + \lambda_j} > \left(\frac{D\beta_j^2(t_2) + b_0^2}{D\beta_i^2(t_2) + b_0^2} \right)^D > \left(\frac{C_D}{1 + \delta} \right)^D = (1 + c(C_D - 1))^D. \quad (40)$$

Recall that $|\beta_i(t_2)| < \frac{1}{C_D} |\beta_j(t_2)|$ and $\beta_j^2(t_2) > CD^{-\frac{2}{D+2}} M^{\frac{2}{D+2}}$. If we choose the constant C_D such that $(1 + c(C_D - 1))^D$ is large enough, the inequality Equation (40) will implies λ_i larger than its upper bound in the definition of set A_1 . (We can let $C_D = 1 + c \cdot \frac{1}{D}$.)

The contraction shows that $\tilde{\lambda}_i(t_2) < \tilde{\lambda}_j(t_2)$ for any $i \in A_1, j \in B_2$. If the sets A_1 and B_2 are not empty when $t = t_1$, then from t_1 to t_2 , the elements of set B_2 will be arranged before those of set A_1 according to the eigenvalue index. We only need $\lambda_i < c \cdot D^{-\frac{D}{D+2}} M^{\frac{2}{D+2}}$.

For the same reason, the elements of set A_2 will be arranged before those of set A_1 at t_2 .

Part 4: A_2 and B_2 will be monotonously nonincreasing

In the following, W.L.O.G we assume $\theta^*, \theta^* > 0$. We prove that given $i \in A_2, j \in B_2$, if $\theta_i^* > \theta_j^*$, we have $\tilde{\lambda}_i(t_2) > \tilde{\lambda}_j(t_2)$.

If $\theta_i^* - \theta_j^* > C_\eta \varepsilon$, we have $z_i > z_j$. Then by Proposition F.1, we have at t_2

$$|\theta_i(t_2) - \theta_i^*| < 2\varepsilon', \quad |\theta_j(t_2) - \theta_j^*| < 2\varepsilon'.$$

If $\lambda_i \geq \lambda_j$, by Equation (38) and monotonicity, we always have $\tilde{\lambda}_i(t) > \tilde{\lambda}_j(t)$.

Now, consider the case where $\lambda_i < \lambda_j$. By the definition of A_1 and B_2 , we have $\lambda_j < c \cdot D^{-\frac{D}{D+2}} \cdot M^{\frac{2}{D+2}}$. Next, we use proof by contradiction. Note that

$$\frac{\theta_i(t_2)}{\theta_j(t_2)} = \frac{\tilde{\lambda}_i^{\frac{1}{2}}(t_2)\beta_i(t_2)}{\tilde{\lambda}_j^{\frac{1}{2}}(t_2)\beta_j(t_2)} \geq C_D.$$

If $\tilde{\lambda}_i(t) \leq \tilde{\lambda}_j(t)$, then $\beta_i(t_2) > C_D \beta_j(t_2)$. By Equation (39), both $\beta_i(t_2)$ and $\beta_j(t_2)$ are much larger than $D^{-\frac{1}{2}} b_0$. It then follows that

$$\left(\frac{D\beta_i^2(t_2) + b_0^2}{D\beta_j^2(t_2) + b_0^2} \right)^D > C^*$$

1728 where C^* is a constant that can be made large enough by choosing C_D . Therefore, using the same
 1729 reason as in Equation (40), we can get
 1730

$$\frac{\beta_i^2(t_2) + \lambda_i}{\beta_j^2(t_2) + \lambda_j} < \frac{1}{C^*},$$

1733 which is impossible because $\beta_i(t_2) > C_D \beta_j(t_2)$ and $\beta_i^2(t_2) > C \lambda_j$.
 1734

1735 **Part 5: B_1 will stay behind A_2, A_3 and B_2**

1736 In the following, let $j \in B_1$. By $y = \theta^* + \xi$, we have $|z_j| < \tilde{\sigma} + \varepsilon'$. By Equation (53) and $|\theta_j| < |z_j|$,
 1737 we have

$$|\beta_j(t_2)| \leq \left(D^{-D/2} |z_j| \right)^{1/(D+2)}.$$

1740 Then by $\tilde{\lambda}_j(t_2) = (\beta_j^2(t_2) + \lambda_j)(D\beta_j^2(t_2) + b_0^2)^D < (1 + \frac{1}{c \cdot D})^D b_0^{2D} (\beta_j^2(t_2) + \lambda_j)$. Then if
 1741 $\lambda_j < c \cdot D^{-D/(D+2)} \varepsilon^{2/(D+2)}$, given any $i \in A_3 \cup A_2 \cup B_2$, $\tilde{\lambda}_i(t_2) > \tilde{\lambda}_j(t_2)$. Otherwise, we have
 1742 $\lambda_j > C \cdot D^{-D/(D+2)} \varepsilon^{2/(D+2)}$, then we have $\tilde{\lambda}_j(t_2) < (1 + \delta) \tilde{\lambda}_j(t_1)$, then by the definition of d^\dagger ,
 1743 at least d^\dagger eigenvalues will larger than $\tilde{\lambda}_j(t_2)$.
 1744

1745 **Part 6: A_3 will be ahead of A_1**

1746 by the same reason between B_1 and A_1 , for given $j \in A_3$, $\tilde{\lambda}_j(t_2) = (\beta_j^2(t_2) + \lambda_j)(D\beta_j^2(t_2) + b_0^2)^D <$
 1747 $(1 + \frac{1}{c \cdot D})^D b_0^{2D} (\beta_j^2(t_2) + \lambda_j)$, and $i \in A_1$, $\lambda_i < c \cdot D^{-D/(D+2)} \varepsilon^{2/(D+2)}$, combined with
 1748

$$|\beta_i(t_2)| \leq \left(D^{-D/2} |z_i| \right)^{1/(D+2)}.$$

1751 then we have $\tilde{\lambda}_j(t_2) > \tilde{\lambda}_i(t_2)$ for c is small and C is large enough.
 1752

1753 **Part 7: Ordering of the spectrum at t_2 and $d^\dagger(t_1) \geq d^\dagger(t_2)$**

1754 To show $d^\dagger(t_2) \leq d^\dagger(t_1)$, it suffices to show $\mathbf{H}_{\theta^*, \tilde{\lambda}(t_2)}(d^\dagger(t_1)) < \mathbf{H}_{\theta^*, \tilde{\lambda}(t_2)}(d^\dagger(t_2))$, which is
 1755 equivalent to prove the following difference
 1756

$$\sum_{i: \pi_{t_1}^{-1}(i) > d^\dagger(t_1)} |\theta_i^*|^2 - \sum_{i: \pi_{t_2}^{-1}(i) > d^\dagger(t_1)} |\theta_i^*|^2 \quad (41)$$

1759 is nonnegative.
 1760

1761 We will make use of $|A_1| + |A_2| + |A_3| = d^\dagger(t_1)$ and consider two possible cases.
 1762

- 1763 Case 1: $|B_2| \leq |A_1|$. Since $B_2 \cup A_2$ is ahead of $A_1 \cup B_1$, we can see that the eigenvalue of
 1764 the last element of $B_2 \cup A_2$ is among the top d^\dagger ones. Because A_3 is ahead of $A_1 \cup B_1$, so
 1765 only some of A_1 is swapped to the later part. Also some of B_1 may arise ahead some of A_1
 1766 . Therefore, to analyze the ordering of eigenvalues $\tilde{\lambda}(t_2)$, we define

$$\begin{aligned} B_{11} &= \{i \in B_1 : \pi_{t_2}^{-1}(i) \leq d^\dagger(t_1)\}, \\ 1767 \quad A_{11} &= \{i \in A_1 : \pi_{t_2}^{-1}(i) > d^\dagger(t_1)\}. \end{aligned} \quad (42)$$

1770 Here A_{11} contains all the elements that move from the top $d^\dagger(t_1)$ part to the later part,
 1771 while B_2 and B_{11} are the elements that move from the later part to the top $d^\dagger(t_1)$ part.
 1772 Therefore, we have $|A_{11}| = |B_2| + |B_{11}|$. Let $C_{B_1} := \min\{(|A_1| - |B_2|)_+, |B_1|\}$. We
 1773 have $|B_{11}| \leq C_{B_1}$.

1774 W.L.O.G., we can write divide A_{11} into two subsets such that $|A_{111}| = |B_2|$ and $|A_{112}| = |B_{11}|$. We can then write Equation (41) as
 1775

$$\|\theta_{B_2}^*\|_2^2 + \|\theta_{B_{11}}^*\|_2^2 - \|\theta_{A_{111}}^*\|_2^2 - \|\theta_{A_{112}}^*\|_2^2. \quad (43)$$

1778 The exchange between A_1 and B_2 yields

$$\|\theta_{B_2}^*\|_2^2 - \|\theta_{A_{111}}^*\|_2^2 \geq |B_2|(M^2 - \tilde{\sigma}^2), \quad (44)$$

1781 and

$$\|\theta_{B_{11}}^*\|_2^2 - \|\theta_{A_{112}}^*\|_2^2 \geq -|B_{11}|\tilde{\sigma}^2 \geq -C_{B_1}\tilde{\sigma}^2.$$

1782 Note the assumption of Theorem 5.2 that $(|B_2| + C_{B_1})\tilde{\sigma}^2 \leq |B_2|M^2$. We add the last two
 1783 inequalities Equation (43) and appendix F.1 together to get
 1784

$$1785 \sum_{i:\pi_{t_1}(i)>d^\dagger(t_1)} |\theta_i^*|^2 - \sum_{i:\pi_{t_2}(i)>d^\dagger(t_1)} |\theta_i^*|^2 \geq 0,$$

1786 where \geq becomes $>$ if $B_2 \neq \emptyset$. By the definition of d^\dagger , $d^\dagger(t_2) \leq d^\dagger(t_1)$.
 1787

- 1788 • Case 2: $|B_2| > |A_1|$. If the eigenvalue of the last element of $B_2 \cup A_2$ is among the top d^\dagger ,
 1789 we follow the exact same proof in Case 1.

1790 Now suppose that the eigenvalue of the last element of $B_2 \cup A_2$ is in the later part. In this
 1791 case, all elements B_1 and A_1 are in the later part. We first identify all the elements that fall
 1792 in the later part at time t_2 : in addition to all elements of B_1 , the following
 1793

$$\begin{aligned} 1794 B_{21} &:= \{i \in B_2 : \pi_{t_2}^{-1}(i) > d^\dagger\}, \\ 1795 A_{11} &:= \{i \in A_1 : \pi_{t_2}^{-1}(i) > d^\dagger\}, \\ 1796 A_{21} &:= \{i \in A_2 : \pi_{t_2}^{-1}(i) > d^\dagger\}, \\ 1797 A_{31} &:= \{i \in A_3 : \pi_{t_2}^{-1}(i) > d^\dagger\}. \\ 1798 \end{aligned}$$

1799 Note that at time t_1 , the elements in the later part are in B_1 , B_{21} , and $B_{22} := B_2 \setminus B_{21}$.
 1800 Therefore, Equation (41) can be written as
 1801

$$1802 \|\theta_{B_{22}}\|^2 - \|\theta_{A_{11}}\|^2 - \|\theta_{A_{21}}\|^2 - \|\theta_{A_{31}}\|^2. \quad (45)$$

1803 By definition of B_2 , A_1 , and A_3 , each squared element in B_2 is larger than that of both A_1
 1804 and A_3 . In addition, since A_2 and B_2 will be monotonously nonincreasing, for any element
 1805 in B_{22} , its squared signal will be no less than that of any element in $\theta_{A_{21}}$. Therefore, we
 1806 conclude that Equation (45) is nonnegative and will be positive if B_{22} is not empty.
 1807

1808 F.2 GENERALIZED SIGNAL RESULTS BY DYNAMIC EQUATION ANALYSIS

1809 **Proposition F.1** (Shrinkage monotonicity and shrinkage time). *Suppose all the events $\{E_k\}$ in
 1810 Lemma F.9 hold. Let $\varepsilon = 2(C_{proxy})^{-1/2} \sqrt{\frac{\ln n \tilde{d}}{n}} \cdot \ln n$, $\varepsilon' = 2(C_{proxy})^{-1/2} \sqrt{\frac{\ln n}{n}}$.*

1811 For any $j \in S$ (as defined in Assumption 5.1), we have
 1812

$$1813 |\theta_j^* - \theta_j(t)| < 2\varepsilon'. \quad \forall t \geq t(\varepsilon) \quad (46)$$

1814 where $t(\varepsilon) = C b_0^{-D} \varepsilon^{-1} \ln n$ for some absolute constant C .
 1815

1816 *Proof.* When all the events E_k in Lemma F.9 hold, we have
 1817

$$1818 \|\xi_S\|_\infty \leq \varepsilon'. \quad (47)$$

1819 Consider $j \in S$. We have $\theta_j^* \geq 8\varepsilon'$ (We let $C_M \geq 8$). By taking $\delta = \varepsilon'$ and also $\kappa = \varepsilon'$ in Lemma
 1820 F.7, we have
 1821

$$1822 |\theta_j^* - \theta_j(t)| \leq 2\varepsilon', \quad \forall t \geq \bar{T}^{app}(\delta),$$

1823 with
 1824

$$1825 \bar{T}^{app}(\delta) \leq T^{\text{sig}} + C_2 D^{\frac{D}{D+2}} (\theta_j^*)^{-\frac{2D+2}{D+2}} \ln^+ \frac{2\theta_j^*}{\delta}, \quad (48)$$

1826 and
 1827

$$1828 T^{\text{sig}} \leq \begin{cases} C_1(\theta_j^*)^{-1} b_0^{-D} \ln\left(\frac{e b_0}{a_{0j} \sqrt{D}}\right) & a_{0j} < b_0 / \sqrt{D}; \\ C_1(\theta_j^*)^{-1} a_{0j}^{-1} \ln\left(\frac{e a_{0j} \sqrt{D}}{b_0}\right) & a_{0j} > b_0 / \sqrt{D}, \text{ and } D = 1; \\ C_1(\theta_j^*)^{-1} D^{-\frac{1}{2}} a_{0j}^{-1} b_0^{-D+1} & a_{0j} > b_0 / \sqrt{D}, \text{ and } D > 1, \end{cases} \quad (49)$$

1829 where both C_1 and C_2 are absolute constants.
 1830

1836 For the choice $b_0 = cD^{\frac{D+1}{D+2}}\varepsilon^{\frac{1}{D+2}}$, the second term on the right-hand side of Equation (48) is
 1837 dominated by the right-hand side of Equation (49), and we can choose c small enough so that the
 1838 summation of the two terms is bounded by $b_0^{-D}\varepsilon^{-1}\ln n$. This justifies our choice of $t(\varepsilon)$.
 1839

□

1840
 1841 **Proposition F.2.** We consider the set R . We let $j \in R$, and suppose all the events $\{E_k\}$ in Lemma
 1842 F.9 hold. Given b_0 and $t(\varepsilon)$ defined in Proposition F.1. For any positive constant δ' , if the eigenvalue
 1843 $\lambda_j < n^{-5}$, and n is large enough, then we have

$$1844 \quad 1845 \quad \tilde{\lambda}_j(t) < 2\lambda_j^{1-2\delta'} b_0^D \cdot n^{1+\delta'}.$$

1846
 1847 *Proof.* Since the events in Lemma F.9 hold, we have $|\xi_j| \leq 2(C_{\text{proxy}})^{-1/2} \sqrt{\frac{\ln \tilde{j} + \ln n}{n}}$, where $\tilde{j} = \frac{\tilde{d}}{\lambda_j}$.
 1848 Since $j \in R$, we have $|\theta_j^*| \leq \tilde{\sigma} \leq \sqrt{c'}\varepsilon$. Since $b_0^D t(\varepsilon) = \varepsilon^{-1} \ln n$, we can check that t is no more
 1849 than the hitting time T_2 defined by Equation (67) in Lemma F.8 as follows.
 1850

1851 Note that

$$1852 \quad 1853 \quad \varepsilon^{-1} \ln n (|\theta_j^*| + |\xi_j|) \leq \sqrt{c'} \ln n + \sqrt{\ln n} \sqrt{\frac{n}{\ln n \tilde{d}}} \cdot \sqrt{\frac{\ln n \tilde{d} + \ln \frac{1}{\lambda_j}}{n}} \\ 1854 \quad 1855 \quad < \ln n + \sqrt{\ln n + \ln \frac{1}{\lambda_j}}.$$

1856 Since $b_0 = c \cdot D^{\frac{D+1}{D+2}}\varepsilon^{\frac{1}{D+2}}$, for n large enough, we have $\lambda_j < n^{-5} < \frac{b_0^2}{D^2}$ and also

$$1857 \quad 1858 \quad \ln \frac{b_0/D}{\lambda_j^{\frac{1}{2}}} = \ln c + \frac{1}{2(D+2)}(\ln n + \ln \ln n \tilde{d}) - \frac{1}{D+2} \ln D + \frac{1}{2} \ln \frac{1}{\lambda_j} > \ln n + \sqrt{\ln n + \ln \frac{1}{\lambda_j}}.$$

1859 It then follows that

$$1860 \quad 1861 \quad \beta_j(t) < \lambda_j^{\frac{1}{2}} \exp(b_0^D t(|\theta_j^*| + |\xi_j|)) \\ 1862 \quad 1863 \quad \leq \lambda_j^{\frac{1}{2}} \exp\left(\sqrt{\ln n} \sqrt{\frac{n}{\ln n \tilde{d}}} \cdot \sqrt{\frac{\ln n \tilde{d} + \ln \frac{1}{\lambda_j}}{n}}\right) \cdot n \\ 1864 \quad 1865 \quad < \lambda_j^{\frac{1}{2}} \exp\left(\sqrt{\ln \frac{1}{\lambda_j}}\right) \cdot \exp(\sqrt{\ln n}) \cdot n \\ 1866 \quad 1867 \quad < \lambda_j^{\frac{1}{2}-\delta'} n^{1+\delta'}.$$

1868 Using $\tilde{\lambda}_j(t) = (\beta_j^2(t) + \lambda_j)(b_0^2 + D\beta_j^2(t))^D$, we obtain the desired result for sufficiently large n . □

1869
 1870 **Remark F.3.** The above proposition provides a very weak upper bound on $\tilde{\lambda}$, but it is sufficient to
 1871 show that any eigenvalue λ_j , such that if given any constant C , $\lambda_j < n^{-C}$, then $\tilde{\lambda}_j(t)$ is also less
 1872 than any polynomial of n^{-1} . Therefore, when considering the eigenvalue ordering problem, such
 1873 signals can be ignored.

1874 F.3 CONSERVATION QUANTITY

1875 We omit the subscript j in the following two sections F.3 and F.4 because all the proofs are similar
 1876 for $j = 1, 2, \dots, d$. By Equation (38), it is easy to see that

$$1877 \quad 1878 \quad \frac{d}{dt} a^2 = \frac{1}{D} \frac{d}{dt} b^2 = \frac{d}{dt} \beta^2 = 2ab^D \beta(\theta^* - \theta + \xi).$$

1879 Consequently, we have

1890
1891
1892

$$a^2(t) - \beta^2(t) \equiv a_0^2, \quad b^2(t) - D\beta^2(t) \equiv b_0^2. \quad (50)$$

1893 Using this, we see that
1894

1895
1896
$$a(t) = (\beta^2(t) + a_0^2)^{1/2}, \quad b(t) = (D\beta^2(t) + b_0^2)^{1/2} > 0.$$

1897 Using these conservation quantities, we can prove the following estimations in terms of β :
1898

1899
1900
$$\begin{aligned} \max(a_0, |\beta|) &\leq a \leq \sqrt{2} \max(a_0, |\beta|) \\ \max(b_0, \sqrt{D}|\beta|) &\leq b \leq \sqrt{2} \max(b_0, \sqrt{D}|\beta|) \end{aligned} \quad (51)$$

1903 which also implies that $|\theta| = |ab^D\beta| \geq D^{D/2}|\beta|^{D+2}$. The evolution of θ . It is direct to compute that
1904

1906
$$\begin{aligned} \dot{\theta} &= \dot{a}b^D\beta + aD\dot{b}^{D-1}\dot{b}\beta + ab^D\dot{\beta} \\ &= \left[(b^D\beta)^2 + (Dab^{D-1}\beta)^2 + (ab^D)^2 \right] (\theta^* - \theta + \xi) \\ &= \theta^2 (a^{-2} + D^2b^{-2} + \beta^{-2}) (\theta^* - \theta + \xi). \end{aligned} \quad (52)$$

1911 And we also have
1912

1913
1914
$$|\theta| = |ab^D\beta| \geq D^{D/2}|\beta|^{D+2} \implies |\beta| \leq \left(D^{-D/2}|\theta| \right)^{1/(D+2)}. \quad (53)$$

1916 Therefore,
1917

1918
1919
$$\theta^2 (a^{-2} + D^2b^{-2} + \beta^{-2}) \geq \theta^2\beta^{-2} \geq D^{-\frac{D}{D+2}}|\theta|^{\frac{2D+2}{D+2}}. \quad (54)$$

1921 F.4 MULTI-LAYER DYNAMIC

1923 We study the dynamic of the ODE for any given j . Before the analysis, we streamline some notations.1924 Assume for some $\kappa_j > 0$, it holds that $|\xi_j| \leq \kappa_j$. (Note that this κ_j can be the high probability
1925 upper bound derived using Lemma F.9.) Since j is given, we drop the the subscript j to simplify
1926 the exposition throughout this subsection; for example, we write λ for λ_j and θ^* for θ_j^* . We write
1927 $\ln^+(x) = \max(1, \ln(x))$ for any $x > 0$.1928 **Lemma F.4** (Monotonicity from equation). *Consider the equation Equation (38). Suppose $y > 0$.*
19291930 1. *$a(t)$, $\beta(t)$, and $\theta(t)$ are all non-negative and increasing.*
19311932 2. *We have*

1933
$$y \geq \theta(t) \geq 0 \quad \forall t \geq 0.$$

1934 3. *Since $y = \theta^* + \xi$ and $|\xi| \leq \kappa$, we have*

1936
$$|\theta^* - \theta(t)| \leq |\theta^*| + \kappa, \quad \forall t \geq 0.$$

1938 4. *$|\theta^* - \theta(t)|$ is decreasing provided that $|\theta^* - \theta(t)| > \kappa$.*
19391940 5. *If $|\theta^* - \theta(t_1)| \leq \kappa$ for some t_1 , we have*

1942
$$|\theta^* - \theta(t)| \leq \kappa \text{ for all } t \geq t_1.$$

1943 If $y < 0$, Items 3, 4, and 5 still hold, while Items 1 and 2 can be modified by symmetry.

1944 *Proof.* Items 1 and 2 are directly implied from Equation (38). Item 3 is implied by Item 2.
 1945

1946 To prove Item 4, consider Equation (52), from which we have
 1947

$$\dot{\theta} = \theta^2 (a^{-2} + D^2 b^{-2} + \beta^{-2}) (y - \theta),$$

1949 which implies $\dot{\theta} \geq 0$.
 1950

1951 Since $|\theta^* - \theta(t)| > \kappa$, we have either $\theta(t) > \theta^* + \kappa$ or $\theta(t) < \theta^* - \kappa$.
 1952

1953 The first case is not possible; otherwise, we have $0 < y = \xi + \theta^* \leq \kappa + \theta^* < \theta \leq y$, which is a
 1954 contradiction. In the second case, we have $|\theta^* - \theta(t)| = \theta^* - \theta(t)$, which is decreasing because
 $\dot{\theta} \geq 0$.
 1955

1956 Item 5 is implied by Item 4.
 1957 \square

1958 **Lemma F.5** (Approaching from below). *Consider the equation Equation (38). Suppose $\theta^* \geq 8\kappa$*
 1959 *(similar results hold for $\theta^* \leq -8\kappa$ by symmetry). Suppose $t_0 \geq 0$ such that $0 \leq \theta(t_0) < \frac{1}{4}\theta^*$. Define*
 1960

$$T^{\text{sig}} = \inf \{s \geq 0 : \theta(t_0 + s) \geq \theta^*/4\}.$$

1961 This is the extra time needed from t_0 for θ to reach $\theta^*/4$. We have
 1962

$$T^{\text{sig}} \leq \begin{cases} 4(\theta^*)^{-1} b_0^{-D} \ln\left(\frac{b_0}{a_0 \sqrt{D}}\right) & a_0 < b_0/\sqrt{D}; \\ 4(\theta^*)^{-1} a_0^{-1} \ln\left(\frac{a_0 \sqrt{D}}{b_0}\right) & a_0 > b_0/\sqrt{D}, \text{ and } D = 1; \\ 4(\theta^*)^{-1} D^{-\frac{1}{2}} a_0^{-1} b_0^{-D+1} & a_0 > b_0/\sqrt{D}, \text{ and } D > 1. \end{cases} \quad (55)$$

1963 *Proof.* Since $|y - \theta^*| = |\xi| \leq \kappa$ and $\theta^* \geq 8\kappa$, we have $y \geq 7\kappa > 0$. Therefore, $\theta(t) \in [0, y]$. For
 1964 any $t \leq t_0 + T^{\text{sig}}$, we use $\theta^* \geq 8\kappa$ to show that
 1965

$$y - \theta(t) = \theta^* - \theta(t) + \xi \geq \frac{3}{4}\theta^* - \kappa \geq \frac{1}{2}\theta^*.$$

1966 Let $r = \min(a_0, b_0/D^{\frac{1}{2}})$ and $R = \max(a_0, b_0/D^{\frac{1}{2}})$. Define the following time point if it exists:
 1967

$$T^{\text{pos},1} = \inf \{s \geq 0 : \beta(t_0 + s) \geq r\}; \quad T^{\text{pos},2} = \inf \{s \geq 0 : \beta(t_0 + s) \geq R\}$$

$$T^{\text{sig}} = \inf \left\{ s \geq 0 : |\theta^* - \theta(t_0 + s)| \leq \frac{3}{4}\theta^* \right\}.$$

1968 We will first bound both $T^{\text{pos},1}$ and $T^{\text{pos},2}$.
 1969

1970 From Equation (38), we have
 1971

$$\dot{\beta}(t) = a(t)b^D(t)[\theta^* + \xi - \theta(t)] \geq \frac{1}{4}\theta^* a(t)b^D(t), \quad \text{for } t \leq t_0 + T^{\text{sig}}. \quad (56)$$

1972 **Stage 1:** $0 \leq s \leq T^{\text{pos},1}$. Note that $\sqrt{2}a_0 > a(t) > a_0$, and $e \cdot b_0^D > b(t)^D = (D\beta(t)^2 + b_0^2)^{\frac{D}{2}} > b_0^D$.
 1973 We have

$$\dot{\beta}(t_0 + s) \geq \frac{1}{4}\theta^* a_0 b_0^D \geq \frac{1}{4}\theta^* a_0 b_0^D,$$

1974 which suggests β increases at least linearly. Therefore, we have
 1975

$$T^{\text{pos},1} \leq 8r (\theta^* a_0 b_0^D)^{-1}. \quad (57)$$

1976 **Stage 2:** $T^{\text{pos},1} \leq s \leq T^{\text{pos},2}$. Consider two cases.
 1977

1978 Case 1: If $a_0 < b_0/\sqrt{D}$, $r = a_0$ and $R = b_0/\sqrt{D}$. Note $a \geq \beta$ in Equation (51). We use
 1979 Equation (56) to get
 1980

1998

$$1999 \quad \dot{\beta}(t_0 + s) \geq \frac{1}{4} \theta^* b_0^D |\beta(t_0 + s)|, \\ 2000$$

2001 By Grönwall's inequality, we have

2002

$$2003 \quad T^{\text{pos},2} - T^{\text{pos},1} \leq 4 (\theta^* b_0^D)^{-1} \ln \frac{b_0}{a_0 \sqrt{D}}. \quad (58) \\ 2004$$

2005

2006 Case 2: If $a_0 > b_0/\sqrt{D}$, $R = a_0$ and $r = b_0/\sqrt{D}$. We use $b \geq \sqrt{D}\beta$ in Equation (51) together with
2007 $a > a_0$, $b > \sqrt{D}|\beta|$ and Equation (56) to get that

2008

$$2009 \quad \dot{\beta}(t_0 + s) \geq \frac{1}{4} \theta^* a_0 D^{\frac{D}{2}} |\beta(t_0 + s)|^D. \\ 2010$$

2011

By comparison theorem, we have

2012

2013

$$2014 \quad T^{\text{pos},2} - T^{\text{pos},1} \leq \begin{cases} 4 (\theta^* a_0)^{-1} \ln \frac{a_0 \sqrt{D}}{b_0}, & \text{if } D = 1; \\ 2015 \quad 4 ((D-1)\theta^* a_0 D^{D/2})^{-1} \left[(b_0/\sqrt{D})^{-(D-1)} - a_0^{-(D-1)} \right], & \text{if } D \geq 2. \end{cases} \\ 2016 \\ 2017 \quad (59)$$

2018

2019 **Stage 3:** If $T^{\text{sig}} \leq T^{\text{pos},2}$, then we can use the for T^{sig} in Stage 2 as a bound for T^{sig} . Now,
2020 we consider the case $T^{\text{pos},2} < T^{\text{sig}}$. We combine Equation (51) with $a > |\beta|$, $b > \sqrt{D}|\beta|$, and
2021 Equation (56) to get

2022

$$2023 \quad \dot{\beta}(t_0 + T^{\text{pos},2} + s) \geq \frac{1}{4} \theta^* D^{D/2} |\beta(T^{\text{pos},2} + s)|^{D+1}, \quad \text{for } s \in [0, T^{\text{sig}} - T^{\text{pos},2}].$$

2024

Beside, we have $\beta(t_0 + T^{\text{pos},2}) = R > 0$. By Lemma F.10, we have

2025

2026

$$2027 \quad T^{\text{sig}} - T^{\text{pos},2} \leq 4 D^{-\frac{D+2}{2}} (\theta^*)^{-1} R^{-D}. \quad (60)$$

2028

We now bound T^{sig} using the summation of Equation (57), Equation (60), and Equation (58) if
2029 $a_0 < b_0/\sqrt{D}$, or the summation of Equation (57), Equation (60), and Equation (59) if $a_0 > b_0/\sqrt{D}$.

2030

If $a_0 < b_0/\sqrt{D}$, we can bound the right hand sides of Equation (57) and Equation (60) by
2031 $8(\theta^*)^{-1} b_0^{-D}$ and $4(\theta^*)^{-1} b_0^{-D}$ respectively.

2032

If $a_0 > b_0/\sqrt{D}$, we can bound the right hand sides of Equation (57) and Equation (60) by
2033 $8(\theta^*)^{-1} D^{-\frac{1}{2}} a_0^{-1} b_0^{-D+1}$ and $4(\theta^*)^{-1} D^{-\frac{1}{2}} a_0^{-1} b_0^{-D+1}$ respectively. Furthermore, if $D > 1$, we
2034 can bound Equation (59) by $4(\theta^*)^{-1} (D-1)^{-1} D^{-\frac{1}{2}} a_0^{-1} b_0^{-D+1}$.

2035

This leads to

2036

$$2037 \quad T^{\text{sig}} \leq \begin{cases} 4(\theta^*)^{-1} b_0^{-D} \left(3 + \ln \left(\frac{b_0}{a_0 \sqrt{D}} \right) \right) & a_0 < b_0/\sqrt{D}; \\ 2038 \quad 4(\theta^*)^{-1} a_0^{-1} \left(3 + \ln \left(\frac{a_0 \sqrt{D}}{b_0} \right) \right) & a_0 > b_0/\sqrt{D}, \text{ and } D = 1; \\ 2039 \quad 16(\theta^*)^{-1} D^{-\frac{1}{2}} a_0^{-1} b_0^{-D+1} & a_0 > b_0/\sqrt{D}, \text{ and } D > 1. \end{cases} \quad (61)$$

2040

2041

2042

2043

Lemma F.6 (Approximation time near θ^*). *Consider the equation Equation (38) with $\theta^* \geq 0$ (a
2044 similar result holds for $\theta^* \leq 0$). Suppose $\theta^* > 8\kappa$. Suppose for some $t_0 \geq 0$ such that*

2045

2046

2047

$$\frac{1}{4} \theta^* \leq \theta(t_0) \leq \theta^* - \kappa.$$

2048

2049 Then, for any $\delta > 0$, we have

2050

2051

$$|\theta^* - \theta(t)| \leq \kappa + \delta, \quad \forall t \geq t_0 + 4^{\frac{2D+2}{D+2}} D^{\frac{D}{D+2}} (\theta^*)^{-\frac{2D+2}{D+2}} \ln^+ \frac{|\theta^* - \theta(t_0)| - \kappa}{\delta}.$$

2052 *Proof.* Given any $\delta > 0$, if $\theta(t_0) \geq \theta^* - \kappa - \delta$, we have $|\theta^* - \theta(t)| \leq \kappa + \delta$ for all $t \geq t_0$ by
 2053 Lemma F.4 (Item 4) and the desired result is proved.
 2054

2055 Next, suppose $\theta(t_0) < \theta^* - \kappa - \delta$. Define

$$2056 T^{\text{app}} = \inf \{s \geq 0 : |\theta^* - \theta(t_0 + s)| \leq \kappa + \delta\}.$$

2057 By Lemma F.4 (Item 4) again, it suffices to provide an upper bound on T^{app} .
 2058

2059 For all $t \geq t_0$, we have $\frac{1}{4}\theta^* \leq \theta(t)$ by Lemma F.4 (Item 1). Consequently, Equation (54) implies that
 2060

$$2061 \theta^2 (a^{-2} + D^2 b^{-2} + \beta^{-2}) \geq D^{-\frac{D}{D+2}} |\theta|^{\frac{2D+2}{D+2}} \geq 4^{-\frac{2D+2}{D+2}} D^{-\frac{D}{D+2}} (\theta^*)^{\frac{2D+2}{D+2}} := c_0.$$

2062 Furthermore, by Equation (52), we have

$$2064 \dot{\theta} = \theta^2 (a^{-2} + D^2 b^{-2} + \beta^{-2}) (\theta^* - \theta + \xi) \geq c_0 (\theta^* - \kappa - \theta).$$

2066 Let $x(s) := \theta^* - \kappa - \theta(t_0 + s)$ with $x(0) = \theta^* - \kappa - \theta(t_0)$. Note that T^{app} is the hitting time of
 2067 $x(s)$ to δ . Applying Lemma F.11 to $x(s)$, we have
 2068

$$2069 2070 2071 T^{\text{app}} \leq c_0^{-1} \ln \frac{|\theta^* - \theta(t_0)| - \kappa}{\delta}.$$

2072 \square

2073 **Lemma F.7.** Consider the equation Equation (38) with $\theta^* \geq 0$ (a similar result holds for $\theta^* \leq 0$).

2075 Suppose $\theta^* \geq 8\kappa$. For two absolute constants C_1, C_2 , we have
 2076

$$2077 2078 |\theta^* - \theta(t)| \leq \kappa + \delta, \quad \forall t \geq \bar{T}^{\text{app}}(\delta),$$

2079 where

$$2080 2081 2082 \bar{T}^{\text{app}}(\delta) := \bar{T}^{\text{sig}} + C_2 D^{\frac{D}{D+2}} (\theta^*)^{-\frac{2D+2}{D+2}} \ln^+ \frac{\theta^*}{\delta}, \quad (62)$$

2084 and

$$2085 2086 2087 2088 \bar{T}^{\text{sig}} := \begin{cases} C_1(\theta^*)^{-1} b_0^{-D} \ln\left(\frac{b_0}{a_0 \sqrt{D}}\right) & a_0 < b_0 / \sqrt{D}; \\ C_1(\theta^*)^{-1} a_0^{-1} \ln\left(\frac{a_0 \sqrt{D}}{b_0}\right) & a_0 > b_0 / \sqrt{D}, \text{ and } D = 1; \\ C_1(\theta^*)^{-1} D^{-\frac{1}{2}} a_0^{-1} b_0^{-D+1} & a_0 > b_0 / \sqrt{D}, \text{ and } D > 1. \end{cases} \quad (63)$$

2090 *Proof.* We will repeatedly apply the monotonicity of Lemma F.4.

2091 Recall T^{sig} defined in Lemma F.5 with $t_0 = 0$ and let t_1 be the upper bound on T^{sig} we found therein.
 2092 Then $\theta(t_1) \geq \frac{\theta^*}{4}$.

2093 We then apply Lemma F.6 with $t_0 = t_1$, and conclude that $|\theta^* - \theta(t)| \leq \kappa + \delta$ for all $t \geq t_1 + t_2$,
 2094 where $t_2 = 4^{\frac{2D+2}{D+2}} D^{\frac{D}{D+2}} (\theta^*)^{-\frac{2D+2}{D+2}} \ln^+ \frac{|\theta^* - \theta(t_1)| - \kappa}{\delta}$. Note that $|\theta^* - \theta(t_1)| - \kappa \leq \theta^*$. We complete
 2095 the proof by defining $\bar{T}^{\text{sig}} = t_1$ and $\bar{T}^{\text{app}}(\delta) = t_1 + 4^{\frac{2D+2}{D+2}} D^{\frac{D}{D+2}} (\theta^*)^{-\frac{2D+2}{D+2}} \ln^+ \frac{\theta^*}{\delta}$.
 2096

2097 \square

2099 **Lemma F.8.** Consider the equation Equation (38). Denote $r' = \min\{a_0, b_0/D\}$, $R' = \max\{a_0, b_0/D\}$. W.L.O.G., We assume that $\theta^* \geq 0$. Define $T_1 = \inf\{t : |\beta(t)| > r'\}$, and
 2100 $T_2 = \inf\{t : |\beta(t)| > R'\}$. If $D \geq 1$, and t satisfies the following:
 2101

$$2103 2104 2105 \sqrt{2e} a_0 b_0^D \int_0^t (|\theta^*| + |\xi|) ds \leq \min(a_0, b_0/D),$$

2106 then we have

2160 F.5 AUXILIARY LEMMA
21612162 The following lemma provides a choice of $\kappa_j \geq |\xi_j|$ with high probability.
21632164 **Lemma F.9.** *Recall S defined by Assumption 5.1 and let $C = 2(C_{\text{proxy}})^{-1/2}$. For $k \in S$, we
2165 introduce the events $\{E_k\}$ as follows:*

2166
$$E_k := \{|\xi_k| \leq Cn^{-1/2}\sqrt{\ln n}\}. \quad (68)$$

2167

2168 For $k \in S^C$, we introduce the events $\{E_k\}$ as follows:
2169

2170
$$E_k := \left\{ |\xi_k| \leq Cn^{-1/2}\sqrt{\ln(n\tilde{k})} \right\}. \quad (69)$$

2171

2172 where $\tilde{k} = \sum_j \lambda_j / \lambda_k$.
21732174 Then, with probability at least $1 - \frac{4}{n}$, all events E_k , $k \in [d]$ hold simultaneously.
21752176 *Proof.* By Assumption 5.1, the noise ξ_k is sub-Gaussian with variance proxy C_{proxy}/n . Therefore,
2177 $\mathbf{P}(|\xi_k| \geq s) \leq 2 \exp(-(2C_{\text{proxy}})^{-1}ns^2)$.
2178If $k \in S$, we have

2179
$$\mathbf{P} \left\{ |\xi_k| \geq 2C_{\text{proxy}}^{-1/2}\sqrt{\frac{\ln n}{n}} \right\} \leq 2 \exp(-2(\ln n)).$$

2180
2181

2182 By the union bound, we have
2183

2184
$$\begin{aligned} \mathbf{P} \{ \cap_{k \in S} E_k \} &\geq 1 - \sum_{k \in S} \mathbf{P} \left\{ |\xi_k| \geq 2C_{\text{proxy}}^{-1/2}\sqrt{\frac{\ln n}{n}} \right\} \\ 2185 &\geq 1 - |S|2 \exp(-2(\ln n)) \\ 2186 &\geq 1 - \frac{2}{n}, \end{aligned} \quad (70)$$

2187
2188
2189

2190 where the last inequality is because $|S|2 \exp(-2(\ln n)) \leq 2n^{-1}$.
21912192 If $k \in S^C$, we have

2193
$$\mathbf{P} \left\{ |\xi_k| \geq 2(C_{\text{proxy}})^{-1/2}\sqrt{\frac{\ln n\tilde{k}}{n}} \right\} \leq 2 \exp \left(-(\ln n + \ln \frac{\sum_j \lambda_j}{\lambda_k}) \right) \leq \frac{2}{n} \cdot \frac{\lambda_k}{\sum_j \lambda_j}, \quad (71)$$

2194
2195
2196

2197 where we recall that $\tilde{k} = \frac{\sum_j \lambda_j}{\lambda_k}$.
2198

2199 By the union bound, we have

2200
$$\begin{aligned} \mathbf{P} \{ \cap_{k \in S^C} E_k \} &\geq 1 - \sum_{k \in S^C} \mathbf{P} \left\{ |\xi_k| \geq 2(C_{\text{proxy}})^{-1/2}\sqrt{\frac{\ln n\tilde{k}}{n}} \right\} \\ 2201 &\geq 1 - \sum_{k \in S^C} \frac{2}{n} \cdot \frac{\lambda_k}{\sum_j \lambda_j} \\ 2202 &\geq 1 - \frac{2}{n}. \end{aligned} \quad (72)$$

2203
2204
2205
2206
2207
2208

2209 We combined the Equation (70) and Equation (72), and we derive the results.
2210□
22112212 The following two lemmas provide convenient upper bounds on hitting times of ODE solutions.
2213**Lemma F.10.** *Let $k > 0$ and $p > 1$.*

2214 • Consider the ODE
 2215

$$2216 \quad \dot{x} \geq kx^p, \quad x(0) = x_0 > 0$$

2218 Then we have
 2219

$$2221 \quad x(t) \geq \left(x_0^{-(p-1)} - (p-1)kt \right)^{-\frac{1}{p-1}}$$

2223 and thus for any $M \geq 0$,
 2224

$$2225 \quad \inf\{t \geq 0 : x(t) \geq M\} \leq \left[(p-1)kx_0^{p-1} \right]^{-1}. \quad (73)$$

2228 • Consider the ODE
 2229

$$2230 \quad \dot{x} \leq -kx^p, \quad x(0) = x_0 > 0.$$

2232 Then we have
 2233

$$2235 \quad x(t) \leq \left(x_0^{-(p-1)} + (p-1)kt \right)^{-\frac{1}{p-1}},$$

2237 and thus for any $M > 0$,
 2238

$$2239 \quad \inf\{t \geq 0 : x(t) \leq M\} \leq \left[(p-1)kM^{p-1} \right]^{-1}. \quad (74)$$

2241 **Lemma F.11.** Let $k > 0$ and $x_0 > 0$.

2243 1. If

$$2245 \quad \dot{x}(t) \geq kx(t), \quad x(0) = x_0,$$

2247 then for all $t \geq 0$, it holds that
 2248

$$2249 \quad x(t) \geq x_0 e^{kt},$$

2251 and for every $M \geq x_0$, we have
 2252

$$2254 \quad \inf\{t \geq 0 : x(t) \geq M\} \leq \frac{1}{k} \log\left(\frac{M}{x_0}\right).$$

2256 2. If

$$2259 \quad \dot{x}(t) \leq -kx(t), \quad x(0) = x_0,$$

2261 then for all $t \geq 0$, it holds that
 2262

$$2263 \quad x(t) \leq x_0 e^{-kt},$$

2265 and for every $0 < M \leq x_0$, we have
 2266

$$2267 \quad \inf\{t \geq 0 : x(t) \leq M\} \leq \frac{1}{k} \log\left(\frac{x_0}{M}\right).$$

2268 **G RELATED WORK ON PRINCIPAL COMPONENT REGRESSION**
2269

2270 As discussed in Section 3.1, the PC estimator serves as a motivating example for the concepts of ESD
2271 and span profile due to its clear illustration of bias-variance trade-offs. However, the ESD and span
2272 profile are designed to characterize the intrinsic difficulty of generalization arising from signal-kernel
2273 alignment, and their definitions do not rely on the PC estimator. Nonetheless, the analysis of PC
2274 estimators, particularly in high-dimensional linear regression, been an active area of recent research.
2275 Below, we briefly summarize some relevant contributions to provide context.
2276

2277 **G.1 PROPORTIONAL ASYMPTOTICS**
2278

2279 Several studies analyze Principal Component Regression (PCR) in the proportional asymptotic setting
2280 where the dimension p and sample size n grow with $p/n \rightarrow \gamma$. In this regime, Xu & Hsu (2019) study
2281 the limiting risk of PCR with Gaussian designs with diagonal covariance. They assume polynomially
2282 decaying eigenvalues or a convergent empirical spectrum, together with an isotropic prior, and they
2283 reveal a “double-descent” risk curve. In a related vein, Wu & Xu (2020) extend the analysis to a
2284 general covariance matrix Σ_x and an anisotropic prior satisfying $\mathbb{E}\beta_*\beta_*^\top = \Sigma_\beta$. They also derive an
2285 exact risk expression and demonstrate how “misalignment” between Σ_x and Σ_β affects risk; here
2286 “alignment” refers to concordance between the orderings of their eigenvalues. Both studies assume
2287 knowledge of the eigenvectors of the population covariance matrix Σ_x to construct the *oracle PCR*.
2288 Gedon et al. (2024) analyze the limiting risk of PCR under a latent factor model and explore the
2289 effect of distribution shift. Green & Romanov (2024) derive the exact limits of estimation risk,
2290 in-sample prediction risk, and out-of-sample prediction risk of PCR under the assumption that both
2291 the empirical spectrum distribution and the distribution of the true signal’s mass over the eigenspaces
2292 of Σ_x converges weakly.
2293

2294 **G.2 NON-ASYMPTOTIC ANALYSIS**
2295

2296 Complementary research develops non-asymptotic guarantees. Agarwal et al. (2019) derive finite-
2297 sample upper bounds on prediction error using $\|\beta^*\|_1^2$ and the rank of the design matrix under latent
2298 factor models, and they explore the robustness of PCR to noise and missing values in the observed
2299 covariates. Bing et al. (2021) consider PCR with an adaptively selected number of components
2300 under latent factor models and provide alternative finite-sample risk bounds using $\|\beta^*\|_2^2$. Huang
2301 et al. (2022) derive non-asymptotic risk bounds for PCR in more general settings by analyzing the
2302 alignment between population and empirical principal components. Hucker & Wahl (2023) derive
2303 non-asymptotic error bounds for PCR in kernel regression.
2304
2305
2306
2307
2308
2309
2310
2311
2312
2313
2314
2315
2316
2317
2318
2319
2320
2321